School of Molecular and Life Sciences

Faculty of Science and Engineering

Characterisation of Insulin at the Interface Between Two Immiscible Electrolyte Solutions

Hum Bahadur Lamichhane

0000-0001-6359-5644

This thesis is presented for the degree of

Master of Philosophy (Chemistry)

of

Curtin University

December 2019

Declaration

To the best of my knowledge and belief, this thesis contains no material previously published by any other person except where due acknowledgement has been made.

This thesis contains no material which has been accepted for the award of any other degree or diploma in any university or institution for higher education.

Hum Bahadur Lamichhane

M.Phil. Candidate

[13th December 2019]

Statement of Contribution by Others

Dr. Terence J. Henares contributed to the design of the electrochemical cell used in this work, and to the design of experiments to characterise that cell.

Dr. Mark J. Hackett contributed to the design and interpretation of the spectroscopic experiments for insulin characterisation.

Prof. Damien W.M. Arrigan contributed to the design and interpretation of the electrochemical experiments for insulin detection and characterisation.

Hum Bahadur Lamichhane

Dr Mark J Hackett

Prof. Damien W.M. Arrigan

Table of Contents

List of Figures

List of Tables

Acknowledgements

The credit for this work goes to my respected Scientific Supervisors, Prof. Damien Arrigan and Dr. Mark Hackett, School of Molecular and Life Sciences, Curtin University. They have provided constant guidance for me to complete this work. I appreciate them for inspiring my research thinking, for showing due patience to listen to my arguments and for helping me to frame this research idea and to adopt the proper approach. Their patience in correcting my writing and captious remarks on the subject has been very valuable for the preparation of this thesis.

I am most grateful to the Chair of my thesis committee, Dr. Franca Jones, School of Molecular and Life Sciences, Curtin University, for her support and expert opinions in my research.

I am also grateful to the entire Electrochemistry and Sensors Group, who have been there for the entire journey of my research, Terence, Ben, Jahir, Bren, Shaheda, Nasibeh, Nazanin who directly and indirectly supported me to successfully accomplish my research on time. And thanks to all of my group members for all the electrochemistry and spectroscopy discussions and lunches as well.

I am also grateful to Dr. Thomas Becker and Mr. Peter Chapman, School of Molecular and Life Sciences, Curtin University, for their help to handle the ATR-FTIR Spectrometer and Raman Spectrometer. I am also thankful to all the academic and administrative staff of the School of Molecular and Life Sciences, Curtin University, for their help during entire research.

Finally, I must express my very profound gratitude to my parents (Tulsi Devi Lamichhane and Late Mr. Ran Bahadur Lamichhane), to my brother (Krishna Bahadur Lamichhane), to my spouse (Sarita Paudel), and to my daughter (Joyana Lamichhane) for providing me with unfailing support and continuous encouragement throughout my years of study and through the process of researching and writing this thesis. This accomplishment would not have been possible without them.

Thank you.

Glossary of Major Symbols

Roman Symbols

Symbols	Definition	Units
A	Area	cm^2
a_i	Activity of species i	-
C	Capacitance	F
C_{dl}	Double-layer capacitance	F
C_i	Concentration of species i	mol cm^{-3}
D_i	Diffusion coefficient	Cm^2 s^{-1}
e^-	Electrons	-
E	Potential	V
E^0	Formal potential	V
E_{eq}	Equilibrium potential	V
F	Faraday's constant	C mol^{-1}
G	Gibbs free energy	J mol^{-1}
G^0	Standard Gibbs free energy	J mol^{-1}
I	Current	A
I_{lim}	Limiting current	A
J	Flux	mol s^{-1} cm^{-2}
ln	Natural logarithm	-
M	Molarity	mol L^{-1}
n	Number of moles of electrons Number of micro interfaces	- -
N	Number of moles	-
o	Organic phase at liquid-liquid interface	-
O	Oxidised species	-
Q	Charge	C
r	Radius	cm
R	Reduced species Resistance	- Ω

	Universal gas constant	J K^{-1} mol^{-1}
t	Time	s
T	Temperature	K
V	Potential difference	V
w	Aqueous phase at liquid-liquid interface	-
x	Distance	cm
z_i	Charge of species i	-

Greek Symbols

Symbols	Definition	Units
α	Phase of a liquid-liquid system	-
α-helix	Secondary structure of protein	-
β-sheet	Secondary structure of protein	-
Δ	Difference	-
Γ	Surface coverage	-
γ_i^{α}	Activity coefficient for species i in phase α	-
μ	Micro- (prefix)	-
$\mu_i^{-\alpha}$	Electrochemical potential of species i in phase α	kJ mol^{-1}
μ_i^{α}	Chemical potential of species i in phase α	kJ mol^{-1}
$\mu_i^{\alpha,0}$	Standard chemical potential of species i in phase α	kJ mol^{-1}
ν	Scan rate Hydrodynamic velocity	V s^{-1} cm s^{-1}
ϕ	Standard Galvani potential difference	V

Glossary of Abbreviations

Abbreviation	Definition
AC	Alternating current
ACT	Aqueous complexation followed by transfer
AdSV	Adsorptive stripping voltammetry
Ag/AgCl	Silver/silver chloride
Aq.	Aqueous phase
ATR	Attenuated total reflection
BSA	Bovine serum albumin
$BTPPA^+$	Bis(triphenylphophoranylidene)ammonium, organic cation
BTPPACl	Bis(triphenylphophoranylidene)ammonium chloride
CA	Chronoamperometry
CE	Counter electrode
Cl^-	Chloride ion
CV	Cyclic voltammetry
Cyt c	Cytochrome c
1,2-DCE	1,2-Dichloroethane
1,6-DCH	1,6-Dichlorohexane
DNA	Deoxyribonucleic acid
EM	Electron microscopy
ESI-MS	Electrostatic spray ionisation mass spectrometry
ET	Electron transfer
FIA	Flow injection analysis
FIT	Facilitated ion transfer
FTIR	Fourier transform infrared
H^+	Hydrogen ion
HB	Haemoglobin
HCl	Hydrochloric acid
IHP	Inner Helmholtz Plane
IT	Ion transfer

ITIES	Interface between two immiscible electrolyte solutions
IUPAC	International union of pure and applied chemistry
KCl	Potassium chloride
KTPBCl	Potassium tetrakis(4-chlorophenyl)borate
LiCl	Lithium chloride
MALDI	Matrix-assisted laser desorption ionisation
MD	Molecular dynamics
MS	Mass spectrometry
NB	Nitrobenzene
NMR	Nuclear magnetic resonance spectroscopy
NPOE	2-nitrophenyl octyl ether
OCP	Open Circuit Potential
Org.	Organic phase
OHP	Outer Helmholtz Plane
PDMMS	Phenyldimethylmethoxy silane
pI	Isoelectric point
PVC	Polyvinyl chloride
QELS	Quasi-elastic light scattering
RE	Reference electrode
SECM	Scanning electrochemical microscopy
SHE	Standard hydrogen electrode
SV	Stripping voltammetry
TIC	Transfer by interfacial complexation
TID	Transfer by interfacial dissociation
TMA^+	Tetramethylammonium ion
TOC	Transfer to the organic phase followed by complexation
$TPrA^+$	Tetrapropylammonium ion
$TPBCl^-$	Tetrakis(4-chlorophenyl)borate, organic anion
WE	Working electrode

Abstract

The study of the structure of insulin at the interface between two immiscible electrolyte solutions (ITIES) following electroadsorption was undertaken in order to identify the structures of the adsorbed insulin and any possible changes that might result. Initial experiments in this thesis focused on the electrochemical study of tetrapropylammonium ion ($TPrA^+$) and insulin at the ITIES. A new electrochemical set up based on a plastic membrane perforated with a millimetre-scale single hole was introduced and was used to study $TPrA^+$ and insulin electrochemistry. Then, secondary structures of insulin were investigated at the newly characterised millimetre-sized ITIES, following electroadsorption, using FTIR and Raman spectroscopies. The understanding of the secondary structures of insulin at the ITIES, and any changes introduced by the electroadsorption, may be beneficial for some biomedical applications.

The electrochemical study of $TPrA^+$ has revealed that voltammetric peak responses (forward as well as backward scans) increase with increasing concentration of $TPrA^+$. Likewise, a voltammetric scan rate study of $TPrA^+$ shows that peak currents (forward as well as backward scans) linearly increase with increasing square root of scan rate. It means that the $TPrA^+$ transfer at the ITIES follows a diffusion-controlled basis. In addition, the peak-peak separation and the ratio of the forward peak current to the backward peak current are found to be *ca*. 59 mV and *ca*. 1, respectively. The diffusion coefficient of $TPrA^+$ in the aqueous phase is reported to be 5.5×10^{-6} cm^2 s^{-1}. These electrochemical parameters validated the new electrochemical cell.

The electrochemical study of insulin shows that peak responses (both forward and backward scans) increase with increasing concentration of aqueous insulin. Similarly, a scan rate study and the nature of the cyclic voltammogram (CV) of insulin show that insulin possesses a diffusion-controlled phenomenon followed by the adsorption/desorption of organic anion-insulin complex at the ITIES. These studies also validate the new millimetre-sized electrochemical set up. Adsorption of the insulin at the interface, in combination with electrochemical ion transfer, may influence insulin secondary structures. Characterising insulin secondary structure at the ITIES may reveal new insight regarding insulin structure and chemical function.

The secondary structures of insulin following electroadsorption are investigated using Fourier transform infrared (FTIR) spectroscopy. Combined β-sheet and irregular helix structures are reported in significant proportions in both solid-state insulin and hydrated films of insulin. However, the secondary structures of electroadsorbed insulin at the ITIES depend on the concentration of aqueous insulin. Combined β-sheet and irregular helix structures are found in larger proportions at high concentrations. On the other hand, at low concentration of aqueous insulin, α-helical structures dominate over the other secondary structures. Other secondary structures like 3_{10}-helix, unordered, and turns remain unaltered at different concentrations. The impact of electroadsorpiton at different potentials on the relative proportions of insulin secondary structures is also investigated. Results show that there is no impact on the secondary structures of electroadsorbed insulin at different adsorption potentials. Nevertheless, the applied potential was a trigger for the adsorption at the ITIES. Likewise, the relative proportions of the secondary structures of electroadsorbed insulin at different adsorption times is investigated. It reveals that the proportions of α-helical and combined β-sheet and irregular helix remain unaffected at different adsorption times. However, the relative proportion of 3_{10}-helix and unordered structure show variation with different adsorption times.

Raman spectroscopy could not detect insulin following electroadsoption, even at 50 µM aqueous insulin, but FTIR spectroscopy could detect 5 µM aqueous insulin. However, electrochemistry could detect 0.5 µM aqueous insulin. So, electrochemistry is the more sensitive technique for detection of insulin at the ITIES. Nevertheless, FTIR spectroscopy is a valuable technique for the determination of secondary structures of insulin following electroadsorption.

Chapter 1. Introduction

The principles of electrochemistry establish the key ideas of electrochemistry at the liquid-liquid interface. The basic concept of electrochemistry, as well as the basic concept of electrochemistry at the liquid-liquid interface, is presented in this chapter. The electrochemistry and Fourier transform infrared (FTIR) spectroscopy study of bio-electroactive molecules at the interface between two immiscible electrolyte solutions (ITIES) are also reported in this chapter. Since a large number of diseases are related to the presence of protein β-sheet secondary structures,[1] knowledge of the secondary structures of insulin at the ITIES might provide fruitful insight to a number of biomedical applications. Hence, an extensive review of the secondary structures of protein is also included in this chapter.

1.1. The basic concepts of electrochemistry

Electrochemistry is a branch of chemistry that deals with the study about the relationship between chemical and electrical processes.[2] Electrochemistry has been broadly categorised into two types: (a) study of chemical or physical changes due to the supply of electrical energy and (b) study of electrical changes due to chemical processes.[3] An electrochemical cell that can be used to produce electrical energy from chemical reactions is called a Voltaic cell or a Galvanic cell. Electrical energy is produced due to the spontaneous redox chemical reactions that occur at the electrodes. On the other hand, electrolytic cells use electrical energy to drive a chemical reaction. Here, to initiate chemical change, electrical energy has to be supplied and the reactions which take place in electrolytic cells are not spontaneous.[3] Different processes occurring in electrochemistry are discussed below.

1.1.1 Electrochemistry at solid electrodes

Solid electrode electrochemistry involves the transfer of charge (i.e. electrons) between the oxidised (or reduced) species and the electrified surface (electrode).[2,4] Carbon, gold, and platinum electrodes are the frequently used solid electrodes.[5] Section 1.1.2 below discusses the electron transfer processes across the solid-liquid interface.

1.1.2 Electron transfer processes

Some of the electroactive species that are present in solution have a tendency to either lose or gain an electron (or electrons). Oxidation is the process in which the electroactive particles lose an electron (or electrons) whereas reduction is that process in which the electroactive particles accept an electron (or electrons) from the solid electrode. Oxidation and reduction are also known as anodic and cathodic processes, respectively. Equations (1) and (2) indicate the oxidation and reduction processes, respectively, where O and R stand for oxidised and reduced species, respectively.[6]

$$\boldsymbol{R \rightarrow O + ne^-} \quad (1)$$

$$\boldsymbol{O + ne^- \rightarrow R} \quad (2)$$

The chemical reactions in which both oxidation and reduction reactions take place simultaneously are known as redox reactions. Equation (3) describes the Gibbs free energy of any redox reaction in terms of activities of the species involved.

$$\boldsymbol{\Delta G = \Delta G^0 + RTln\frac{a_O}{a_R}} \quad (3)$$

where ΔG and ΔG^0, respectively, indicate the Gibbs free energy and standard Gibbs free energy of the system in J mol^{-1}. Also, R and T denote the universal gas constant and temperature (K), respectively. The value of R is 8.314 J mol^{-1} K^{-1}. In addition, a_O and a_R, respectively, represent the activities of the oxidised and reduced species. Here, the unit of activity is mol L^{-1}. The Gibbs free energy of any redox reaction will change with the change in the ratio of activities of the oxidised and reduced species. The standard Gibbs free energy (J mol^{-1}) of any redox reaction can be correlated with the standard electrode potential. The relationship between the standard electrode potential (E^0) and standard Gibbs free energy of any redox reaction is illustrated in equation (4).

$$\boldsymbol{\Delta G^0 = -nFE^0} \quad (4)$$

where n is the number of moles of electrons involved in the redox reaction and F is known as the Faraday constant (96485 C mol^{-1}) whereas the other terms are as already defined. This equation is widely used for the prediction of whether the processes are spontaneous or nonspontaneous. For any spontaneous redox reaction $E^0_{cell} > 0$, while for nonspontaneous redox reactions $E^0_{cell} < 0$. For any

redox reaction, the equilibrium electrode potential is provided by the Nernst equation which is shown in equation (5). If the reactions are kinetically and thermodynamically feasible, the Nernst equation will apply.[3,7]

$$\boldsymbol{E = E^0 + \frac{RT}{nF} ln \frac{a_O}{a_R}} \quad (5)$$

where E denotes the potential difference (V). All other terms used in equation (5) are already defined. Equation (5) successfully explains the potential of an electrode with the change in the ratio of activity of the redox species in solution at the electrode surface.

1.1.3 Faradaic and non-Faradaic reactions

In any electrochemical cell, two electrochemical processes (i.e. faradaic and non-faradaic reactions) always occur. The oxidation or reduction reactions that generate electric energy in the form of a current are called faradaic reactions. The current which is obtained by faradaic reactions is called the faradaic current. Faradaic reactions follow Faraday's law.[7] Faraday's law, which is shown in equation (6), describes the relationship between chemical reactions and the electricity passed through the electrochemical cell.

$$\boldsymbol{Q = nFN} \quad (6)$$

where Q, n, F, and N represent the charge (C), the number of electrons involved, Faraday's constant (96485 C mol^{-1}), and the number of moles of reacting species (mol), respectively. However, non-faradaic reactions do not associate with redox reactions at the interface, rather they associate with the accumulation of charge at the interface. The current which is related to non-faradaic reactions is called non-faradaic current, and the structure which is associated with the non-faradaic current is called the electrical double layer[2,5,8] which is described in section 1.1.4.

1.1.4 The Electrical double Layer

When an electrode is immersed in a liquid solution of an electrolyte, a solid-liquid interface is formed. Similarly, when two mutually immiscible liquid electrolytic solutions come into contact, it gives a liquid-liquid interface. The interface of the latter type is used in this thesis. In both types of interfaces, a potential difference is

developed across the interface and an electrical double layer is formed at the interface. This double layer is made up of the charges on the electrode surface and the charges of the electrolyte ions and is in close contiguity with the electrode. Helmholtz[2,3] proposed the basic model of the electrical double layer in order to explain the non-faradaic current at electrodes. This model assumed that the double layer is made up of charges on the electrode surface and the charges of the electrolyte ions in the electrolytic solution close to the electrode surface. Here, the electrical double layer acts as a capacitor. Figures 1 (A) and 1 (B) represent Helmholtz's electrical double layer and a capacitor, respectively.

A capacitor is an electrical device that consists of a pair of metal electrodes that are parallel to each other and these metal electrodes are separated by dielectric medium. When a potential is imposed on the capacitor, then electrical charges are stored on the metal electrodes. The capacitance of the capacitor can be calculated by equation (7).[2]

$$\boldsymbol{C = \frac{Q}{E}} \tag{7}$$

where Q, E, and C indicate the charges accumulated on the capacitor (C), applied potential on the capacitor (V), and capacitance (F), respectively. Any capacitor will store electrical charges until Q in Equation (7) is fully satisfied. As a result, the non-faradaic current will transfer through the capacitor. It means that the capacitance of double layer, C_{dl}, varies according to the applied potential and hence the capacitance of double layer is a characteristic of the interface that exists between the electrode and electrolytic solution.

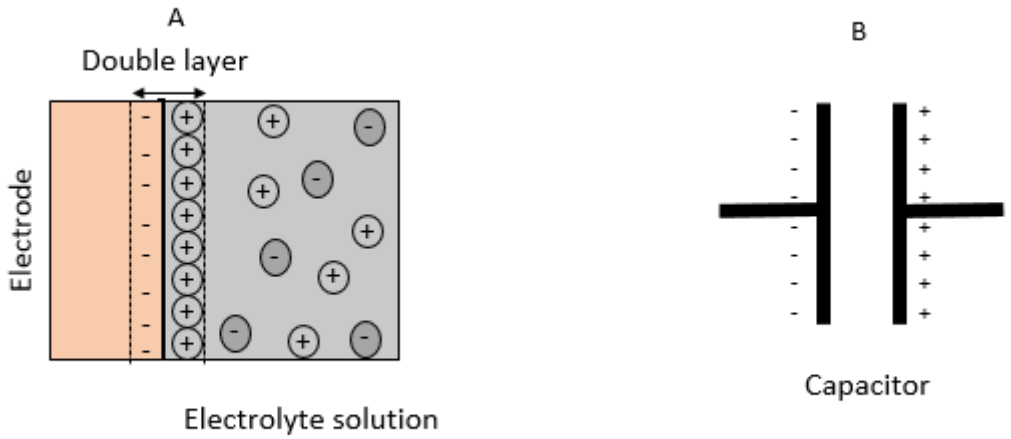

Figure 1: (A) Schematic representation of Helmholtz's electrical double layer model and (B) Schematic representation of a capacitor.

The study of the double layer has been conducted and modified over the years. Gouy and Chapman launched a new idea of the diffuse layer and they proposed that any charged particle in the solution cannot be restricted to the electrode surface.[2] Since the number of charged particles is less in dilute solutions and hence to counterbalance the charges that are located on the electrode surface, it is necessary that a thicker layer in close proximity to the electrode surface would form. This thicker layer that is present in the vicinity of the electrode is called the diffuse layer and this diffuse layer is as shown in Figure 2. With increase in distance of ions from the electrode surface, the electrostatic force is decreased and hence the concentration of counter ions is decreased. Similarly, the thickness of the diffuse layer also depends on the applied potentials. As the applied potential is increased, the electrostatic force decreases and hence the thickness of the diffuse layer will also decrease.

According to Helmholtz, Gouy, and Chapman, ions are point charges that could come close to the electrode surface without any hindrance.[2] Because of the finite size of the electrolyte ions, however, ions could not arbitrarily come to the surface of the electrode if the distance is less than the ionic radius of approaching ions. In order to overcome the limitation of previous models, Stern proposed another model by considering the plane of closest approach known as the Outer Helmholtz

Plane (OHP) for the centre of ions at a certain distance, X_2 (Figure 2).[9] Likewise, Grahame made some improvement on the Stern model by considering the term Inner Helmholtz Plane (IHP).[10] IHP is made up of the adsorbed ionic species and these species may be strongly held on the electrode surface and this plane is the distance X_1 from the metallic surface to the centre of the adsorbed species, as depicted in Figure 2.

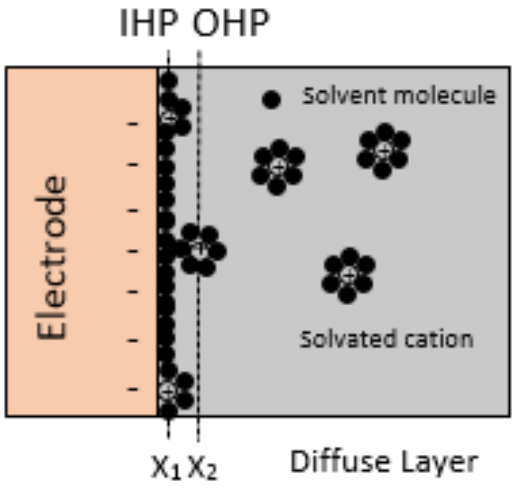

Figure 2: The electrical double layer model given by Stern and Grahame showing outer and inner Helmholtz planes (The idea of this figure was adopted from Grahame [10]).

1.1.5 Mass transport

The movement of electroactive particles in the electrolytic solution towards or away from the interface is known as mass transport and is often measured in the form of flux (J). In any electrolytic solution, mass transport can be described by three mechanisms:

(1) Diffusion - occurs due to concentration gradients.

(2) Migration - occurs due to the impact of an electric field.

(3) Convection - occurs due to mechanical forces like temperature variation or stirring.[2,5]

The Nernst-Plank equation describes the mass transport of any ionic species (i) to the electrode as the flux which is shown in equation (8).

$$\boldsymbol{J_i(x) = -D_i \frac{\partial C_i(x)}{\partial x} - \frac{z_i F}{RT} D_i C_i \frac{\partial \emptyset(x)}{\partial x} + C_i \nu(x)} \quad (8)$$

where, $\boldsymbol{J_i, D_i, C_i}$ and $\boldsymbol{z_i}$ are the Flux (mol cm^{-2} s^{-1}), diffusion coefficient (cm^2 s^{-1}), concentration (mol cm^{-3}), and charge of the electroactive species (i), respectively, and $\nu(x)$ shows the hydrodynamic velocity (cm s^{-1}). Similarly, $\frac{\partial C_i(x)}{\partial x}$ and $\frac{\partial \emptyset(x)}{\partial x}$ are the concentration gradient and potential gradient along the x – axis, respectively.[2,5] Many factors like temperature, viscosity, and molecular size of electroactive species are responsible for the value of the diffusion coefficient of the species.[11] At standard temperature (298 K), the diffusion coefficient of the diffusing species vary from 10^{-6} to 10^{-5} cm^2 s^{-1} at aqueous conditions.[5,12]

By running the electrochemical cell in the presence of excess electrolyte and at stationary solution conditions, the mass transport caused by migration and convection can be minimised. At this condition, the mass transport of the species is limited by diffusion process[8,13] and such process is mathematically described by Fick's first law as shown in equation (9).

$$\boldsymbol{J_i(x,t) = -D_i \frac{\partial C_i(x,t)}{\partial x}} \quad (9)$$

This equation (9) helps to calculate the diffusion flux of electrolytic species at time t at x distance from the electrode at its concentration C_i. Similarly, equation (10) exhibits Fick's second law, which helps to explain the diffusional flux with time.

$$\boldsymbol{\frac{\partial C_i(x,t)}{\partial x} = D_i \frac{\partial^2 C_i(x,t)}{\partial x^2}} \quad (10)$$

Likewise, equation (11) gives the direct relationship between current and flux and is used to calculate the rate of charge flow.

$$\boldsymbol{i = -nFAJ\ (x,t)} \quad (11)$$

Combining equations (9) and (11) gives equation (12).

$$\boldsymbol{i = nFAD \frac{\partial C_i(x,t)}{\partial x}} \quad (12)$$

In equation (12), $n, F, and\ A$, respectively, represent the number of electrons exchanged during the process, Faraday's constant and area of the electrode. It gives the diffusional current on suppression of the other modes of mass transport (convection and migration).

1.2. Electrochemistry at the ITIES

1.2.1. Introduction to the ITIES

When two mutually immiscible (or poorly miscible) solutions, one containing hydrophilic electrolyte (e.g. LiCl) and other having hydrophobic electrolytes (e.g. bis(triphenylphosphoranylidene)ammonium tetrakis(4-chlorophenyl)borate (BTPPATPBCl), are brought in contact with each other, then an interface between the two immiscible electrolyte solutions (ITIES) is formed. The hydrophobic electrolyte should be dissolved in organic solvents (e.g. 1,2-dichloroethane (1,2-DCE), 1,6-dichlorohexane (1,6-DCH)) which are polar and with sufficient dielectric permittivity to dissolve and dissociate the organic electrolyte.[14,15] At the ITIES, often ion transfers take place from one medium to other,[16] and redox reactions can occur but in special conditions.[17,18] Because of many advantages of the ITIES, these days, many researchers have applied electrochemistry at the ITIES. Those ions or ionisable species which cannot be easily oxidised or reduced can be detected by using the ITIES because the transfer of these ions across the ITIES produces a current.[15] So, electrochemistry at the ITIES has been widely used for the label-free detection of various biomolecular species.[19] In addition, the ITIES in the different length scales like macro[16,20], micro[21], and nano[22,23] has been used by different researchers to study the various ionic or ionisable species.

Nernst and Riesenfeld initiated electrochemical studies at the ITIES in 1902 using water-phenol-water interfaces.[24] In 1963, Blank and Feig[25] also added some valuable works on the field of electrochemical studies at the ITIES. Later, Gavach et al.[26] observed the polarisable nature of the ITIES, and concluded that charge transfer at the ITIES could be due to the Galvani potential difference across the interface. Like Gavach's work, later, Koryta and co-workers have considered the polarisability of the interface, and they announced that the charge transfer behaviour across the ITIES was found to be similar with redox species at conventional solid electrodes.[27] This paved the way to study the charge transfer behaviour of various redox species at the ITIES. Using a four-electrode system, Samec and co-workers, investigated the kinetic nature of various charge transfer processes at the ITIES.[16]

Not only different biomolecules (e.g. choline,[28] noradrenaline,[29] acetylcholine,[30] dopamine,[31] insulin,[32] lysozyme,[33] and haemoglobin[34]), drugs (e.g.

metoprolol,[35] and daunorubicin[36]), carbohydrates (e.g. heparin)[37,38] but also DNA[39,40] have been extensively studied using electrochemistry at the ITIES by different researchers. In addition, the electrochemical behaviour of various food substances like aspartame and acesulfame K has also been studied by using the ITIES.[41] These substances have ionic characters and these substances are widely used for the manufacture of sugar-free liquid refreshment. Likewise, different analytical techniques like scanning electrochemical microscopy (SECM),[42] capillary electrophoresis,[43] ion chromatography,[44] and flow injection analysis (FIA)[45] have been widely assimilated with electrochemistry at the ITIES.

1.2.2. Structure of the ITIES

In order to describe the structure of the ITIES, by making some modifications to the Gouy-Chapman theory, Verwey and Niessen announced a theoretical model of the structure of the ITIES.[5,46] According to this theory, the ITIES consists of two back to back diffuse layers, one having large proportions of positive charges, while the other has large proportions of negative charges. Gavach and co-workers, however, have introduced the idea of a rigid non-ionic layer of oriented molecules which are aligned in a particular orientation that isolates the back-to-back diffuse layers.[26] In addition, Girault and Schiffrin proposed the formation of an intermixed solvent layer at the interface as shown in Figure 3, and according to them the composition of this layer does not remain constant.[47,48] According to Schmickler et al., the thickness of this mixed solvent layer varies according to the miscibility of two solvents chosen.[49] Likewise, the width of water-alkane interfaces was examined by Schlossman et al. using synchrotron X-ray reflectivity.[50] This group also performed molecular dynamics (MD) simulations to calculate the distribution of ions.[51] Moreover, Mitrinovic et al. also used X-ray reflectivity to analyse the thickness of water-alkane interfaces, and successfully determined the thickness of it, which was found to be 3.5 – 6 Å.[52] By using neutron reflection and scanning electrochemical microscopy (SECM), Strutwolf et al. were able to calculate the root mean square roughness of the water-dichloroethane interface.[53] Afterward, by considering the impact of the capillary waves, capillary wave theory described the non-linear polarisation of the double layer.[54]

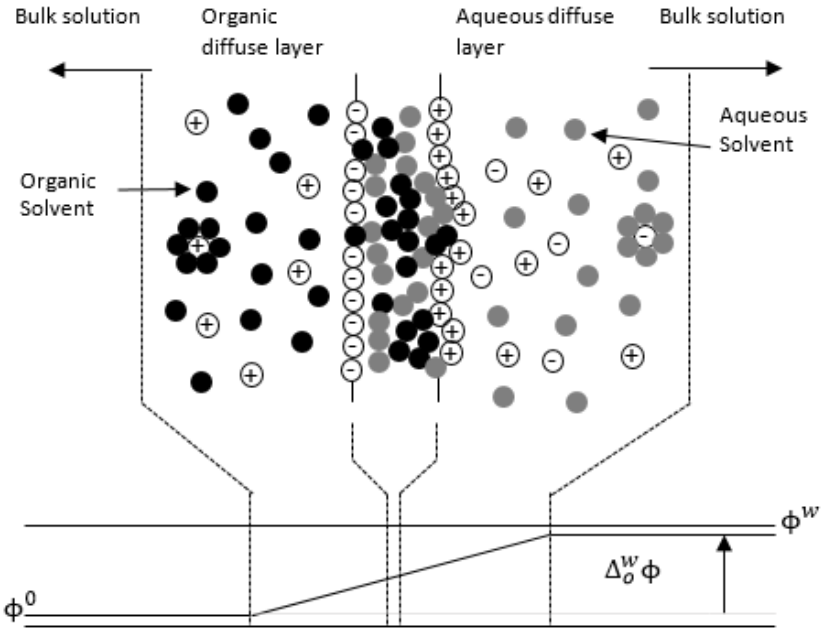

Figure 3: Figure demonstrating the electrical double layer which is formed at the ITIES. Darker and lighter shaded circles, respectively, represent the organic and aqueous solvents. ϕ^o, ϕ^w, and $\Delta_o^w\phi$, respectively, denote the potential in the aqueous phase, the potential in the organic phase, and the Galvani potential difference across the ITIES.

1.2.3. Thermodynamic overview of the ITIES

When two mutually immiscible electrolyte solutions are brought into contact, an ITIES is formed. At the ITIES, because of the separation of charges, a difference in Galvani potential, $\Delta_o^w\phi$, is developed. The equilibrium Galvani potential difference at the ITIES is given by equation (13):[6,14]

$$\boldsymbol{\Delta_o^w\phi = \phi^w - \phi^o} \qquad (13)$$

where ϕ^w and ϕ^o are the aqueous phase (w) and organic phase (o) potentials, respectively. Using this equation the potential of either phase at the interface can also be calculated.

Any electrochemical species has an electrochemical potential at a particular point in space. However, the electrochemical potential of any electrochemical ion (i) at the equilibrium state is constant everywhere. The electrochemical potential at equilibrium can be written by the following equation (14):[2,3]

$$\bar{\mu}_i^w = \bar{\mu}_i^o \quad (14)$$

where $\bar{\mu}_i^w$ and $\bar{\mu}_i^o$ are the electrochemical potentials of an ion (i) in water and organic phase, respectively.

According to thermodynamics, the work required to migrate an ion (i) from a vacuum phase to a liquid phase (α) is given by equation (15):[2]

$$\bar{\mu}_i^\alpha = \mu_i^\alpha + z_i F\phi^\alpha \quad (15)$$

where μ_i^α and z_i are the chemical potential in phase (α) and charge of the ion (i), respectively. Likewise, the term $z_i F\phi^\alpha$ shows the electrical work responsible for the electrochemical potential.

For any species, the chemical potential and the electrochemical potential are related by equation (16):[2]

$$\mu_i^\alpha = \mu_i^{\alpha,0} + RTln\alpha_i^\alpha \quad (16)$$

where $\mu_i^{\alpha,0}$ and α_i^α are the standard chemical potential and activity of the ion (i), respectively. Factors like temperature, pressure, and solution compositions have a large influence on the activity of the ion. Equation (17) shows the relationship between activity and concentration.

$$\alpha_i^\alpha = \gamma_i^\alpha C_i^\alpha \quad (17)$$

where γ_i^α and C_i^α represent the activity coefficient and concentration of ion (i), respectively.

Combining equations (15) and (16), a new equation (18) defined as follows:

$$\bar{\mu}_i^\alpha = \mu_i^{\alpha,0} + RTln\alpha_i^\alpha + z_i F\phi^\alpha \quad (18)$$

As already discussed when the electrochemical potential of ion (i) is equal in both phases, then there exists a thermodynamic equilibrium in the system. So, combining equation (14) and equation (18), the following equation (19) is defined:[3]

$$\mu_i^{w,0} + RTln\alpha_i^w + z_i F\phi^w = \mu_i^{o,0} + RTln\alpha_i^o + z_i F\phi^o \quad (19)$$

On rearranging equation (19), the Galvani potential difference at the interface can be written as shown in equation (20):[3]

$$\Delta_o^w \phi = \phi^w - \phi^o = \frac{\mu_i^{o,0} - \mu_i^{w,0}}{z_i F} + \frac{RT}{z_i F} \ln\left(\frac{\alpha_i^o}{\alpha_i^w}\right) \quad (20)$$

Equation (21) describes the relationship between the difference in standard chemical potentials and the standard Gibbs energy of ion transfer, $\Delta G_{transfer,i}^{0,w\to o}$ using standard ion transfer potential, $\Delta_o^w \phi_i^o$.[2]

$$\Delta_o^w \boldsymbol{\phi}_i^o = \frac{\Delta G_{transfer,i}^{0,w\rightarrow o}}{z_i F} = \frac{\mu_i^{o,0} - \mu_i^{w,0}}{z_i F} \quad (21)$$

where $\mu_i^{\alpha,0}$ represent the standard chemical potential of ion (i) in different phases (α) (w-aqueous phase and o-organic phase). Combining equations (20) and (21), we get the Nernst equation at the ITIES as shown in equation (22).[2,14,15,55]

$$\Delta_o^w \boldsymbol{\phi} = \boldsymbol{\phi}^w - \boldsymbol{\phi}^o = \Delta_o^w \boldsymbol{\phi}_i^o + \frac{RT}{z_i F} \ln \left(\frac{\alpha_i^o}{\alpha_i^w} \right) \quad (22)$$

On altering the potential at the interface, the value of $\frac{\alpha_i^o}{\alpha_i^w}$ should be changed as the value of $\Delta_o^w \phi_i^o$ remains constant at given conditions. The value of $\frac{\alpha_i^o}{\alpha_i^w}$ will change only when a certain portion of equilibrated ions migrate from one phase to the other, which is responsible for generating an electric current. Therefore, a graph between the measured current and the applied potential at the interface can be obtained which is called a voltammogram, the same as that from the solid electrode-electrolyte condition. Likewise, the potential difference at the ITIES can be controlled by varying the activities of the common ion in both phases.

The Nernst equation i.e. equation (22), can also be written by the different way by considering the activity coefficient (γ) and concentration (C) of ionic species (i) as shown in equation (23):

$$\Delta_o^w \boldsymbol{\phi} = \Delta_o^w \boldsymbol{\phi}_i^o + \frac{RT}{z_i F} \ln \left(\frac{\gamma_i^o C_i^o}{\gamma_i^w C_i^w} \right) \quad (23)$$

Equation (23) can be re-written in terms of activity coefficient by replacing the standard Galvani transfer potential and activity coefficients with the formal transfer potential ($\Delta_o^w \phi_i^{o'}$) (equation 24). Similarly, equation (25) can be defined for the case of the concentration of species (i) in either phase.[56]

$$\Delta_o^w \boldsymbol{\phi}_i^{o'} = \Delta_o^w \boldsymbol{\phi}_i^o + \frac{RT}{z_i F} \ln \left(\frac{\gamma_i^o}{\gamma_i^w} \right) \quad (24)$$

$$\Delta_o^w \boldsymbol{\phi} = \Delta_o^w \boldsymbol{\phi}_i^{o'} + \frac{RT}{z_i F} \ln \left(\frac{C_i^o}{C_i^w} \right) \quad (25)$$

1.2.4. Classification of the ITIES

The interface between the two immiscible electrolyte solutions (ITIES) can be classified as either polarisable or non-polarisable in the same way as a solid-liquid interface. Polarisation at the ITIES takes place only when both phases show excess charges, negative in one phase and positive in the other phase.[57] If the aqueous and the organic phases, respectively, contain more hydrophilic (A^+B^-) and more hydrophobic (C^+D^-) electrolytes, it results in a polarisable interface as shown in Figure 4 (A). In contrast, a non-polarisable interface, as shown in Figure 4 (B), can be achieved in two ways: first, when both phases contain the same binary electrolyte (A^+B^-) and, second, when both phases contain electrolytes having a common ion (A^+). In the first case, from equation (22), the Nernst equations for cation (A^+) and the anion (B^-) can be written as follows (when both cation and anion have charges +1 and -1, respectively):

$$\Delta_o^w \boldsymbol{\phi} = \Delta_o^w \boldsymbol{\phi}_{A^+}^o + \frac{RT}{z_i F} \ln \left(\frac{\alpha_{A^+}^o}{\alpha_{A^+}^w}\right) \tag{26}$$

$$\Delta_o^w \boldsymbol{\phi} = \Delta_o^w \boldsymbol{\phi}_{B^-}^o + \frac{RT}{z_i F} \ln \left(\frac{\alpha_{B^-}^o}{\alpha_{B^-}^w}\right) \tag{27}$$

At the ITIES, due to the difference in solubility of (A^+) in both mediums, a distribution potential is established and this potential is not affected by concentration. So, the Nernst equation can be re-defined in terms of the activity coefficient as shown in equation (28).

$$\Delta_o^w \boldsymbol{\phi} = \frac{\Delta_o^w \boldsymbol{\phi}_{A^+}^{o'} + \Delta_o^w \boldsymbol{\phi}_{B^-}^{o'}}{2} + \frac{RT}{2F} \ln \left(\frac{\gamma_{A^+}^o \gamma_{B^-}^w}{\gamma_{A^+}^w \gamma_{B^-}^o}\right) \tag{28}$$

However, in the second case, the Galvani potential difference across the ITIES is governed by (A^+) because (B^-) and (C^+) ions are hydrophilic and hydrophobic in nature, respectively, and they do not distribute across the interface. So, equation (28) can be simplified and rewritten as follows:

$$\Delta_o^w \boldsymbol{\phi} = \Delta_o^w \boldsymbol{\phi}_{A^+}^o + \frac{RT}{F} \ln \left(\frac{\alpha_{A^+}^o}{\alpha_{A^+}^w}\right) \tag{29}$$

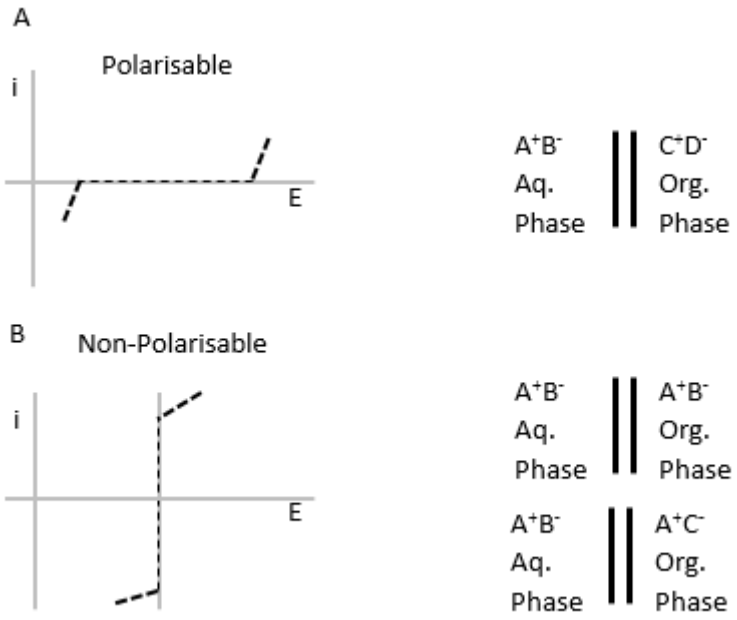

Figure 4: (A) Figure representing the polarisable interface between the two immiscible electrolyte solutions A^+B^- (Hydrophilic) and C^+D^- (Hydrophobic). (B) Figure showing the non-polarisable interface between the two immiscible electrolytic solutions either containing same electrolyte A^+B^- or containing different electrolytes having one ion common (i.e. A^+B^- and A^+C^-) where B^- and C^- are highly hydrophilic and hydrophobic, respectively.

1.2.5. The potential window at the ITIES

The potential window of the ITIES can be described using a cyclic voltammogram (CV) as shown in Figure 5, which is obtained by using 10 mM hydrochloric acid (HCl) as the aqueous electrolyte and 10 mM bis(triphenylphosphoranylidene)ammonium tetrakis(4-chlorophenyl)borate (BTPPATPBCl) as the organic electrolyte. The aqueous and the organic solvents, in this case, are deionised water and 1,2-dichloroethane (1,2-DCE), respectively. In the cyclic voltammogram (Figure 5) two points, one lower and the other higher potential, were chosen and the potential was scanned between these two points while the current of different magnitude was recorded. On the forward scan, a positive potential is maintained on the interface (low to high potential), which results in a positive current. In contrast, on the backward scan, a negative current is transferred through the interface (high to low potential). Here the positive (for forward direction) and

negative (for backward direction) currents simply represent the direction of current that arises due to the movement of ions.

In Figure 5, the CV of only the background electrolyte is divided into three different compartments. The dashed line boxes represent the compartments. On scanning at lower potentials (0.0 to 0.22 V), the $BTPPA^+$ ions from the organic phase are transferred to the aqueous phase and at the same time the Cl^- ions from the aqueous phase are transferred to the organic phase. On further scanning to higher potentials (0.22 to 0.72 V), background electrolyte ions did not show any transfer. Nevertheless, on further increase in potential (0.72 to 0.80 V), again ions of the background electrolyte undergo transfer. In this case, the current is caused by the transfer of $TPBCl^-$ ions from the organic to the aqueous phase and the transfer of H^+ from the aqueous to the organic phase simultaneously. When the potential is reversed from higher to lower potential (0.8 to 0.0 V), the previously transferred ions are returned to their original phases as shown in Figure 5. On backward scanning the potential from 0.8 to 0.72 V, the $TPBCl^-$ions returned to the organic phase and at the same time H^+ transferred back to its aqueous phase. Similarly, at the potential between 0.72 to 0.22 V, the transfer of electrolyte ions did not take place. On further scanning back to 0.0 V from 0.22 V, $BTPPA^+$ ions are transferred back to the organic phase and at the same time Cl^- ions from the organic phase are transferred back to the aqueous phase. In Figure 5, the potential region between 0.22 to 0.72 V is known as the potential window. The current in this region arises due to the charging of interface. The current which is associated with the potential window is known as a charging current. The range of potential window is determined by the forward and backward transfer of background electrolyte ions. In this region, ions of the background electrolytes do not transfer at all. Thus, those analytes which have a tendency to transfer within the potential window without the hindrance of the background electrolyte can be analysed. Larger potential windows can be obtained by choosing highly hydrophilic electrolytes in the aqueous phase and highly hydrophobic electrolytes in the organic phase. The range of potential window also depends upon the salting-out effect (i.e. salt-induced precipitation).[58]

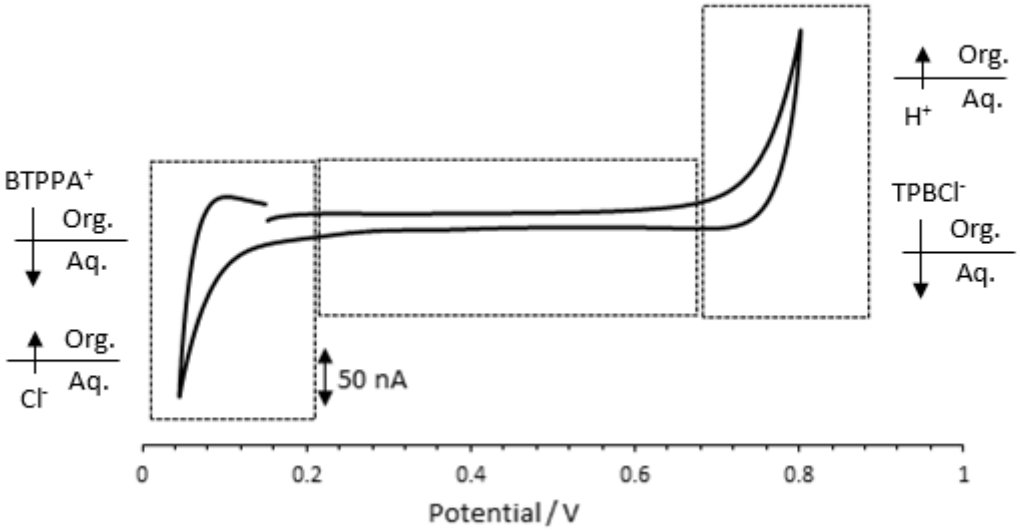

Figure 5: The cyclic voltammogram of 10 mM BTPPATPBCl (gelled in 1,2-DCE and 10 % w/v PVC) as the organic phase and 10 mM HCl as the aqueous phase. The signal on the extreme left and right boxes indicate the background electrolyte transfer while in the middle box shows the potential window where background electrolytes do not transfer. Ag/AgCl electrodes were applied as counter and reference electrodes, containing one in each phase. 10 mV s^{-1} scan rate was used. Full electrochemical cell notation used to produce this data:

$Ag|AgCl|BTPPACl(1\ mM), LiCl(10\ mM)_{aq}|BTPPATPBCl(10\ mM)\ 1,2\text{-}DCE_{org}||HCl(10mM)_{aq}|AgCl|Ag$

1.2.6. Different modes of charge transfer across the ITIES

There are different modes of charge transfer across the ITIES. They are: ion transfer (IT), facilitated ion transfer (FIT), and electron transfer (ET). IT is the simplest mode of charge transfer. It is feasible only when the applied potential difference across the interface overcomes the Gibbs energy of transfer for that ion.[14] In a FIT, a complex[59], which is formed by the combination of a ligand and ion, is responsible for the transfer of the charges. In this case, the transfer energy of the ion is lowered by the presence of the ligand so that it transfers within the potential window. FIT is of different types: (a) transfer by interfacial complexation (TIC), (b) transfer to the organic phase followed by complexation (TOC), (c) transfer by interfacial dissociation (TID), and (d) aqueous complexation followed by transfer (ACT). ET is another mode

of charge transfer across the interface. This mode of charge transfer is possible if each phase contains redox-active species. Figure 6 summarises all three types of charge transfer processes across the interface.

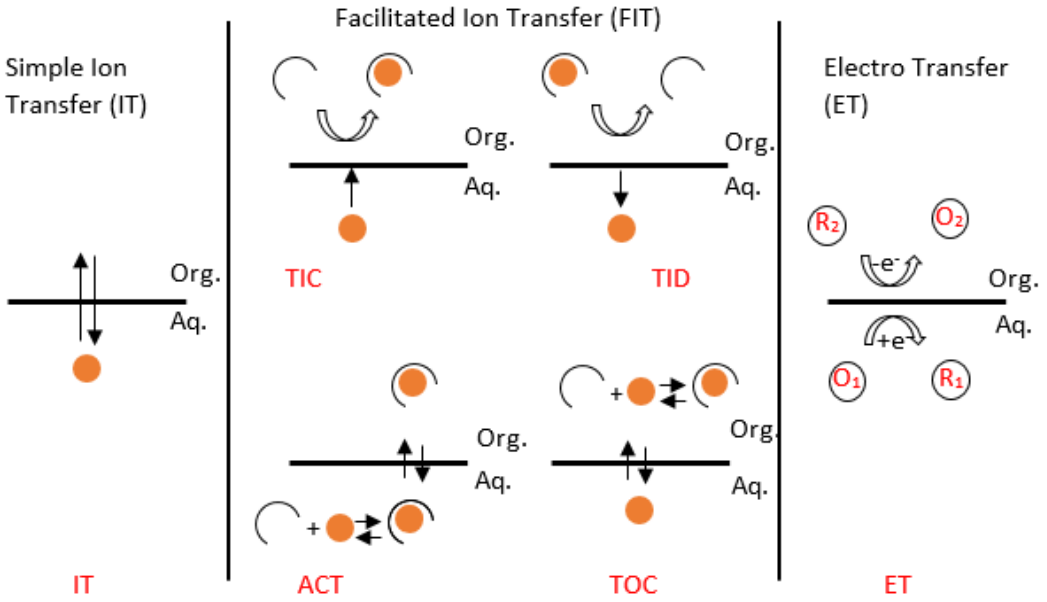

Figure 6: Schematic representation of possible charge transfer processes across the interface (i.e. Simple ion transfer (IT), Facilitated ion transfer (FIT), and Electron transfer (ET)) and different types of FIT: Transfer by interfacial complexation (TIC), Transfer via interfacial dissociation (TID), Transfer to the organic phase followed by complexation (TOC), and Aqueous complexation followed by transfer (ACT). (The idea of this figure was adopted from Samec et al.[14])

1.2.7. Gelled ITIES

Mechanical stability is a major problem of the ITIES. Over time, different researchers used gelled ITIES to study different analytes. Senda and co-workers for the first time used the gelled ITIES using a gelled organic electrolyte.[60] They analysed the transfer of tetramethylammonium ions (TMA^+) and picrate ions using gels.[60] They have used polyvinyl chloride-nitrobenzene gel/water interface and agar-water gel/nitrobenzene interface to see the electrochemical behaviour of TMA^+. Usually, the organic phase is gelled, but the aqueous phase has also been gelled for some experiments. Although gellification increases the resistance (R) of the cell, by using

miniaturised ITIES, such impact can be reduced. As a jellifying component, polyvinyl chloride (PVC) is the most common one. Different types of PVC based gelled ITIES like PVC-nitrophenyl octyl ether (NPOE),[61] PVC-nitrobenzene (NB),[62] PVC-1,6-dichlorohexane (DCH)[63,64] and PVC-1,2-dichloroethane (DCE)[65] have been used by different researchers. Fantini et al. have used agarose gel (i.e. aqueous phase gel) for the liquid-liquid extraction of ions.[66]

1.2.8. Interfacial geometry of the ITIES

Different geometry like recessed, inlaid, and hemisphere of the interface result in different voltammograms at the solid-liquid electrochemical system.[67,68] In liquid-liquid electrochemistry, the interfacial geometry has also played a crucial role in the voltammetric behaviours. For example, the interface may be formed by locating it within a hole or pore in a membrane. If the pore is completely filled with the organic phase, then it gives an inlaid geometry, as shown in Figures 7 (A) and 7 (B). In this condition, ions undergo radial diffusion when transferring from the aqueous to the organic phase. But, on back transferring the ions from the organic to the aqueous phase, these ions follow linear diffusion. The inlaid geometry is true in case of micro-ITIES. Inlaid geometry is also possible when the pore is completely filled with the aqueous phase. However, the transferring ions then have different diffusion patterns. In this case, radial diffusion occurs when ions transfer from organic to the aqueous phase, while transferring the ions from aqueous to the organic phase, linear diffusion takes place. A recessed geometry may appear if the pore is equally filled with both phases as shown in Figures 7 (C) and 7 (D). In this condition, the combination of radial and linear diffusion is shown, depending on the timescale of the experiment. The interfacial geometry of the ITIES is mainly affected by the wetting properties and hydrophobicity of the membrane used to contain the pores.[69]

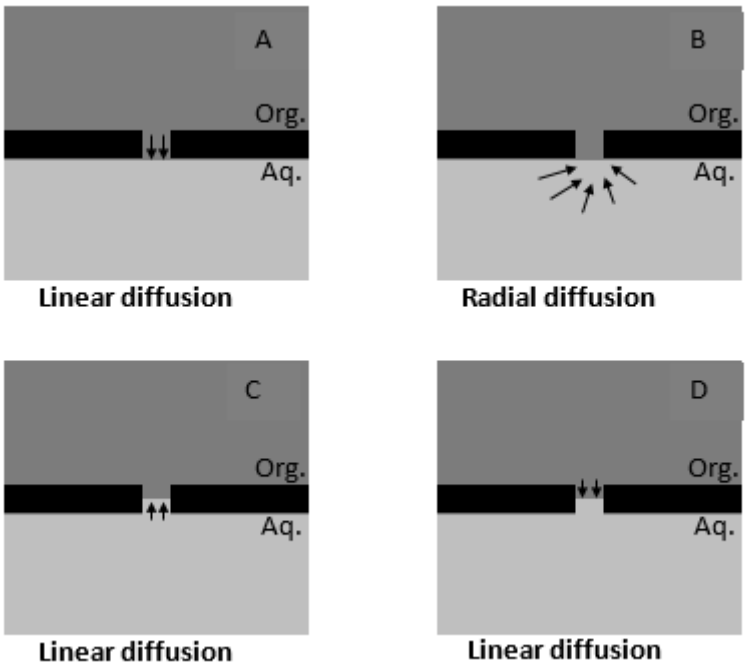

Figure 7: Figure demonstrating the different mode of diffusing profile: (A) linear diffusion from the organic to the aqueous phase, (B) radial diffusion from the aqueous to the organic phase, (C) linear diffusion from the aqueous to the organic phase, and (D) linear diffusion from the organic to the aqueous phase.

1.3. Bio-electroactive molecules at the ITIES

Different biological molecules have been extensively studied at the ITIES. Vanysek and co-workers for the first time investigated the electrochemical behaviour of biomolecules (e.g. bovine serum albumin (BSA), ovalbumin, colicine E_3) using an aqueous-nitrobenzene interface.[70] Electrochemistry of different bio-molecules like neurotransmitters (e.g. dopamine,[71] noradrenaline[29]) amino acids,[72] peptides,[73,74] ionisable drug molecules[15] (e.g. propranolol,[75] warfarin,[76] daunorubicin,[36] metoprolol[35]), carbohydrates (e.g. biopolymer heparin,[77]) biomacromolecules (e.g. proteins)[34,63,78,79] have been studied over time.

The ITIES has been widely used for the study of the electrochemical behaviour of various proteins[63,80,81] not only because it provides a label-free detection strategy but also because it minimises the amount of analytes used.[19] Vanysek and co-workers for the first time reported the behaviour of proteins at the ITIES.[70] Likewise, Karyakin

et al. were able to observe the transfer behaviour of protein at the ITIES using surfactant.[82] Likewise, Amemiya et al. in 2003 conducted the electrochemistry of protamine at polarised liquid/liquid interfaces.[83,84] Protamines were also investigated at the ITIES using cyclic voltammetry, quasi-elastic light scattering (QELS) and conductometry.[85] It revealed that protamine exhibits the facilitated transfer into the organic phase. O'Sullivan and Arrigan explored the electrochemical behaviour of various proteins like myoglobin, haemoglobin, and cytochrome c at the ITIES using bis(2-ethylhexyl) sulfosuccinate as a surfactant.[79,86] They found that the signal in the presence of the surfactant was due to the complex formed between the protein and surfactant. Herzog et al. also contributed to analyse the electrochemical behaviour of protein digested with the enzyme at the ITIES.[34] They found the different responses of protein after digestion with enzyme. They also observed the conformation change of haemoglobin at the ITIES.

Using the adsorptive stripping technique at the ITIES, Alvarez de Eulate and Arrigan were able to detect nano-molar concentration of lysozyme using a suitable adsorption potential.[87] Recently, these researchers investigated the influence of electrodeposition on the formation of cytochrome c oligomer at the ITIES.[80]

In the literature, the ITIES was used for the electrochemical analysis of insulin[32] applying different techniques. By using alternating current (AC) voltammetry, Thomsen et al. have studied the adsorption kinetics of insulin at 1,2 – dichloroethane-aqueous interface.[88] Likewise, Kivlehan et al. studied the electrochemical nature of bovine insulin at the interface.[32] They found that the electrochemical response is due to the formation of a complex between the positively charged insulin and anion of the organic phase followed by adsorption at interface. Electrochemical adsorption of insulin at the soft interface was subsequently established by O'Sullivan et al., using adsorptive stripping voltammetry (AdSV).[89] They were able to investigate the selective identification of insulin from the aqueous mixtures of albumin and insulin by applying suitable adsorption potentials. However, despite studies of its electrochemical detection, there have been few studies of protein structures at the ITIES.

1.4. Structures of proteins

Proteins are made up of amino acid units. Some protein may contain hundreds of amino acid units while some may contain hundreds of thousands of amino acid units.[90] They play a crucial role in life. In the cell, proteins actively participate in various biological functions. Various enzymatic chemistries along with various transport processes are controlled by protein molecules. Four different types of structures of proteins were reported in the literature.[91] The different types of structures of proteins are: (a) primary structure (peptide bonds link the amino acids), (b) secondary structure (hydrogen bond is responsible for inter and intra-molecular interactions), (c) tertiary structure (obtained due to the side-chain interaction of components of secondary structures), and quaternary structure (formed due to the accumulation of individual polypeptide chains in a single unit). Among these four structures, secondary structures of proteins are widely studied. α-helix, 3_{10} helix, irregular helix, β-sheet, unordered, and turn are common examples of secondary structures of insulin.[92–95] Since β-sheet secondary structures have been implicated in many diseases like Alzheimer's disease, Prion disease, Parkinson's disease, and Amyotrophic diseases,[1,96] the secondary structures of proteins have been widely studied by different researchers over time. Different methods like Fourier transform infrared (FTIR) spectroscopy, X-ray crystallography, nuclear magnetic resonance (NMR) spectrometry, Raman spectroscopy, Mass spectrometry (MS) and circular dichroism (CD) spectroscopy have been widely used for the study of secondary structures of proteins.[97–111] Nonetheless, despite studies of other secondary structures, there have been few studies of protein structures at the ITIES.

1.5. Mass Spectrometry (MS) and Fourier transform infrared (FTIR) spectroscopy studies of proteins at the ITIES.

Although proteins have been extensively studied by various researchers using the different techniques as mentioned above (section 1.4), reports of structural study of proteins at the ITIES is limited. In 2014, Arrigan and co-workers studied one protein, lysozyme, at the ITIES.[81] They used electrostatic spray ionization mass spectrometry (ESI-MS) to analyse the tertiary structure of lysozyme following

electroadsorption and they were able to open up a new technique for the identification of the tertiary structure of proteins that interact with the ITIES.

FTIR spectroscopy is one of the most widely used techniques for the analysis of protein secondary structure. In FTIR spectra, the amide I band which arises due to the C=O stretching vibration is the most useful absorption band to analyse the secondary structures of proteins. The different secondary structural components of proteins are related to the frequencies of the amide I band components. In addition, second derivatives of the amide I band successfully provide information about the individual components of secondary structures of proteins.[112,113] Booth et al. in 2019 have analysed the secondary structure of proteins following electroadsorption at the ITIES using FTIR spectroscopy.[105] Proteins like lysozyme, myoglobin, cytochrome c, and haemoglobin were investigated by them. From the FTIR data, they reported that except for lysozyme, the proteins showed antiparallel β-sheet aggregates and this was possible because of the interaction of these proteins with the anion of the organic phase of the ITIES. However, the structure of lysozyme remained unchanged at the ITIES. These results of FTIR spectroscopy were supported by data obtained from matrix-assisted laser desorption/ionisation time of flight mass spectroscopy (MALDI ToF MS).[105] Nevertheless, the structural analysis of insulin at the ITIES has not been studied yet.

1.6. Insulin and its secondary structures

Insulin, which controls glucose in blood, consists of 51 amino acid units. Different diseases like Diabetes mellitus, Insulinoma, and Polycystic ovary syndrome are common diseases that are related with insulin. Insulin possesses different secondary structures like α-helix, 3_{10}-helix, irregular helix, β-sheet, unordered, and turn.[110,111] Over time, different techniques as mention above (section 1.4) have been widely used to study the secondary structures of proteins.

In 1983 Williams[114] studied the secondary structures of insulin using Raman spectroscopy and found larger proportions of combined β-sheet and irregular helix as shown in table 1. Likewise, Wei et al. in 1991 investigated the secondary structure of insulin using FTIR spectroscopy and compared their results with the X-ray crystallography data of the secondary structures of insulin as shown in Table 1.[110]

Table 1 shows that combined β-sheet and irregular helix were found in remarkable proportions, while the other secondary structures were found in lower proportions. The results of FTIR they reported were found in good agreement with the results reported by Williams as shown in Table 1.[114] Xie and Tsou also reported larger proportions of combined β-sheet and irregular helix, in agreement with other researchers.[111] The different relative proportions of secondary structures reported by Xie and Tsou were shown in Table 1. Furthermore, Vecchio et al. in 1996 also reported the presence of significant proportions of combined β-sheet and irregular helix in the insulin as shown in Table 1.[99]

Table 1: Summary of relative proportions of secondary structures of insulin (%) as reported by different researchers.

Authors	Relative proportions (%)							Source of insulin	Method
	α-helix	3_{10}-helix	Irregular helix	β-sheet	unordered	Turn	Combined β-sheet and irregular helix		
Williams[114]	33	-	16	24	9	15	40	Not specified	Raman
Wei et al.[110]	17.5 21	12.2 11.8	23.6 17.6	13.9 19.6	26.7 13.7	6.1 15.6	37.5 37.2	Bovine	FTIR X-ray
Xie and Tsou[111]	15.9	16.6	13.2	30.9	12.4	11.1	44.1	Porcine	FTIR
Vecchio et al.[99]	18.9	11	15.5	23	21.3	9.4	38.5	Bovine	FTIR

Over time, many scientists have conducted the study of the secondary structure of insulin because a large number of diseases[1] are related to the β-sheet secondary structures. It was found that the immunogenicity of insulin increased while the biological activity of insulin decreased due to the formation of aggregates on injecting insulin into the bloodstream.[115] Therefore, it is crucial to know if any structural change of insulin occurs in various conditions. Bouchard et al. studied the impact of temperature on the formation of Bovine insulin fibrils in acidic conditions using FTIR, CD and electron microscopy (EM).[102] They have observed that insulin possesses substantially alpha-helical form at pH 2 (without heating). But, at 70˚C, most of the alpha form has changed into β-sheet forms that lead to the formation of fibrils. Such fibrils formation of insulin on heating (or agitation) was also studied by Nielsen et al. using bovine insulin and their results were in good agreement with Bouchard et al. who studied insulin in acid solution.[100] Mass spectrometry was used

by Nettleton et al. to study Bovine insulin behaviour under similar conditions to Bouchard et al. at pH 2.[116] They have found that insulin essentially exists as a monomeric form but observed insulin aggregation in solution which was not detected by Bouchard and co-workers. The Nettleton et al. results were in agreement with the results of human insulin conducted by Hua and Weiss[103] in similar conditions, using 2D NMR in 20% acetic acid. Similarly, Nault and co-workers have characterised bovine insulin behaviour at hydrophobic surfaces on a silicon prism functionalized by phenyldimethylmethoxy silane (PDMMS) using ATR-FTIR spectroscopy.[117] They have found that insulin possessed conformational changes on interaction with a hydrophobic surface. Yeo et al. analyzed the secondary structures of microparticulate insulin powders (Bovine insulin) using Raman spectroscopy at two different temperatures (i.e. 25° and 35°C) and compared with the secondary structures of commercially available insulin (Total helix = 46 % and total β-sheet = 30 %).[118] They observed a decrease in α-helical (11 %) and a remarkable increase in β-sheet (60 %) components in microparticulate insulin. But, this change was slightly greater at 35°C (α-helical = 10 % and β-sheet = 65 %). However, the proportion of the random coil (commercial powder = 10 %, microparticulate insulin at 25°= 8 % and microparticulate insulin at 35°=7 %) and β-turn (commercial powder = 24 %, microparticulate insulin at 25° = 29 % and microparticulate insulin at 35° = 24 %) remains unaltered in both cases. Although different researchers have studied the secondary structure of proteins, few researchers were focused on the analysis of the secondary structure of proteins at the ITIES following electroadsorption. So, the literature reviews show that the spectroscopic study of the secondary structure of electroadsorbed insulin at the ITIES is still unknown.

1.7. Aims of this research work

The aims of this research work are as follows:

- The design and development of plastic-based single pore ITIES and its characterisation by the transfer of tetrapropylammonium ions ($TPrA^+$) across the interface.
- Analysing the electrochemical behaviour of insulin at the ITIES.

- Investigating the secondary structures of insulin following electroadsorption at the ITIES using FTIR spectroscopy.
- Comparing the sensitivity of electrochemistry, FTIR spectroscopy and Raman spectroscopy for the detection of insulin at the ITIES.

Cyclic voltammetry (CV) was applied in order to justify the newly developed plastic-based ITIES and $TPrA^+$ ions transfer was used to study its electrochemical behaviour; these results were compared with previously published data.

Then, the electrochemistry of insulin at the interface was discussed. This was followed by using FTIR spectroscopy to study the secondary structures of insulin following electroadsorption. Finally, comparing the sensitivity of electrochemistry, FTIR spectroscopy and Raman spectroscopy for the detection of insulin was discussed. These results are explained in chapter 3.

In chapter 4, the overall conclusions and any suggestions for further works are presented.

Chapter 2. Experimental procedures

This chapter first discusses the electrochemical arrangement of the ITIES. Secondly, it discusses the various reagents used in this thesis. Thirdly, it discusses the preparation and arrangement of the macro-ITIES. After that, it discusses the different electrochemical techniques (i.e. Cyclic Voltammetry (CV), Stripping Voltammetry (SV), and Chronoamperometry (CA)) and electrochemical measurements. Finally, this chapter discusses the measurements of spectra and techniques for their analysis of FTIR spectroscopy and Raman spectroscopy.

2.1 Electrochemical arrangement of the ITIES

2.1.1 Electrochemical cell

Different researchers have used different types of electrochemical set up to study analytes at the ITIES. A four-electrode cell was used by the Samec et al. at the ITIES.[16,119] A Four-electrode electrochemical set up is made up of two counter and two reference electrodes, as shown in Figure 8. Each phase is connected with one reference and one counter electrode. The ohmic drop, which is developed by the resistive solution, can be counterbalanced by using such an electrochemical set up. In millimetre or centimetre sized ITIES, the resistance is often high; thus, such resistance can be compensated using this type of cell. The new electrochemical system can be characterised using the voltammetry of the ITIES in a four-electrode system. Since the resistance caused by the organic phase is reduced on lowering the surface area of the ITIES, so, a two-electrode cell set up having miniaturised ITIES can also be used to study various analytes.

Two silver/silver chloride electrodes (Ag/AgCl), both serving as counter and reference electrodes, containing one in each phase were employed in this set up as shown in Figure 9. The ITIES used in this work was created with a single pore in a plastic membrane (Melinex S, polyethylene terephthalate). A polyvinyl chloride (PVC) based organogel in 1,2-dichloroethane (1,2-DCE) was packed in the glass cylinder, and this gel containing a cylinder was inserted into the beaker containing the aqueous medium. The interface is formed when both phases come into contact with each other. All the voltammograms presented in chapter 3, unless otherwise stated, were measured in this two-electrode set up. This set up was used in this research work

because the magnitude of current that flows through the system lies in the nanoampere (nA) scale and hence there is less ohmic drop.

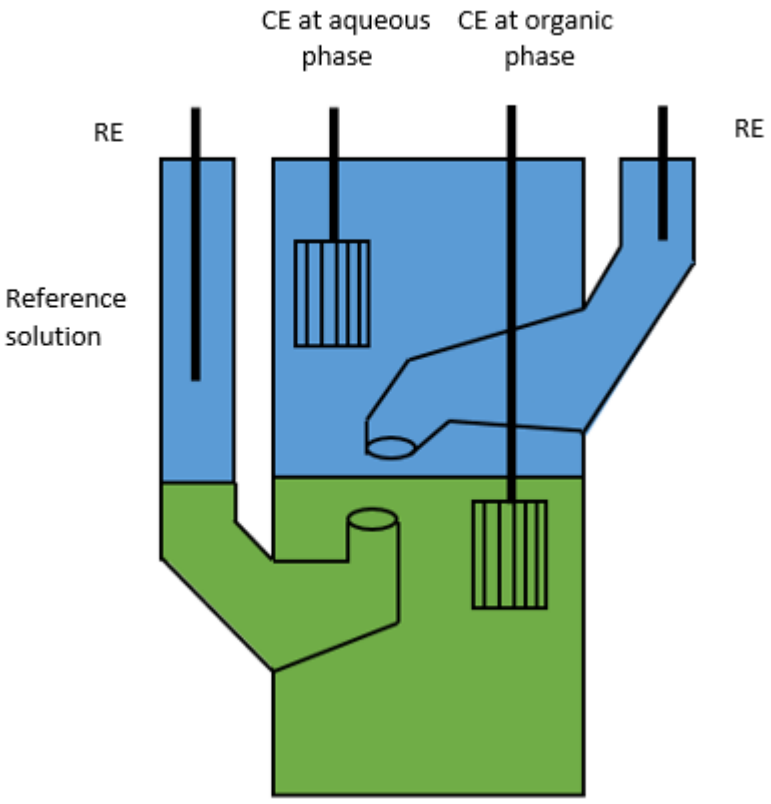

Figure 8: Schematic representation of a four-electrode cell for electrochemistry at the ITIES, where RE and CE, respectively, indicate the reference electrode and counter electrode.

Since reference solution and organic phase are in the cell, a non-polarisable interface is formed between them. The interface between the organogel and aqueous phase, however, is polarisable, and by the application of external voltage through the two Ag/AgCl electrodes, the change in potential difference across the interface can be controlled. An Autolab PGSTAT101 electrochemical workstation (Metrohm, The Netherlands) was used for electrochemical measurements and was operated with the supplied NOVA software. To prevent the impact of external charges, the whole electrochemical cell was enclosed in a Faraday cage. Solutions were not stirred and all experiments were at laboratory temperature (25˚C).

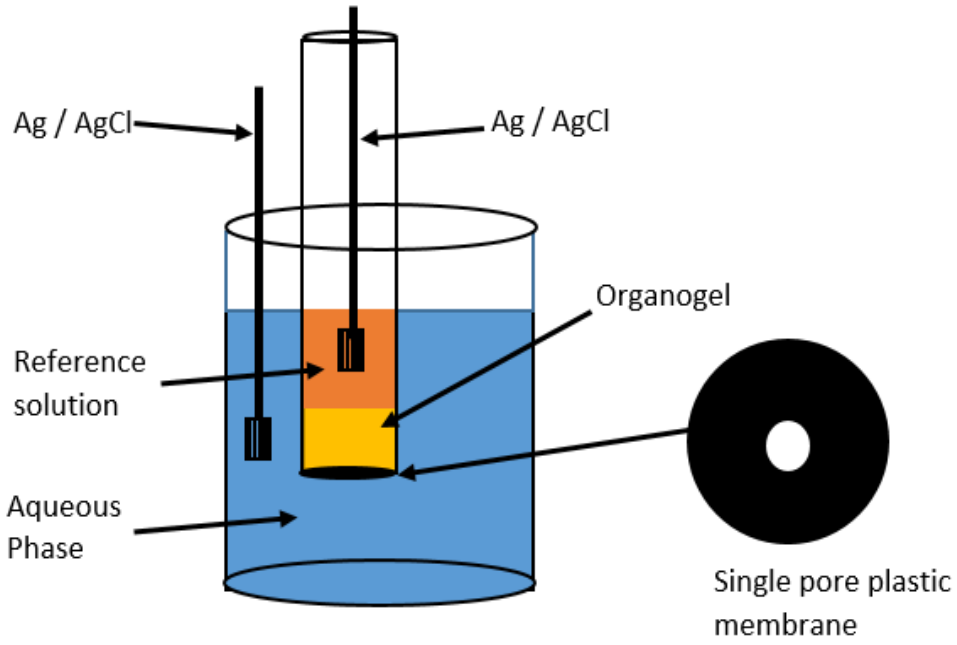

Figure 9: Figure demonstrating the two electrode macro ITIES with single pore plastic membrane.

2.1.2 Electrodes and electrolytes.

Different materials like gold, platinum, silver, and carbon that are conductive can be used as electrodes in different areas. In this research, silver/silver chloride (Ag/AgCl) was employed as the reference electrode (RE). Equation (30) shows the standard half-cell reaction of the Ag/AgCl electrode.

$$\boldsymbol{AgCl(s) + e^{-} \rightarrow Ag(s) + Cl^{-}(aq)} \qquad (30)$$

When this electrode is dipped into the aqueous phase containing chloride ions, then a non-polarisable interface is formed around it. Then, two non-polarisable interfaces are formed by the Ag/AgCl electrode, one at the aqueous phase (e.g. HCl as electrolyte provides Cl^{-}) and another at the reference electrolytic solution (BTPPACl as an electrolyte provides Cl^{-}). The potential of this electrode can be calculated by the Nernst equation provided below in equation (31). It shows that the potential varies according to the variation of activity of chloride ions (Cl^{-}). According to the International Union of Pure and Applied Chemistry (IUPAC), the standard potential of the Ag/AgCl/KCl (1 mM) electrode is +0.222 V when it coupled with the

standard hydrogen electrode (SHE).[120] NaCl or KCl (from 1.0 mM to saturated concentrations) can be used as a source of chloride.[2]

$$E_{Ag/AgCl} = E^{0}{}_{Ag/AgCl} - \frac{RT}{F} lna_{Cl^-} \quad (31)$$

When the organogel (having hydrophobic electrolyte) is brought into contact with an aqueous hydrochloric acid (hydrophilic electrolyte) phase, a polarisable ITIES is formed as discussed in chapter 1. The charge transfer process of interest occurs at this interface; thus, this interface behaves as a working electrode. By changing the potential across the interface, the transfer behaviour of ions across the ITIES can be studied.

Nevertheless, a non-polarisable interface is formed between the reference electrolytic solution and the organogel which is due to the presence of a common ion (i.e. $BTPPA^+$) in both phases.[55] In the non-polarisable interface, there is no change in potential taking place, although, the current is passed through the electrochemical cell.

2.2 Reagents

All reagents including insulin (insulin from bovine pancreas, product codes: 1002743779, 1002726793, 1002878501) were purchased from Sigma-Aldrich Australia. These reagents were used in the experiment without any further purification. The organic electrolyte salt bis(triphenylphosphoranylidene)ammonium tetrakis(4-chlorophenyl)borate (BTPPATPBCl) was prepared by metathesis of equimolar amounts of bis(triphenylphosphoranylidene)ammonium chloride (BTPPACl) and potassium tetrakis(4-chlorophenyl)borate (KTPBCl). This salt was prepared by using a solvent which is prepared by mixing water and methanol in the ratio of 1:2.

For the preparation of this salt, first, 0.5740 g BTPPACl and 0.4926 g of KTPBCl were dissolved in 5 mL solvent separately to form the clear solutions. Then, the clear solution of BTPPACl was added dropwise with stirring into the clear solution of KTPBCl until complete precipitation. Here, a white precipitate of BTPPATPBCl having some impurities was produced. To remove the impurities, like KCl, this precipitate was washed with the above-mentioned solvent several times, vacuum-filtered using a

Buchner funnel and dried in a desiccator overnight. Then, the dried salt was dissolved in minimum acetone. By adding methanol dropwise, the crystal product of BTPPATPBCl was obtained and this salt was again isolated using a Buchner funnel. In this way, obtained BTPPATPBCl was then subjected to overnight drying in a desiccator and stored in the fridge for further use. The other electrolyte solutions needed in this research were 1 mM BTPPACl (in 10 mM aqueous LiCl), 10 mM aqueous HCl, and 2.5 mM insulin (in 10 mM aqueous HCl).

2.3 Macro ITIES

The interface between the two immiscible electrolytic solutions (ITIES) used in this research was created with a single pore in the plastic membrane (Melinex S, polyethylene terephthalate) having a diameter of 1.56 mm. This diameter was measured by using a USB Digital Microscope with 300× magnification and 5 M pixels image sensor. The pore was made in the middle of the plastic membrane using a hand punch that was purchased from a local fabric supply shop. The plastic membrane thickness was also measured using a Dino-Lite Edge / 5MP AM7515 series microscope and was found to be 0.13 mm. The total geometric area of this single pore was 0.019 cm^2 and hence the interface also had this geometric area. The single pore plastic membrane was sealed using 100 % silicone sealant onto the mouth of a glass cylinder as shown in Figure 10.

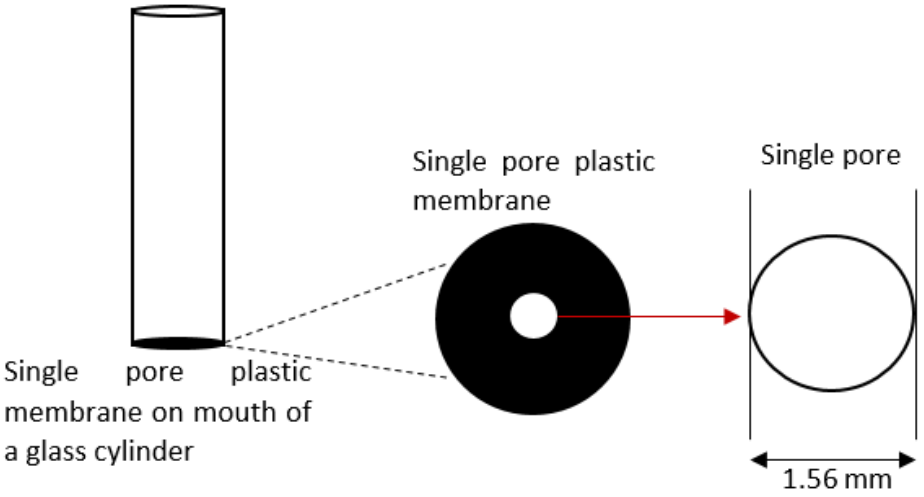

Figure 10: A schematic representation of a single pore plastic membrane having diameter 1.56 mm attached to the end of cylinder pipette.

Organogel was prepared by using BTPPATPBCl and low molecular weight polyvinyl chloride (PVC). 1,2-Dichloroethane (1,2-DCE) was used as an organic solvent. During the preparation of organogel, the concentration of BTPPATPBCl and PVC were maintained at 10 mM and 10 % (w/v), respectively. To prepare the organogel, first, the calculated weight of BTPPATPBCl was taken in a vial and dissolved in a calculated volume of 1,2-DCE. Then, the required weight of low molecular weight PVC was added into that vial. After that, by using a magnetic stirrer/hot plate, this mixture was heated up to 60˚C to form the organogel. Then, 100 µL of that organogel was introduced into the glass cylinder containing the single pore plastic membrane using a pipette. Then 1 hour after preparation, this set up was inserted into the beaker containing 10 mM HCl as shown in Figure 9. Then, the organic reference solution (composition: 1 mM BTPPACl in 10 mM LiCl) was added in the glass cylinder containing the organogel such that the height of the reference solution and the solution in the beaker should be equal. By using this ITIES, the electrochemical measurements were performed. The electrochemical set up used in this case was summarised by **scheme 2** as shown below.

Ag | AgCl	1mM BTPPACl in 10 mM LiCl	10 mM BTPPATPBCl gel with 1,2-DCE (10 % w/v PVC)	x μM analyte in 10 mM HCl	AgCl	Ag

Scheme 2: Schematic representation of the electrochemical cell used. x indicated the concentrations of various analytes used in this study.

2.4 Electrochemical techniques

2.4.1 Cyclic voltammetry

One of the most widely used electrochemical techniques is cyclic voltammetry and this technique is extensively applied to study the kinetics, diffusion, adsorption, reversibility, and number of charges (or electrons) transferred in reactions of various analytes of interest.[5,121] In this technique, an initial potential, E_1, was applied to a particular system and scanned to maximum potential, E_2, and then switched back to the initial potential, E_1, at the same scan rate, ν, as shown in Figure 11. E_1 is usually chosen so that no reaction occurs at that applied potential. The two extreme potentials (i.e. E_1 and E_2) at the ITIES will be selected depending upon the ion transfer behaviour of ions of interest. The region between these two potentials is known as potential window, the region where the analytes of interest will be transferred across the interface. The selection of the potential window should be done properly otherwise the current signal of analytes to be studied could be masked by the background electrolytes transfer.

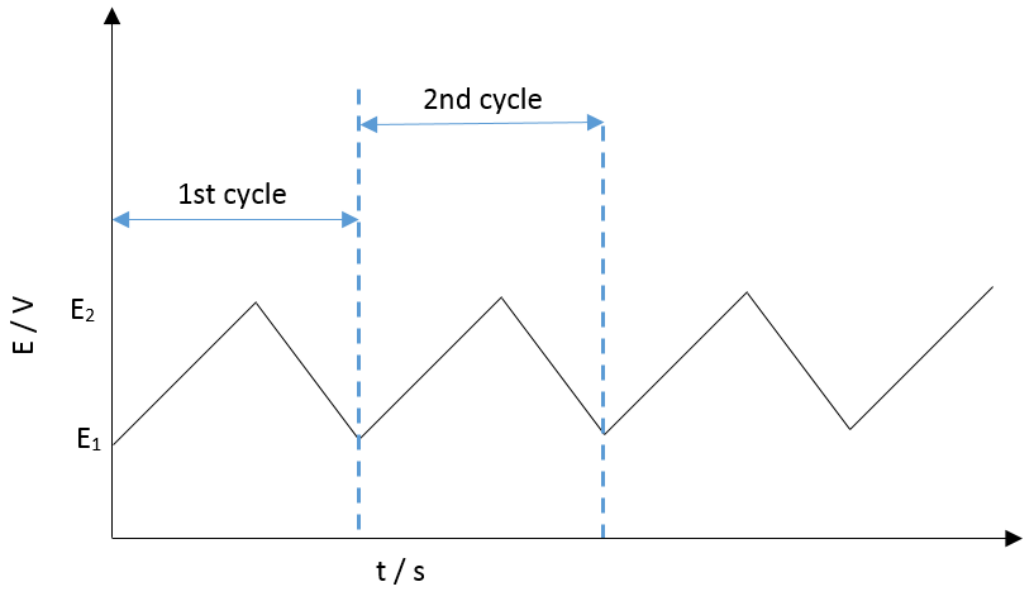

Figure 11: The waveform of cyclic voltammetry describing the relationship between applied potential and time.

The nature of CV varies according to the types of the ITIES used. The CVs obtained after the use of micro and millimetre interfaces are shown in Figure 12 (A) and 12(B), respectively. Figure 12 (A) is obtained due to the unsymmetrical diffusion (radial diffusion on the forward scan and linear diffusion on the reverse scan); however, Figure 12 (B) results due to the linear diffusion of the charged particles in both scan directions.

For a reversible process, the peak current arises due to the linear diffusion of charged particles and can be calculated by using the Randles-Sevcik equation as shown in equation (32).

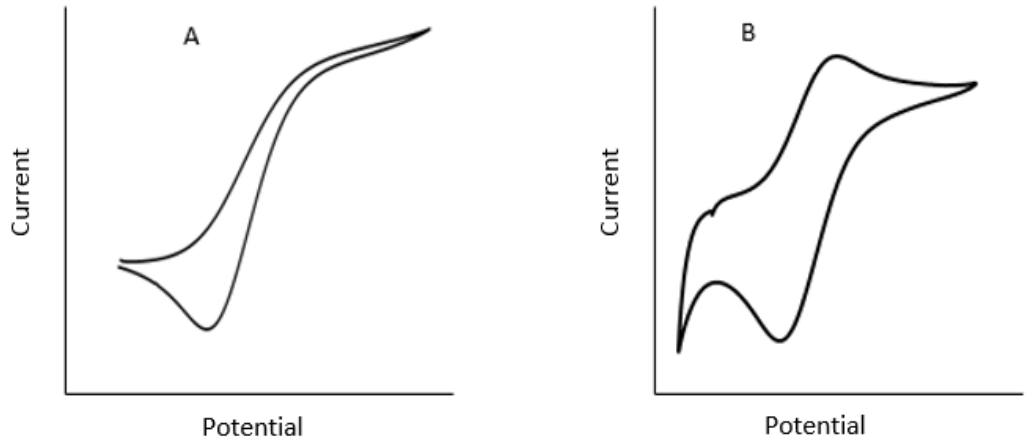

Figure 12: Figures representing cyclic voltammograms due to transfer of cation in (A) micro ITIES (forward transfer controlled by radial diffusion but the backward transfer is controlled by linear diffusion) and (B) milli ITIES (both forward and backward transfer are linear diffusion-controlled).

$$\boldsymbol{I_p = \left(2.69.10^5\right) z_i^{3/2} A D_i^{1/2} C_i \nu^{1/2}} \quad (32)$$

where I_p , z_i, D_i and C_i are the peak current, the charge, the diffusion coefficient, and the concentration of species (i), respectively. Similarly, A represents the area of the interface. This equation reveals that the peak current is directly proportional to the square root of the scan rate ($\nu^{1/2}$). This equation is derived on the assumptions that the interface is flat, background electrolytes are present in excess amount, and the diffusion process is one dimensional .[2]

This equation (32) can be used to calculate the diffusion coefficient of the species that transfers through the ITIES. For singly charged species that follow the reversible process, the ratio between the forward and backward peak current ($I_{p,w\to o}/\ I_{p,o\to w}$) should be ~1 and the peak-peak separation ($E_{p,w\to o}/\ E_{p,o\to w}$) should be ~ 59 mV / z_i at 25°C.[21] Nevertheless, the equation (32) can be re-written as shown in equation (33) (for quasi-reversible processes).

$$\boldsymbol{I_p = \left(2.99 \times 10^5\right) z (\alpha z_i)^{1/2} A D_i^{1/2} C_i \nu^{1/2}} \quad (33)$$

where α and z indicate transfer coefficient and charge for the charge transfer step, respectively. Other terms used in this equation are already defined.

Likewise, if adsorption occurs at the interface, the peak current for the adsorption process can be determined by using equation (34) as shown below. It indicates that the peak current is proportional to the scan rate (ν) of that experiment.

$$\boldsymbol{I_p = \frac{z_i^2 F^2 \Gamma A v}{4RT}} \quad (34)$$

where the terms $z_i, F, \Gamma, R,$ and T, respectively, represent the charge of the transferred ions, Faraday's constant, surface coverage of the interface, the universal gas constant, and temperature of the system.

Similarly, equation (35) can be used to see the behaviour of the adsorption process. It shows that for the adsorption process, the charge accumulated (Q) is proportional to the surface coverage (Γ) at the interface.[2]

$$\boldsymbol{Q = z_i F A \Gamma} \quad (35)$$

However, for the radial diffusion, which is observed in micro ITIES array, the steady state current can be calculated by using equation (36). This equation is applicable only when the interface is inlaid as discussed in chapter 1.

$$\boldsymbol{I_{lim} = n4z_i FDCr} \quad (36)$$

where I_{lim}, n, z_i, F, D, C, and r indicate the limiting current, number of micro interfaces, charges of ionic species, Faraday's constant, diffusion coefficient, bulk concentration, and radius of the interface, respectively.

2.4.2 Stripping voltammetry

Stripping Voltammetry (SV) is an important electrochemical technique that is often used to enhance the detection limit of analytes.[122,123] It involves two steps, (1) pre-concentration and (2) detection step, as shown in Figure 13. In the first step, a fixed potential is applied up to a certain period of time for the adsorption or extraction of species to be analysed and in the second step, for the detection of the analyte, the potential is scanned either in a positive or in a negative direction such that the accumulated analyte returns back to their original phase.

Adsorptive stripping voltammetry (AdSV) is one type of SV in which the species of interest was adsorbed on the interface in the pre-concentration step at a certain time at a fixed potential and then followed by scanning of the potential that acts as the

detection step. Based on the CV of the analyte, suitable adsorption potential can be selected.

In this thesis, the suitable adsorption potential in the pre-concentration step was selected to be 0.70 V. Then, this adsorption potential was applied to the interface by choosing different pre-concentration times followed by voltammetric scan to the lower potential of 0.30 V.

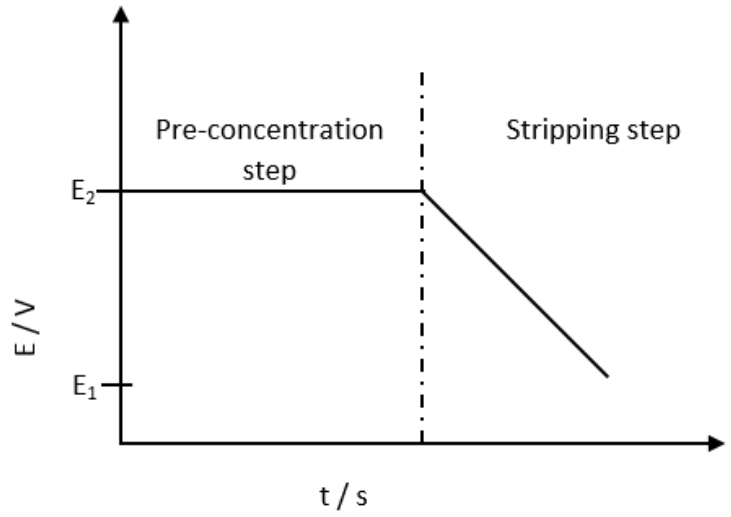

Figure 13: A waveform illustrating the different steps involved in the stripping voltammetry.

2.4.3 Chronoamperometry

Chronoamperometry (CA) is an electrochemical technique that can be used for the determination of the mechanism and kinetics of various electrochemical processes. By stepping the potential of the interface, the variation of current with time can be monitored. A typical waveform of potential step chronoamperometry is shown in Figure 14. Here, the potential of the interface is stepped from E_1 (Initial potential) to E_2 (final potential). There is no flow of current at E_1; however, charge transfer takes place at E_2. Figure 15 is a chronoamperogram which describes the variation of current with time.[2,11]

For linear diffusion that occurs at a macroelectrode, the Cottrell equation (equation (37)) well describes the relationship between current and time.[121]

$$|\boldsymbol{I}| = \frac{\boldsymbol{z_i FAD^{1/2} C}}{\boldsymbol{\pi^{1/2} t^{1/2}}} \quad (37)$$

where $|I|$, z_i, F, A, t, D, and C are the diffusion-limited current (A), charges of ions, the Faraday constant, the surface coverage of the interface (cm^2), time (s), the diffusion coefficient of ionic species (cm^2 / s), and bulk concentration (mol / cm^3), respectively.

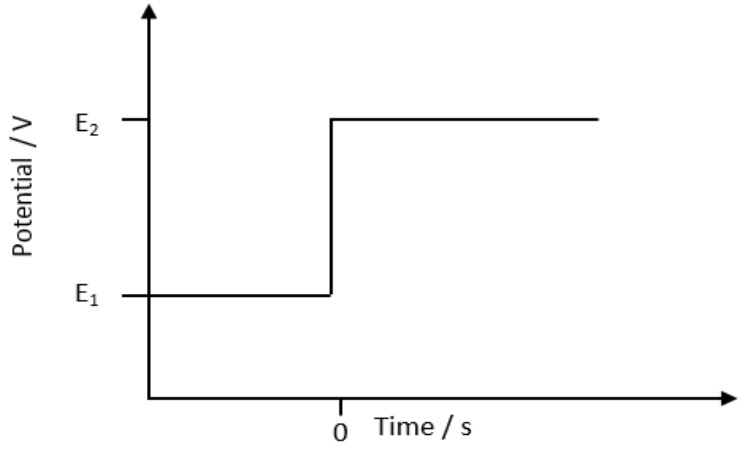

Figure 14: Potential-time waveform showing steps in chronoamperometry.

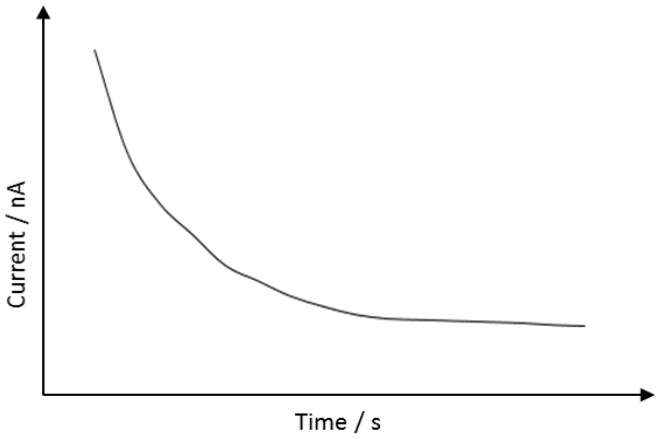

Figure 15: Figure illustrating a chronoamperogram.

2.5 Electrochemical measurements

Voltammetric measurements were performed using a 10 mV / s scan rate for all the experiments unless otherwise stated. In these measurements Ag/AgCl electrodes were applied as counter and reference electrodes, containing one in each phase as shown in Figure 9. A blank cyclic voltammogram was measured on each fresh cell to confirm that there was no drift in the potential scale. CVs of tetrapropylammonium ion ($TPrA^+$) were measured at the ITIES located at the single pore plastic membrane at different concentrations and different scan rates. Likewise, CVs of insulin were measured at the scan rate of 10 mV / s by maintaining different insulin concentrations in the aqueous phase, and the results were compared with previously reported data. Similarly, different scan rate study was performed using a fixed concentration of insulin in the aqueous phase. Then, the impact of the scan rate on the transfer behaviour of insulin was analysed and compared with the previously reported data. Similarly, AdSV was employed to identify the detection limit of insulin.

Similarly, CA was applied for the adsorption of insulin at the interface. Different potentials like 0.35, 0.50, 0.60, 0.65, 0.70, and 0.75 V were applied to the interface for adsorption at different times. The different adsorption time was discussed in the corresponding chapters. The CA results were also discussed in chapter 3. Also, surface coverage of insulin at the ITIES was studied using CAs. Here, the charges accumulate at the interface during adsorption at a fixed adsorption time was correlated with surface coverage using equation (35).

For surface coverage study of insulin, a fixed potential (i.e. 0.70 V) was applied to the interface for 30 min. The surface excess concentrations of adsorbed insulin at four different concentrations (i.e. 5, 20, 50, and 100 µM) were calculated in terms of monolayers using surface coverage. Likewise, by keeping the fixed concentrations of aqueous insulin (20 µM), the surface coverage of insulin at the ITIES at different times was also monitored. The spectra of electroadsorbed insulin were measured with FTIR spectroscopy.

2.6 FTIR spectroscopy

FTIR spectroscopy is a widely used technique to analyse various materials. Since almost all compounds possess a characteristics IR spectra, this technique can be widely used for the qualitative as well as quantitative analysis of various compounds. In this study, ATR-FTIR measurements were done on a Thermofisher Scientific Nicolet iS50 FTIR spectrometer (Massachusetts, USA) using a diamond ATR crystal. Spectra were collected with 64 co-added scans and 4 cm^{-1} spectral resolution in 96 s. The wavenumber range of the spectral window collected was 4000-400 cm^{-1}. A background spectrum of the blank diamond ATR crystal was collected under the same conditions every time before measuring the FTIR spectra of adsorbed insulin.

FTIR spectra of solid-state insulin were recorded by placing the insulin on the diamond ATR crystal. Also, the FTIR spectra of aqueous insulin, referred to in the Results and Discussions as films of hydrated insulin, were recorded. In this measurement, 2.5 µL of 2.5 mM aqueous insulin (dissolved in 10 mM HCl) was directly added onto the diamond ATR crystal and was subjected to complete evaporation followed by spectra measurement. Similarly, organogels (10 mM BTPPATPBCl-1,2-DCE (10 % w/v PVC) were properly covered and stored overnight in the laboratory. Then FTIR spectra of the organogel were also measured by adding this gel onto the diamond ATR crystal as shown in Figure 16. The organogels containing insulin (after electroadsorption) were properly covered and stored overnight in the laboratory. Then, spectra of electroadsorbed insulin were measured by placing the organogel containing insulin at the ATR crystal. All data were discussed in chapter 3.

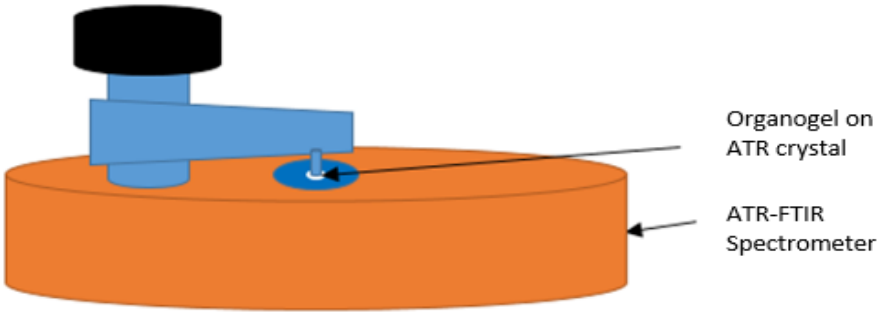

Figure 16: Schematic representation of ATR-FTIR spectrometer showing organogel on the ATR crystal.

After measuring the FTIR spectra of organogel, electroadsorbed insulin, hydrated film of aqueous insulin and solid-state insulin using FTIR spectroscopy, the amide I region (1600 - 1700 cm^{-1})[111] of the different spectra were analysed using second derivative and curve fitting techniques. In order to determine the second derivatives of the amide I region, 21 smoothing points were taken, using a Savitzky-Golay function. The software OPUS 7.0 was used for spectra analysis. Likewise, the Local least square method was applied for 30 s iteration time in the curve fitting technique.[124] On the basis of infrared spectra of insulin with known crystallographic data, the different deconvoluted peak frequencies of the different types of secondary structures of insulin were assigned in the curve fitting technique. In this thesis, based on the literature, the insulin deconvoluted peak positions that were assigned in curve fitting technique were 1693, 1690, 1680, 1660, 1656, 1649, 1637, and 1620 cm^{-1}.[100,110,111] In this study, 1637, 1649, 1656, and 1660 cm^{-1} were assigned as combined β-sheet and irregular helix, unordered, α-helix, and 3_{10}-helix, respectively.[100,110,111] Likewise, wavenumber 1680 and 1690 cm^{-1} were assigned as turn.[110] Similarly, 1693 and 1620 cm^{-1} were assigned as an extended chain.[110] Table 2 shows the vibrational frequencies of insulin spectra used in peak assignment. All the results of FTIR spectra of organogel, electroadsorbed insulin, hydrated film of aqueous insulin, and solid-state insulin were discussed in the Results and Discussion chapter.

Table 2. The vibrational frequencies of insulin spectra used in peak assignment of the different secondary structures of insulin.[100,110,111,125]

Secondary structures	Peak position (cm^{-1})
α-helix	1656
3_{10}-helix	1660
Combined β-sheet and irregular helix	1637
Unordered	1649
Turn	1680 1690
Extended chain	1693 1620

2.7 Raman spectroscopy

Raman spectroscopy is a branch of spectroscopy that deals with the study about the inelastic scattering of monochromatic light. In this analysis, the frequency of scattered light is shifted by the frequency of a vibrational mode, relative to the incident excitation light source. Raman spectroscopy provides the structural

fingerprint of molecules to be analysed.[126] The most important reason to choose Raman spectroscopy is that it offers better spatial resolution (shorter wavelength of light) and also that it may be more suited to real-time analysis as it is less affected by H_2O. In this thesis, Raman spectroscopy measurements were performed with an Alpha300SAR+ confocal Raman microscope (WiTec GmbH, Ulm, Germany) utilising a 20x/0.4NA objective (Zeiss, Jena, Germany) and a frequency doubled Nd:YAG laser (λ = 532 nm). The 600 lines/mm grating in the spectrometer provides a spectral resolution of 1 rel. cm^{-1}. A minimum of 100 accumulations at an integration time of 100 ms was recorded for single spectrum data. The instrument is controlled with the manufacturer's Control Four software. Data were post-processed using the WITec Project Four+4.1 software (WITec GmbH, Ulm, Germany). Before recording the Raman spectra of the corresponding sample, a background spectrum of Silicon was collected all the time and used for spectral calibration. By using this confocal Raman spectrometer, the Raman spectra of organogel and electroadsorbed insulin were collected and these spectra were discussed in the chapter 3.

Chapter 3. Results and discussions

3.1 Electrochemical behaviour of tetrapropylammonium ions at the ITIES

3.1.1 Cyclic voltammetry of tetrapropylammonium ions at different concentrations

The electrochemical behaviour of tetrapropylammonium ions ($TPrA^+$) was investigated by different researchers at liquid-liquid interfaces.[37,127–132] These reports show that the $TPrA^+$ ion transfer is linearly dependent on the concentrations and the square root of the scan rate. In addition, the peak-peak separation and the ratio of forward peak current and backward peak current of $TPrA^+$ ion transfer were found to be $\sim$ 59 mV and $\sim$ 1, respectively.[127,129] These behaviours are consistent with reversible, linear diffusion-controlled behaviour.

In this research also the electrochemical behaviour of $TPrA^+$ ions was as a way to validate new electrochemical set up. In this research, a two-electrode system at the water/1,2 -DCE organogel interface was used. Cyclic voltammetry was performed to investigate the transfer behavior of $TPrA^+$ ions at the ITIES located at a single pore in a plastic membrane. Figure 17 represents the cyclic voltammograms (CVs) in the absence (dashed line) and the presence of 120 µM $TPrA^+$ (solid line) along with background electrolyte. Figure 17 shows that the background electrolyte's ions do not show any transfer behaviour at the potential between 0.10 V to 0.50 V. However, the current appeared in the range of 0.10 V to 0.50 V is due to the charging current. The range of potential related to the charging current is known as the potential window. So, those analytes that can be transferred within this potential window could be analysed in the presence of the background electrolytes. On adding 120 µM $TPrA^+$ to aqueous electrolytic phase, two distinct peaks appeared, one for the forward and one for the backward voltammetric scans. The forward response appeared due to the transfer of $TPrA^+$ ions from the aqueous phase to the organic phase. However, on the back transferring of $TPrA^+$ from the organic phase, the backward response was observed. Thus, $TPrA^+$ ions can be analysed using this set up. Nonetheless, in Figure 17, the forward and backward currents at the potential < 0.1 V in the presence and absence of $TPrA^+$ ions were due to the transfer of background electrolytes ions. The forward current at potential < 0.1 V was due to the simultaneous transfer of $BTPPA^+$

ion from the organic phase to the aqueous phase and Cl^- from the aqueous phase to the organic phase. Whilst, the backward current at the potential < 0.1 V was due to the back transfer of $BTPPA^+$ from the aqueous phase to the organic phase and Cl^- from the organic phase to the aqueous phase.

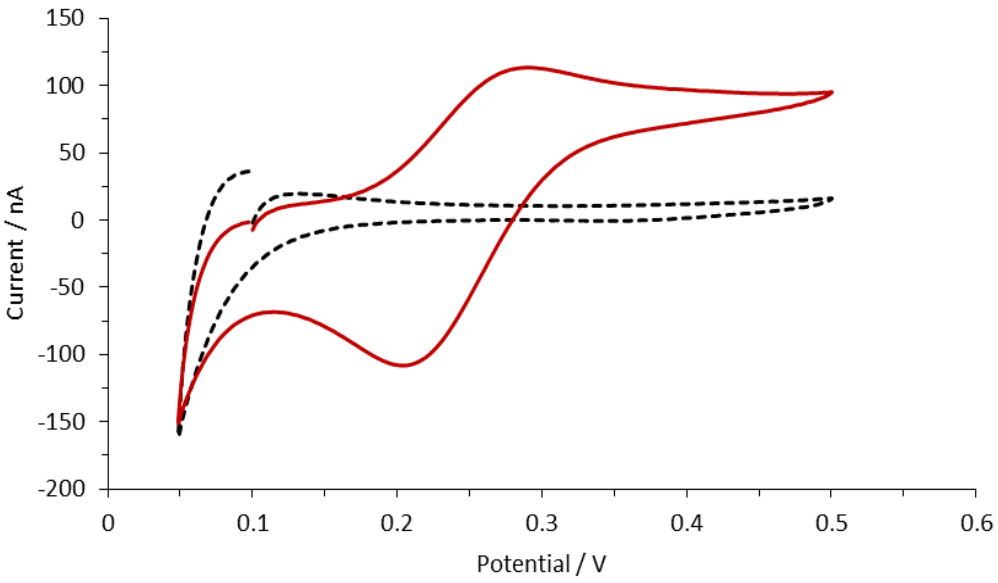

Figure 17: The CVs in the presence and absence of $TPrA^+$. Scan rate is 10 mV / s and the concentration of $TPrA^+$ is 120 µM. The blank experiment is shown as the dashed line while the $TPrA^+$ transfer is shown as the solid line.

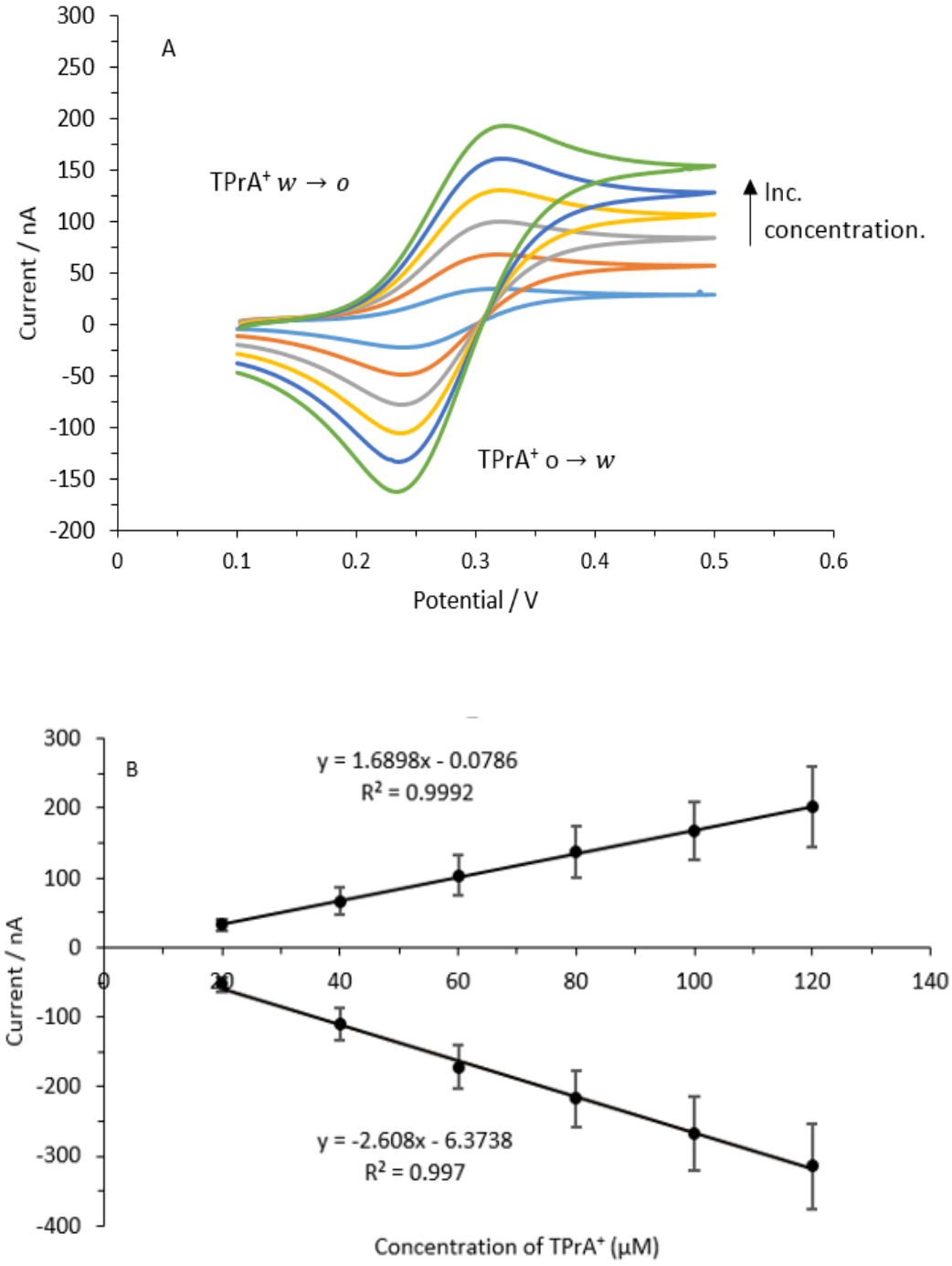

Figure 18: (A) CVs showing transfer of $TPrA^+$ at different concentrations (i.e. 20, 40, 60, 80, 100, and 120 µM) (20 to 120 µM, increasing as directed by the arrow direction). (B) A plot of peak current against $TPrA^+$ Concentrations. 10 mM aqueous HCl as the aqueous phase. 10 mM BTPPATPBCl-1,2-DCE (10 % w/v PVC) organogel as organic phase. 10 mV s^{-1} scan rate. Errors are calculated from standard deviations of three trials.

The electrochemical behaviour of $TPrA^+$ ion transfer at different concentrations at the ITIES was discussed in this portion. Figure 18(A) shows the cyclic voltammograms (CVs) of the $TPrA^+$ ions at different concentrations at 10 mV scan rate and it shows that the peak response of $TPrA^+$ ions increases with increase in concentration. Figure 18(B) shows the variation of the peak current of $TPrA^+$ ions with the increase in the concentration of $TPrA^+$ ions in the aqueous phase. Figure 18(B) shows that the current (forward and backward) due to the transfer of the $TPrA^+$ ions is directly proportional to the concentration of $TPrA^+$ ions in the aqueous phase.

Literature reviews show that for singly charged species, in any reversible cyclic voltammetry, the peak-peak separation and the ratio of forward peak current to the backward peak current are $\sim$ 59 mV and $\sim$ 1, respectively.[133,134] In addition, the peak potential is independent of the scan rate and the peak current is directly proportional to the square root of the scan rate.[133,134] The peak-peak separation for the transfer of $TPrA^+$ at the ITIES is *ca.* 59 V and the ratio of forward peak current (I_{fp}) to the backward peak current (I_{bp}) is *ca.* 1 which are consistent with the data already recorded for the singly charged species.[133,134] Likewise, the peak potential of $TPrA^+$ ions transfer is independent of concentrations of $TPrA^+$ ions which is as recorded elsewhere in the literature.[130] The $TPrA^+$ ions transfer was investigated by Samec and co-workers using a four-electrode system at the nitrobenzene/water interface. They reported the linear relationship between the concentrations of $TPrA^+$ with the peak current obtained due to the transfer of $TPrA^+$ ions. The result of $TPrA^+$ transfer across the ITIES obtained in this research at different concentrations is also consistent with the Samec results.[127,130]

3.1.2 Cyclic voltammetry of tetrapropylammonium ions at different scan rates

Cyclic voltammetry at different scan rates was performed to investigate the transfer behavior of tetrapropylammonium ions ($TPrA^+$) at the ITIES located at a single pore in a plastic membrane having a diameter of 1.56 mm. Figure 19 (A) represents CVs of 100 µM $TPrA^+$ ions at different scan rates (ranges from 10 mV to 70 mV). The forward and backward peak responses in the CVs appeared due to the transfer of $TPrA^+$ ions. The forward peak response is due to the transfer of $TPrA^+$ from the aqueous to the organic phase, whilst the backward peak response is because of

back transfer of $TPrA^+$ ions from organic to the aqueous phase. Samec et al. reported similar results to explain the $TPrA^+$ transfer with a four-electrode system using a nitrobenzene/water interface.[127] Figure 19(A) clearly shows that the amount of current response flowing through the interface rises with increase in scan rate. In addition, Figure 19(B) also shows that the current (both forward and backward) due to the transfer of $TPrA^+$ ions is directly proportional to the square root of the scan rate. Since the $TPrA^+$ ion transfer shows a direct relationship between the peak current and the square root of the scan rate, it means that the transfer behaviour of $TPrA^+$ ion is diffusion-controlled. [14,127,130] It means that the $TPrA^+$ ions at the ITIES strictly follow the Randles-Sevcik equation[133] which is as shown in equation (32). The diffusion coefficient (D_{TPrA+}) of $TPrA^+$ ion in the aqueous phase was calculated using this equation which was found to be 5.5×10^{-6} cm^2 s^{-1}. This data is in good agreement with the data reported elsewhere (literature value of $D_{TPrA+} = 8.5 \times 10^{-6}$ cm^2 s^{-1}).[14,134]

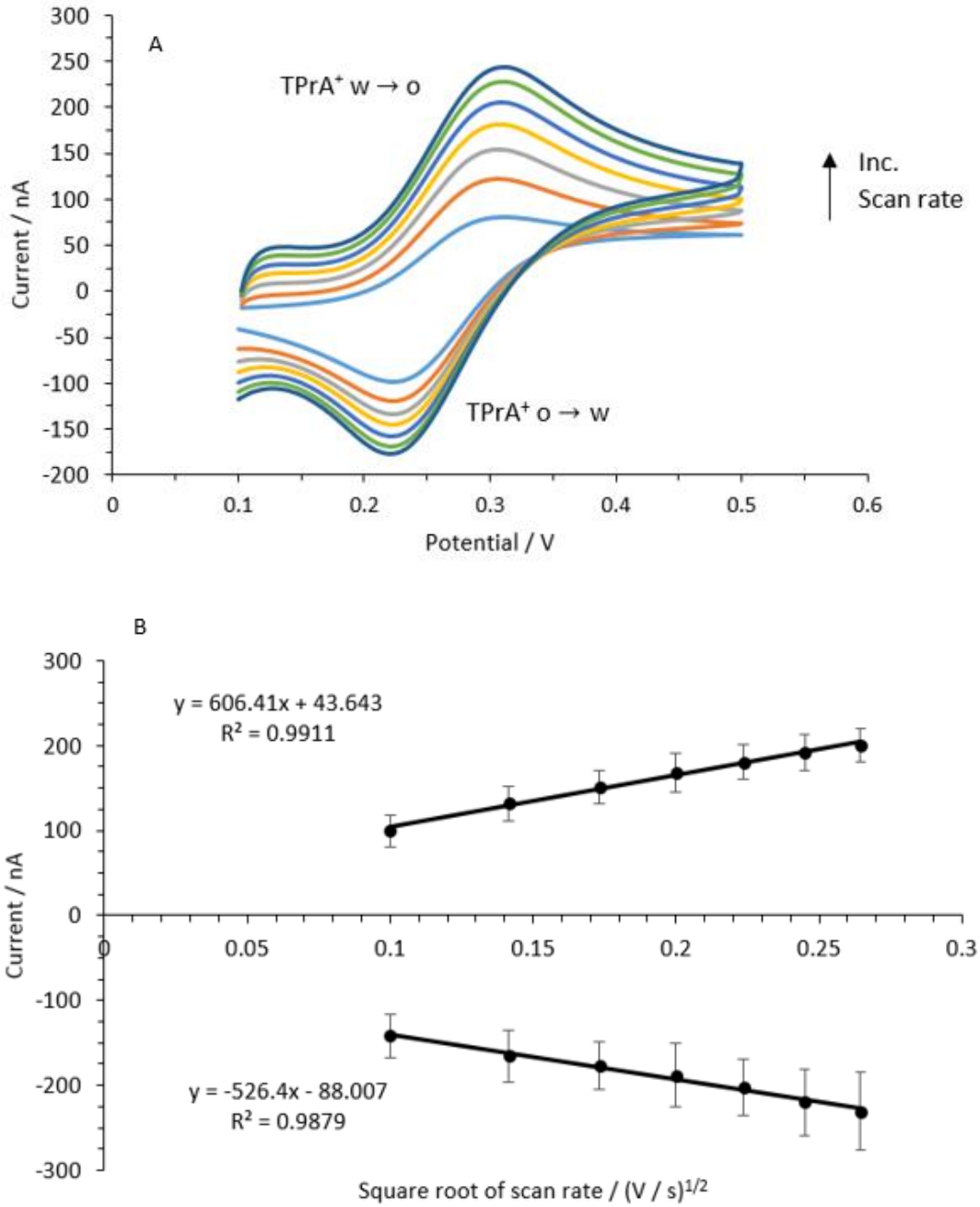

Figure 19: (A) CVs showing transfer of $TPrA^+$ ions at different scan rates (i.e. 10, 20, 30, 40, 50, 60, and 70 mV/s) (10 to 70 mV/s, increasing as directed by the arrow direction). (B) A plot of peak current against the square root of the scan rate. 10 mM HCl is used as the aqueous phase. 10 mM BTPPATPBCl-1,2-DCE (10 % w/v PVC) as the organic phase. Error bars are the standard deviations of three trials.

As already defined that for singly charged species the ratio of forward peak current to the backward peak current (I_f/I_b) and peak-peak separation were found to be ~ 1 and ~ 59 mV, respectively.[133] This research showed that the (I_f/I_b) and peak-peak separation of $TPrA^+$ transfer were *ca.* 1 and *ca.* 59 mV, respectively. Similarly, the diffusion coefficient value of $TPrA^+$ that was calculated in new electrochemical cell was in good agreement with the literature value (Literature value of $D_{TPrA+} = 8.5 \times 10^{-6}$ cm^2 s^{-1}).[14,134] These electrochemical parameters validated the new electrochemical cell. Thus, this electrochemical cell was further used to study the electrochemical behaviour of insulin.

3.2 Electrochemical behaviour of insulin at the ITIES

3.2.1 Cyclic voltammetry of insulin at different concentrations of insulin.

The electrochemical behaviour of insulin at liquid-liquid interfaces has previously been investigated by several other researchers.[32,88,89] O'Sullivan et al. using the adsorptive stripping voltammetry (AdSV) technique at an array of microscale ITIES studied the electrochemical behaviour of insulin. They were able to investigate the lowest limit of detection of insulin concentration (i.e. 10 nM) of insulin at the microscale ITIES applying the potential-controlled adsorption followed by voltammetric desorption.[89] Likewise, Kivlehan et al. conducted the electrochemical behaviour of insulin at the ITIES using a four-electrode system. They also studied the effect of pH on the electrochemical behaviour of insulin at the ITIES. They concluded that the pH of the solution and organic electrolyte ions have a great impact on the electrochemical behaviour of insulin. According to them, acidic pH below the isoelectronic point (pI) is the favourable detection condition for insulin at the ITIES. In addition, the anion of the organic electrolytes having less hydrophobicity is the favourable condition for the response of insulin at the ITIES.[32] Thomsen et al. also studied the transfer behaviour of insulin at the ITIES using a four-electrode system.[88] They have chosen 1,2-DCE as the organic phase and 10 mM phosphate buffer as the aqueous phase. They reported the adsorptive nature of insulin at the ITIES by observing the variation of interfacial capacitance.

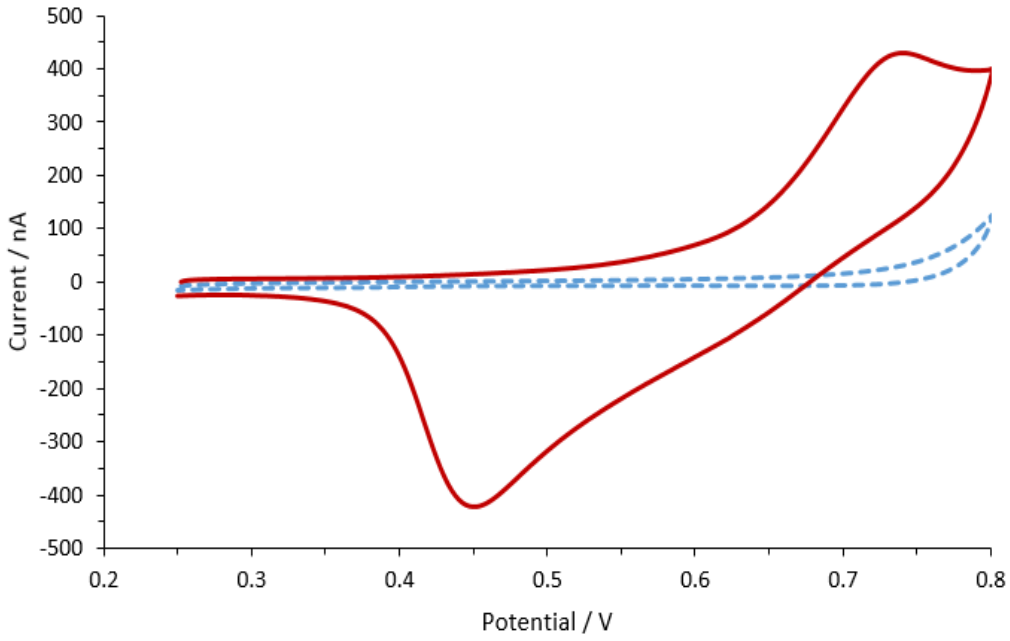

Figure 20: CVs in the presence and absence of insulin at 10 mM HCl as an aqueous phase. 10 mM BTPPATPBCl-1,2-DCE (10 % w/v PVC) as the organic phase. Dashed line indicates the blank, while solid line indicates the 60 µM insulin. Scan rate: 10 mV s^{-1}.

In this thesis, a new electrochemical cell (scheme 2 is shown on page 52) was further characterised by observing the electrochemical behaviour of insulin at the ITIES. All experiments were conducted in the acidic medium using 10 mM aqueous HCl because at this condition insulin is highly susceptible to protonation and gets adsorbed on the interface.[32] In other words, below the isoelectronic point (~ 5.5),[135,136] insulin exists in a cationic charged form and at a suitable potential, it adsorbs on the interface.

Figure 20 represents CVs in the presence and absence (blank) of insulin in the aqueous phase. The dashed line and solid line represent the CVs in the absence and presence of insulin in the aqueous phase, respectively. The CV in the absence of insulin at the aqueous phase is a control experiment. Here, the current is due to the charging of the double layers at the ITIES. The response, in this case, is due to the lack of transfer of background electrolytes at the potential range between 0.25 to 0.75V as shown in Figure 20. The range of potential at which only the current is responsible for charging the double layer where the background electrolytes do not transfer is known as the potential window. Nonetheless, the solid line CV indicates the charge

transfer behaviour of insulin at the ITIES. Since the transfer of insulin occurs within the potential window, thus, the electrochemical behaviour of insulin can be studied in the presence of background electrolytes. In this case, the forward peak response is due to the insulin-facilitated transfer of the organic phase anion.[32] Similarly, the backward peak response is due to the back transfer of the organic phase anion from the interface to the organic phase. At the interface, the anion of the organic phase interacts with insulin to form a complex species and this complex species adsorbed on the interface. Since in the reverse scan the current decreased abruptly to a baseline current, this feature of CV shows that the adsorption/desorption phenomenon occurs. A similar phenomenon has been reported to insulin and other protein like Cyt c.[32,137]

Figure 21 (A) represents the CVs that illustrated the variation of current with potential at different concentrations of insulin in the aqueous phase. It shows that suitable potential for forward and backward peak responses at the interface were 0.70 V and 0.46 V, respectively. It demonstrates that the peak currents (both forward and backward peak current) linearly vary with the concentration of insulin. It means that with the increase in the concentration of insulin, the peak responses were increased as shown in Figure 21 (B). However, with the increase in the concentration of insulin, transfer peak potential remains unchanged in both forward and backward processes. In addition, the shape of the peaks was found to be different than the shape of the peaks that were observed in the simple reversible ion-transfer process for $TPrA^+$ ions. The different shapes of the peaks may be because of a process that involves insulin facilitated ion transfer of organic anion followed by different conformational rearrangements of this complex at the interface which was reported elsewhere in the literature.[32]

This experiment concluded that (a) peak current linearly varies with the concentration of insulin in the aqueous phase, (b) peak potential does not change with the change in concentration of the insulin, (c) different shape of the peaks for forward and backward scans are due to the different conformational rearrangements of a complex of insulin at the ITIES. The results reported in this thesis were found to

agree with that found in the literature.[32] This electrochemical behaviour of insulin at the ITIES characterised the new electrochemical cell used in this research.

Figure 22 shows the relationship between the peak charges (both forward and backward) at the different concentrations of insulin. It reveals that the increase in the concentration of insulin the charges that accumulate at the ITIES is increased. However, the backward peak charges are greater than forward peak charges. It could be due to the high concentration of elctroadsorbed insulin at the gel ITIES and this gel phase prevents the electroadsorbed species diffusing away from the interface.

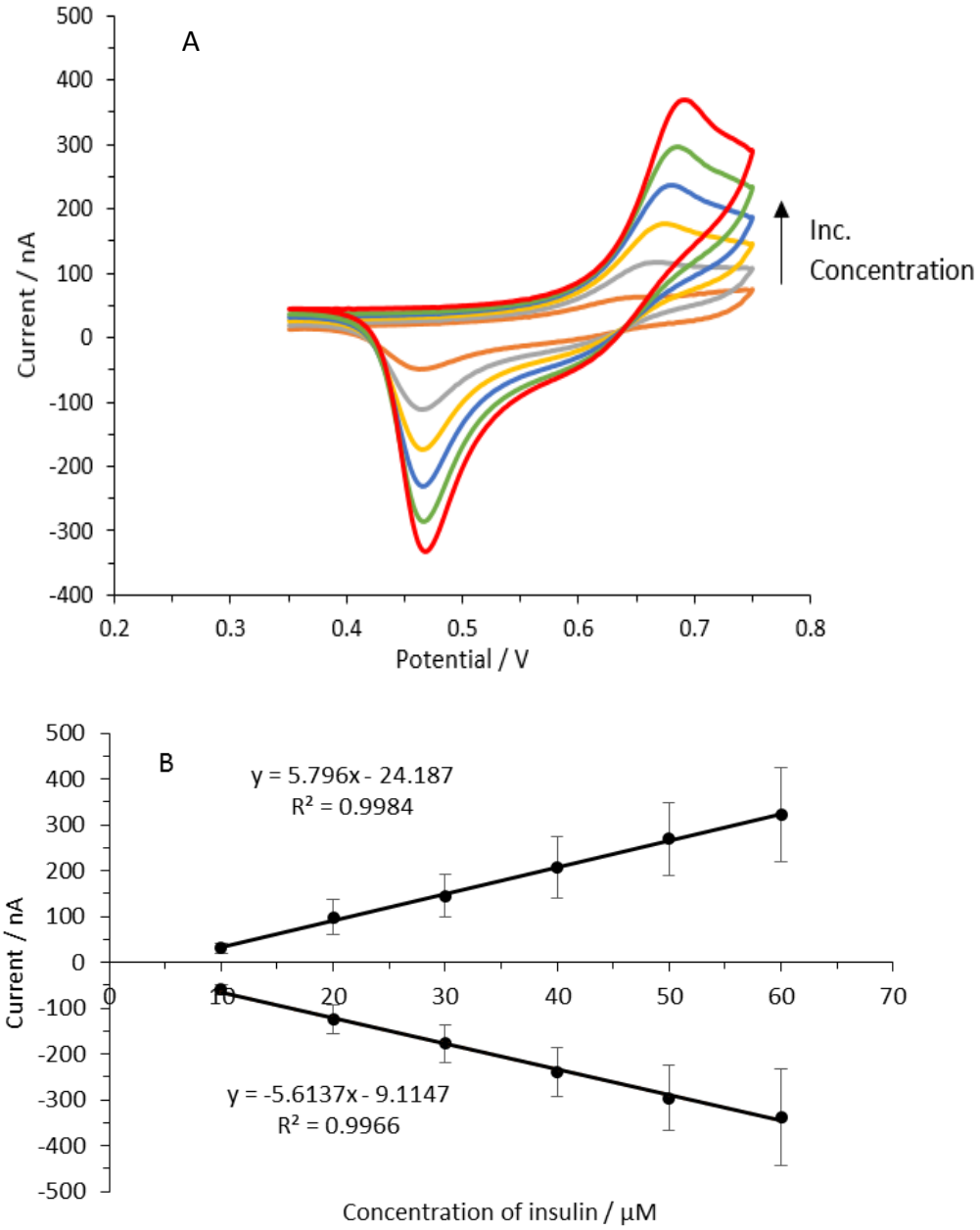

Figure 21: (A) CVs of insulin at different concentrations (i.e. 10 µM, 20 µM, 30 µM, 40 µM, 50 µM, and 60 µM) (10 to 60 µM, increasing as directed by the arrow direction). (B) A plot indicates a relation between peak currents and concentrations of insulin at forward and backward scans. 10 mM HCl as the aqueous phase. 10 mM BTPPATPBCl-1,2-DCE (10 % w/v PVC) as the organic phase. Scan rate: 10 mV s^{-1}. Error bars are the standard deviations of three independent experiments in the same conditions.

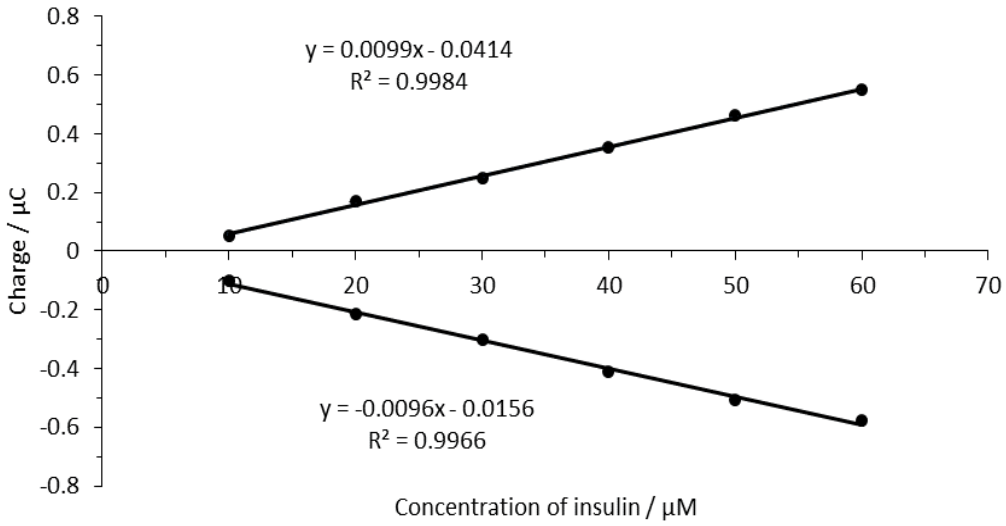

Figure 22: Plot showing the relation between peak charges and concentration of insulin (i.e. 10, 20, 30, 40, 50, and 60 µM). 10 mM HCl as the aqueous phase. 10 mM BTPPATPBCl-1,2-DCE (10 % w/v PVC) as the organic phase. Scan rate: 10 mV s^{-1}. Errors calculated from the standard deviation of three trials where no error bars are visible, they are smaller than the symbol size.

3.2.2 Cyclic voltammetry of insulin at different scan rates.

In this section, the impact of the scan rate on cyclic voltammogram (CV) of insulin was discussed. The data were generated by performing a series of experiments using 10 mM HCl as an aqueous electrolytic solution and 10 mM BTPPATPBCl-1,2-DCE (10 % w / v PVC) as an organic electrolyte. Figure 23 (A) represents a CV of 40 µM insulin at different scan rates. This Figure illustrated the effect of the scan rate on the peak responses. With the increase in the scan rate, both forward and backward peak responses increase as documented in the literature.[32] However, the peak potentials at different scan rates remain unchanged.

A linear relationship between the peak current and square root of the scan rate was established which is as shown in Figure 23(B). It shows that both forward and backward peak currents linearly varied with the square root of the scan rate ($(\nu)^{1/2}$). Although the linear dependency of backward peak current with the square root of the scan rate ($(\nu)^{1/2}$) describes the linear diffusion-controlled transfer across the interface, the shape of CVs exhibits the adsorption/desorption process (i.e. lack of diffusional tailing) in the CV. Hence, the scan rate study and the nature of the CV

of insulin indicates the diffusion-controlled ion transfer process, followed by the adsorption of complex species at the interface. The complex is formed due to the interaction of anion of the organic phase and the positively charged insulin at the interface. These results were in good agreement with the results reported at the ITIES using insulin at a four-electrode system.[32] Amemiya and co-workers using protamine reported similar results at the ITIES.[83] Likewise, Shinshi et al. also reported similar results for other proteins like Cyt c at the ITIES.[137] Hence, this electrochemical study of insulin also characterised the new electrochemical cell used in this research work. The adsorption basis of the insulin electrochemical response has been reported previously[32,88,89] and also give up a way to study insulin structure following its adsorption.

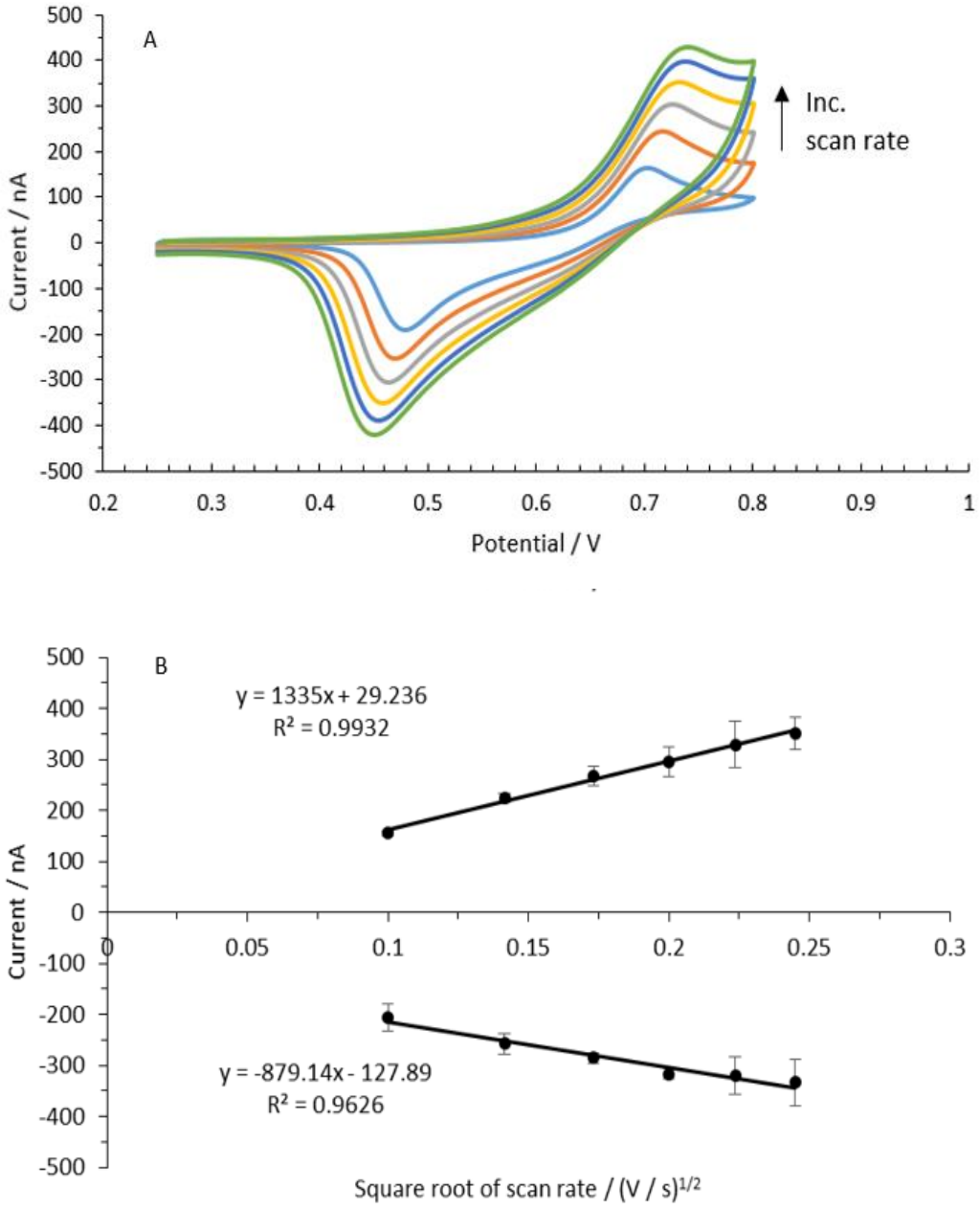

Figure 23: (A) CVs response of insulin at different scan rate: 10 mV s^{-1}; 20 mV s^{-1}; 30 mV s^{-1}; 40 mV s^{-1}; 50 mV s^{-1}; 60 mV s^{-1} (10 to 60 mV s^{-1}, increasing as directed by the arrow direction). (Aq): 10 mM HCl + 40 µM insulin. 10 mM HCl is used as the aqueous phase. 10 mM BTPPATPBCl-1,2-DCE (10 % w/v PVC). (B) Current response to $(\nu)^{1/2}$ for forward and backward peaks. Standard deviations of three trials are used to calculate error bars.

3.2.3 Adsorptive stripping voltammetry of insulin

Different proteins like insulin, lysozyme, and haemoglobin have been studied at the ITIES using adsorptive stripping voltammetry.[63,87,89] O'Sullivan and co-workers detected the lowest concentration of insulin (i.e. 10 nM) using adsorptive stripping voltammetry (AdSV) at a micro-ITIES array.[89] In this thesis, the lowest detection limit of insulin at the macro ITIES was investigated. To find out the lowest detection limit of insulin, a suitable adsorption potential (i.e. 0.70 V) was selected. Then, this potential was applied to the interface for a specific period of time to adsorb the insulin. After that, the detection step (voltammetry) was taken by scanning to the lower potentials (i.e. 0.35 V) at which any adsorbed protein desorbed to give the response. Figures 24(A) and 24(B) show the resulting voltammograms of 0.1 µM and 0.5 µM of insulin at different pre-concentration times, respectively. Stripping peaks were not observed in 0.1 µM insulin at different pre-concentration times as shown in Figure 24 (A). Even at 150 s pre-concentration time, desorption peak was not seen at 0.1 µM insulin. Likewise, no stripping peak was observed at 0.5 µM insulin at 20 s pre-concentration time. Nonetheless, a small stripping peak appeared at 40 s pre-concentration time at this concentration of insulin as shown in Figure 24 (B). In addition, the stripping peak increased with increasing pre-concentration time as shown in Figure 24 (B). Here, before adding the insulin in the aqueous phase, the AdSV of blanks were conducted at all times. Blank did not show any stripping peak as shown in Figure 24 (C). From this experiment, the lowest concentration of insulin was found to be 0.5 µM. Nonetheless, O'Sullivan et al. using a micro-ITIES array recorded the lowest detection limit of insulin, 10 nM.[89] To find out the lowest detection limit of insulin, they also used the AdSV for 450 s pre-concentration time. The lower detection limit of the micro ITIES as compared to the macro ITIES could be due to the less resistivity of the micro ITIES and more pre-concentration time that used in the micro ITIES.

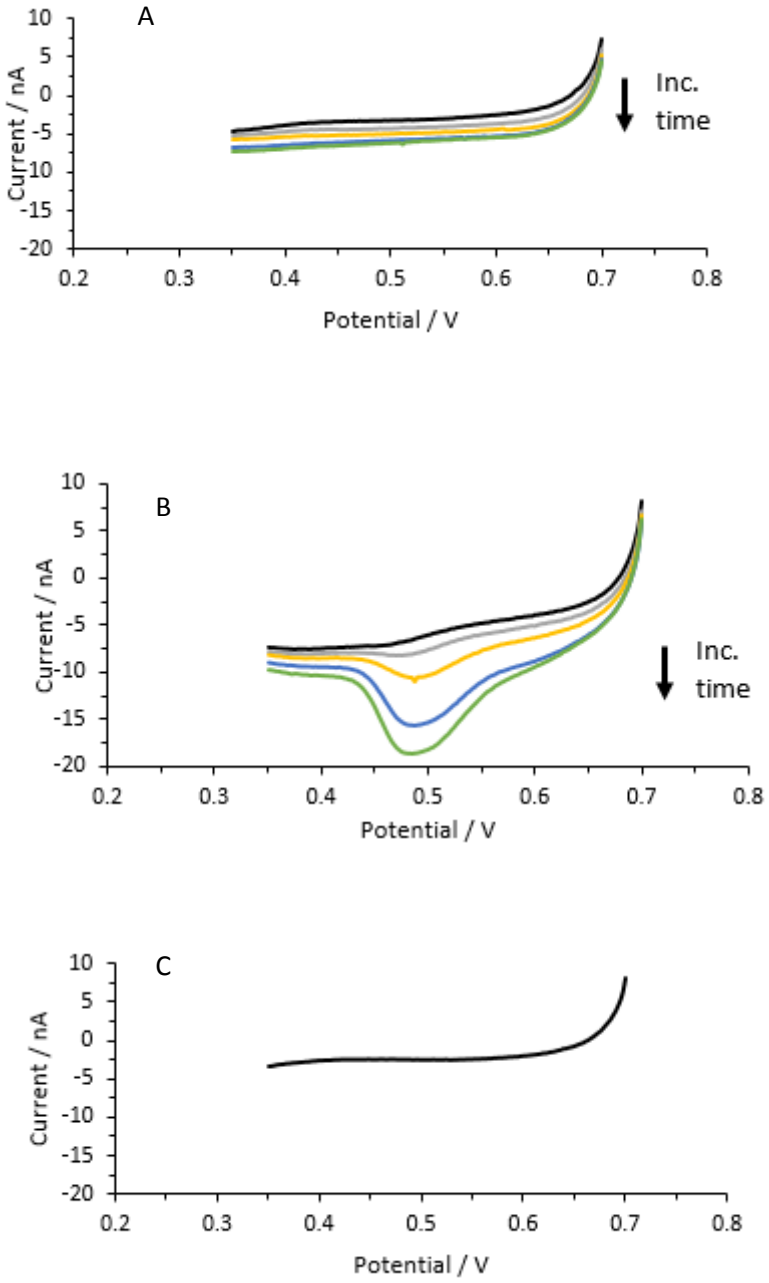

Figure 24: (A) AdSVs of 0.1 µM insulin at various pre-concentration times (i.e. 20 (black line), 40 (grey line), 60 (yellow line), 120 (blue line), and 150 s (green line)). (B) AdSVs of 0.5 µM insulin at various pre-concentration times (i.e. 20 (black line), 40 (grey line), 60 (yellow line), 120 (blue line), and 150 s (green line)). (C) AdSV of 10 mM HCl at 20 s pre-concentration time. 10 mM HCl as the aqueous phase. 10 mM BTPPATPBCl-1,2-DCE (10 % w/v PVC) as the organic phase. Scan rate: 10 mV s^{-1}.

3.2.4 Surface coverage study of insulin

The surface excess concentrations of adsorbed insulin at four different concentrations (i.e. 5, 20, 50, and 100 μM) were calculated using surface coverage analysis. For this analysis, insulin was adsorbed at the constant applied potential for a certain time and the current measured as a function of time. For the adsorption of insulin 0.70 V potential was applied to the interface for 30 min in all cases. A blank CV was measured on each fresh cell to ensure no drifting on the potential scale. All the data were recorded at 10 mM aqueous HCl. This electrochemical study was done using a cell which was shown in scheme 2 (as shown in page 52). Figures 25 (A) describes the relationship between current and adsorption time at different concentrations whereas Figure 25 (B) illustrates the variation of charges with time at different concentrations of insulin at a fixed potential. In this case, charge in Figure 25 (B) is the integrated current. Figure 25(A) reveals that at the specific potential and given adsorption time, the current remains unaltered at fix concentration. But, with the increase in the concentration of insulin in the aqueous phase, the response of current is increased. The current at 100 μM insulin is highest, while the current at 5 μM is recorded to be least among the four different concentrations. These results show that the large current at higher concentration of insulin is due to more anion transfer from the organic phase to the interface. These higher concentrations of anions lead to more insulin deposition at the interface. Unlike the current, at the given applied potential, the amount of charge accumulated at the interface is increased with increase in time (Figure 25 (B)). This increase in charges at the interface is due to the accumulation of more insulin-anion complex. Likewise, the amount of charges that accumulate at the interface is also increased with the increase in the concentration of aqueous insulin. It reveals that with the increase in aqueous insulin, more insulin is deposited at the interface. So, charge accumulation is favourable at high insulin concentration with greater adsorption time.

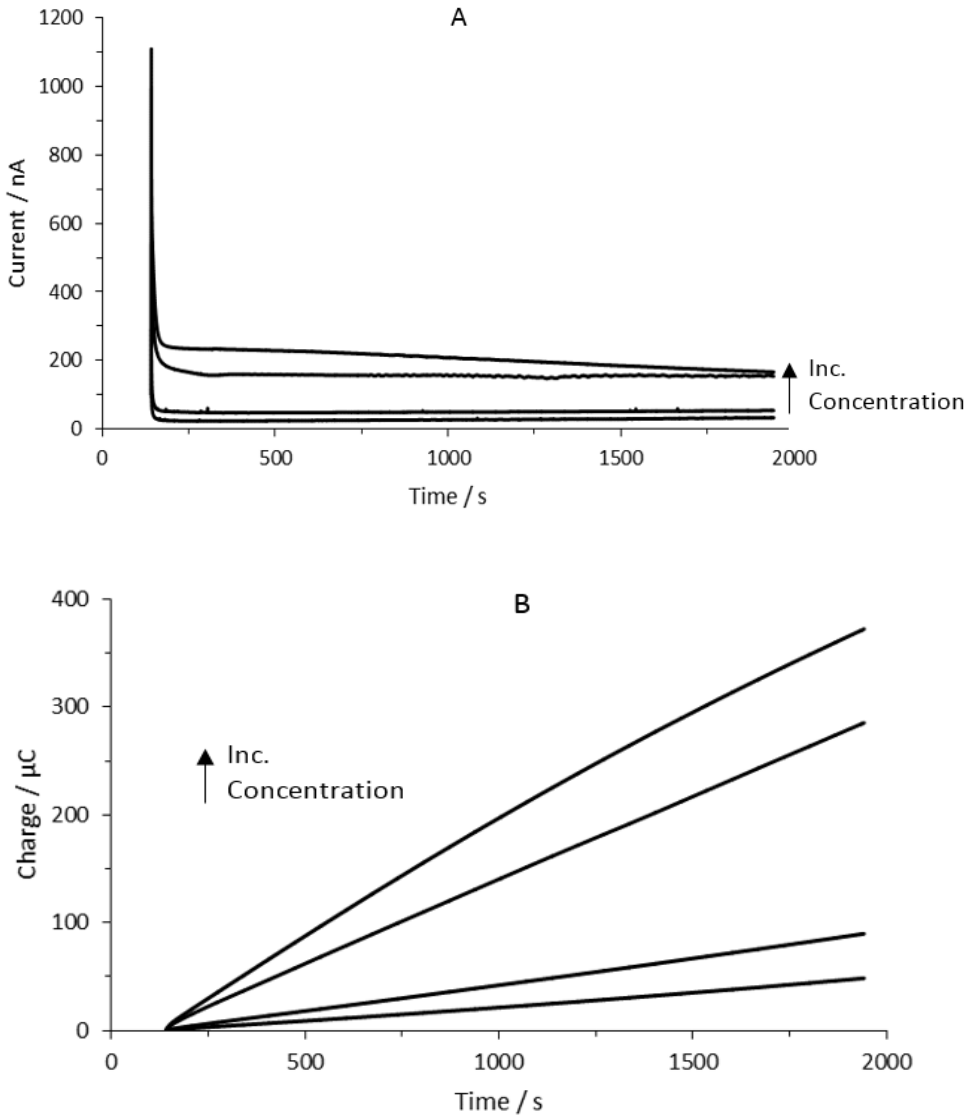

Figure 25: (A) Chronoamperograms of insulin at different concentrations. (B) Figure showing the relationship between adsorbed charge and adsorption time at different concentrations of insulin. 5, 20, 50, and 100 µM Insulin (5 to 100 µM, increasing as directed by the arrow direction) concentrations are maintained. 0.70 V adsorption potential for 30 min adsorption time. 10 mM HCl as the aqueous phase. 10 mM BTPPATPBCl-1,2-DCE (10 % w/v PVC) as the organic phase.

By analysing the accumulated charge at the interface, the surface coverage of the insulin at the interface can be studied. In order to determine the surface coverage of the insulin, the charge flowing through the system at a specified period of time was calculated and substituted in equation (35). The charge that accumulated at 30

min adsorption time was considered to calculate the surface coverage at different concentrations.

Figure 26 (A) indicates the experimental surface coverage at different concentrations of aqueous insulin (i.e. 5, 20, 50, and 100 μM) which were 1.8, 10.9, 19.6, and 25.8 nmol cm^{-2}, respectively. These results show that with the increase in the concentration of insulin in the aqueous phase, the surface coverage of insulin at the interface is increased. These surface coverage data were used to determine the number of monolayers formed at the interface. From the literature, the theoretical monolayer of insulin was found to be 0.0252 nmol cm^{-2}.[89] Hence, the number of monolayers around the interface when 5, 20, 50, and 100 μM insulin were maintained in the aqueous phase were estimated to be 73, 431, 779, and 1025 monolayers, respectively. It clearly indicates that with the increase in the concentration of insulin at the aqueous phase, multilayers of insulin around the interface increases. Similar results were reported by O'Sullivan et al. for insulin using micro ITIES.[89] For the concentration ranges between 10-1000 nM of insulin, they found between 0.1 and 1 monolayer of insulin at the ITIES. Hence, higher the insulin concentration in the aqueous phase, multilayers formation of insulin is favourable.

In addition Figure 26 (B) describes the relationship between surface covered by the insulin at different adsorption times (i.e. 5, 10, 20, and 30 min) at fixed insulin concentration (20 μM). The surface coverage at 5, 10, 20, and 30 min adsorption times were determined to be 1.5, 2.9, 5.6, and 10.9 nmol cm^{-2}, respectively. Similarly, the number of monolayers formed on the interface were 59, 116, 223, and 431 at 5, 10, 20, and 30 min adsorption times, respectively. Thus, the surface coverage of insulin at the interface varies with adsorption time at fixed concentration and potential.

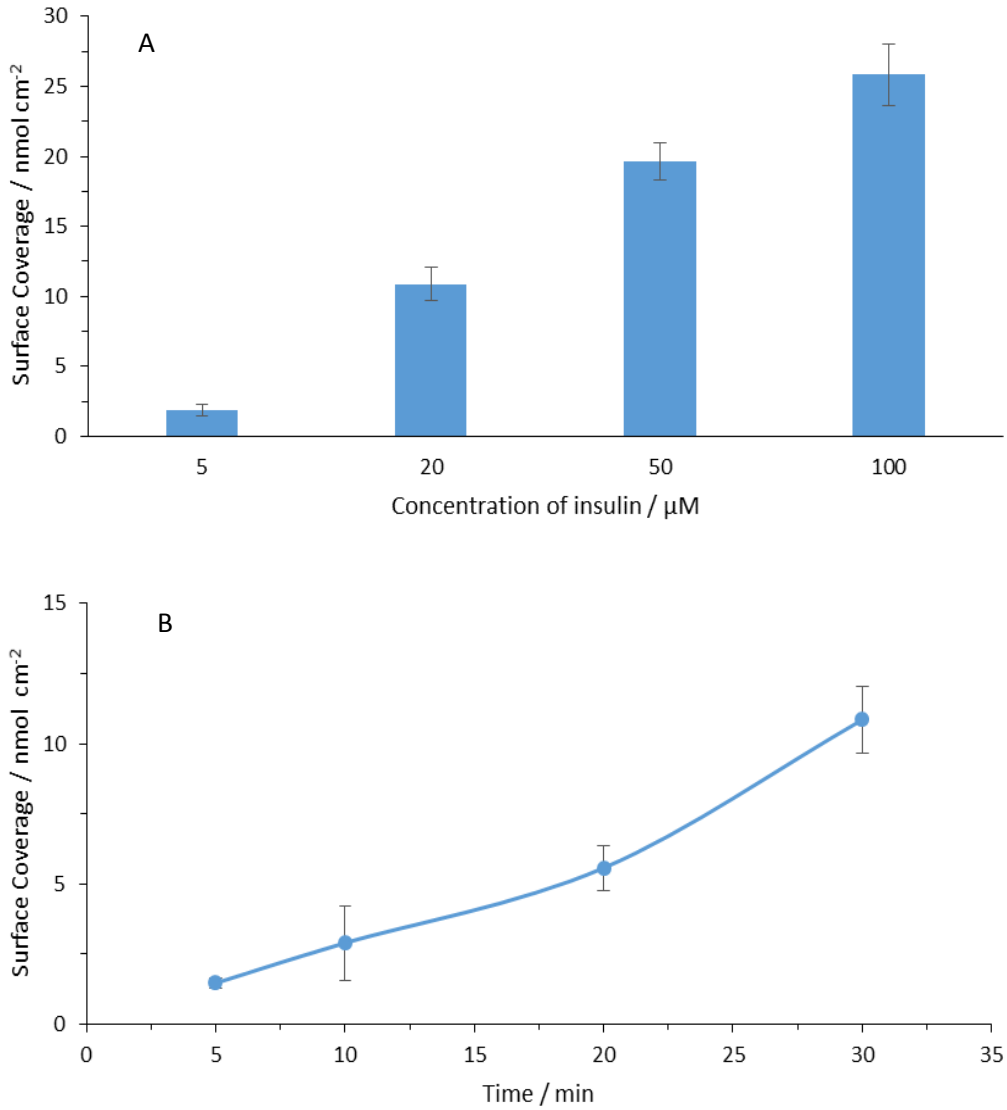

Figure 26: (A) Figure illustrating the relationship between surface coverage and insulin concentrations (i.e. 5, 20, 50, and 100 µM). 0.70 V adsorbed potential for 30 min adsorption time. (B) Figure describing the variation of surface coverage with different adsorption time (i.e. 5, 10, 20, and 30 min). 20 µM insulin concentration and 0.70 V potential are maintained. 10 mM HCl as the aqueous phase. 10 mM BTPPATPBCl-1,2-DCE (10 % w/v PVC) as the organic phase. Error bars are obtained from the standard deviations of three trials.

This experiment concludes that insulin can form multilayers around the interface and these multilayers increase with the increase in the concentration of insulin at the aqueous phase. The multilayer formation of insulin was also affected by the adsorption time. It means that the greater the adsorption time, the multilayer

formation will increase at the ITIES. So, a high concentration of insulin with high adsorption time is favourable for the adsorption of insulin at the ITIES. The results of multilayers formation of insulin at the ITIES was supported by the study of other proteins like haemoglobin and lysozyme.[63,87] Hence, this adsorbed insulin can be characterised using FTIR spectra analysis.

3.3 FTIR study of the secondary structures of insulin

3.3.1 FTIR spectra of organogel

In this research, the organogel was used for the study of secondary structures of electroadsorbed insulin. This approach is based on the report of Booth et al. published in 2019, who reported FTIR spectroscopic analysis of protein secondary structures (lysozyme, myoglobin, Cyt c, and haemoglobin) following electroadsorption at the aqueous/organogel interface.[105] The gel was prepared by using BTPPATPBCl (organic electrolyte), 1,2- dichloroethane (as a solvent), and PVC (as a jellifying agent). The concentrations of BTPPATPBCl and PVC were maintained at 10 mM and 10 % w/v, respectively, while preparing the gel. The FTIR spectra of the organogel were measured by placing the gel directly into physical contact with the diamond ATR crystal. Figure 27 (A) indicates the spectrum of the organogel in the region of amide I spectrum bands. Similarly, Figure 27 (B) indicates the spectrum in the region of amide I band of organogel in the presence of 100 µM aqueous insulin at open circuit potential (OCP). No amide I band appears in the spectra of organogel and no amide I band appears in the spectra recorded from the organogel prepared in the presence of 100 µM insulin in OCP. These results, indicate that 1) spectroscopic interference from the organogel, with respect to analysis of protein secondary structure, is not a concern, 2) spontaneous adsorption of the protein at the interface does not occur. Therefore, these experiments confirm that the organogel is useful for the analysis of secondary structures of insulin following electroadsorption at the interface.

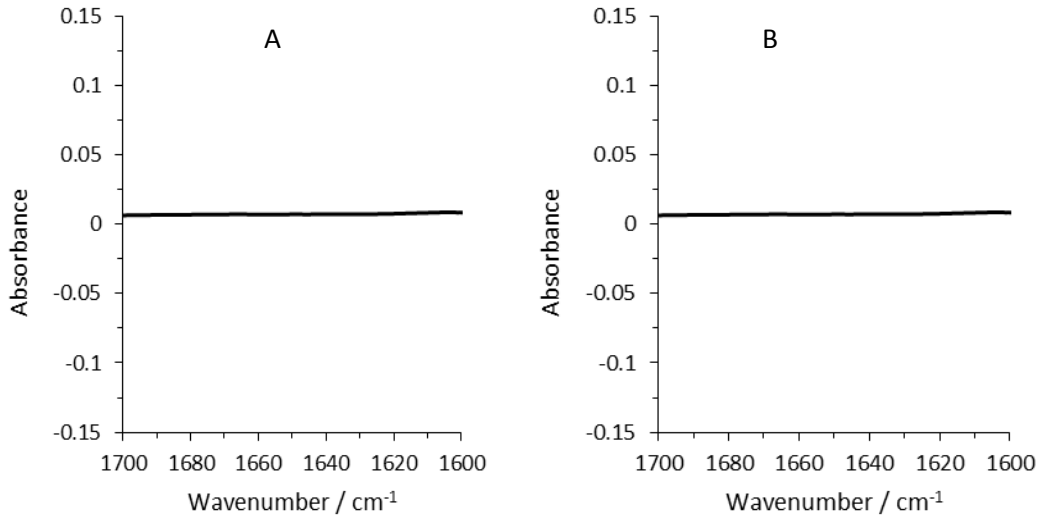

Figure 27: Amide I band in FTIR spectra of (A) 10 mM BTPPATPBCl-1,2-DCE (10 % w/v PVC) organogel and (B) 10 mM BTPPATPBCl-1,2-DCE (10 % w/v PVC) organogel in 100 µM insulin in 30 min adsorption time at open circuit potential. Spectral resolution: 4 cm^{-1}

3.3.2 FTIR spectra of solid-state insulin

The FTIR spectra of solid-state insulin were measured as control experiments, to determine native protein secondary structure. FTIR spectra of solid-state insulin were recorded by adding the solid (insulin powder) directly onto the diamond ATR crystal. The background spectra of blank ATR crystals were recorded before measuring the spectra of solid-state insulin for each case. Figure 28 (A) and 28 (B) illustrate the amide I band and the second derivative of the amide I band from FTIR spectra recorded for solid-state insulin, respectively. Not surprisingly, a distinct amide I band can be seen for solid-state insulin. This amide I peak is due to the C=O stretching of the carbonyl group involved in the peptide linkage present in the insulin. To further deconvolve the amide I band into underlying components, to facilitate protein secondary structure determination, the information about the secondary structures of the insulin, the second derivatives of the amide I regions were used.[100,110,111] Figure 28 (B) represents the second derivative of the amide I band of solid-state insulin. The second derivative of this solid-state insulin shows peaks located at the wavenumbers of 1656, 1649, and 1637 cm^{-1}, respectively. The peaks that appear at 1656 and 1649

cm^{-1} correspond to α-helical and unordered structures, respectively.[100,110,111] Similarly, the peak at 1637 cm^{-1} can be assigned to the existence of either β-sheet and/or irregular helix[100,110,111] because the vibrational frequencies of β-sheet and irregular helix are almost the same. Likewise, the ordinary curve fitting technique was unable to resolve the β-sheet and irregular helix. So, in this research, they were assigned as combined β-sheet and irregular helix (i.e. sum of β-sheet and irregular helix). To determine the relative proportions of protein secondary structures, the curve fitting technique (described in chapter 2) was used. In order to determine the second derivatives of the amide I region, 21 smoothing points were taken using the Savitzky-Golay function, which was the minimum number of smoothing points that yielded an acceptable signal-to-noise ratio. Likewise, a linear background was subtracted using a rubber-band correction method, as provided in the OPUS software.

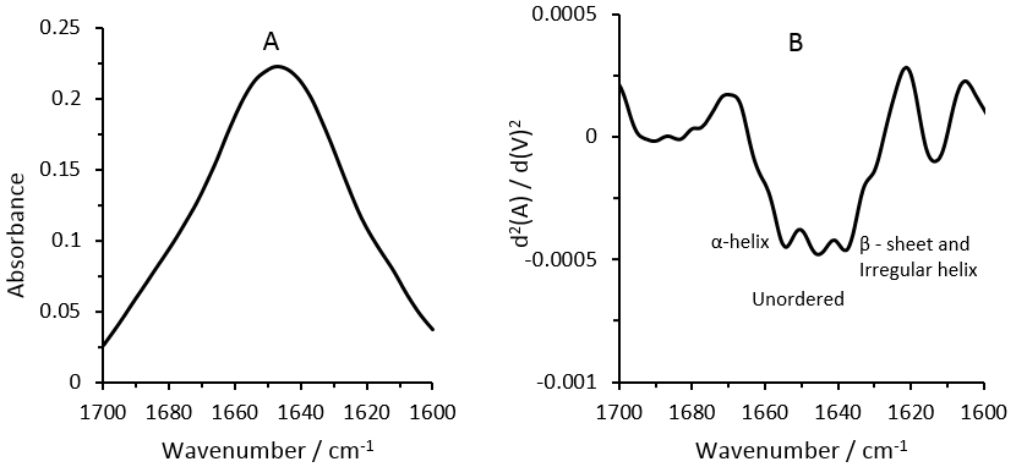

Figure 28: FTIR spectra of solid-state insulin representing: (A) amide I band and (B) the second derivative of the amide I band. 4 cm^{-1} spectral resolution.

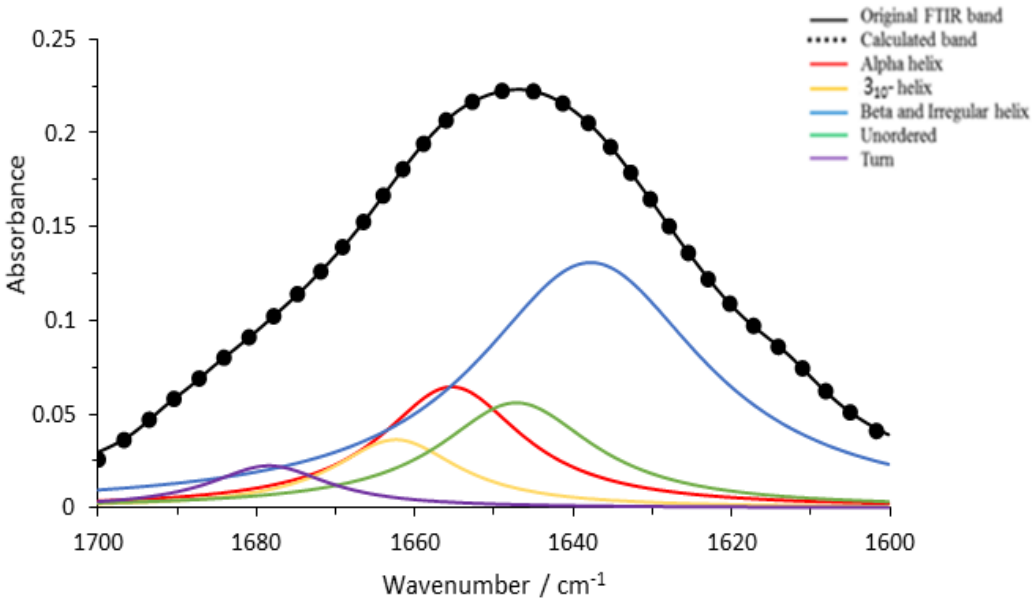

Figure 29: Curve fitted FTIR spectra of solid-state insulin showing the original FTIR band, calculated band and the individual component bands (i.e. α-helix (red line), 3_{10}-helix (yellow line), combined β-sheet and irregular helix (blue line), unordered (green line), and turn (violet line)).

The curve fitted spectra of solid-state insulin are shown in Figure 29. This Figure shows the deconvoluted peaks and their arithmetical sums, together with the experimental spectrum. In Figure 29 the black solid line indicates the original FTIR band and the black dashed line indicates the calculated band, respectively. Similarly, red, yellow, blue, green, and violet solid lines correspond to α-helix, 3_{10}-helix, combined β-sheet and irregular helix, unordered, and turn, respectively. The vibrational frequencies of α-helix, 3_{10}-helix, combined β-sheet and irregular helix, unordered, and turns correspond to 1656, 1660, 1637, 1649, and 1680 cm^{-1}, respectively, in solid-state insulin.[100,110,111] The relative proportions of the secondary structures of solid-state insulin have been presented in Figure 30. It revealed that the majority of the secondary structure of solid-state insulin is due to the combined β-sheet and irregular helix and the relative proportion of these structures is 47.8 %. A similar response was observed by Wei et al.[110] using X-ray diffraction regarding the combined β-sheet and irregular helix (37.2 %) in solid-state insulin. Likewise, large

proportions of combined β-sheet and irregular helix (i.e. 40 %) were also reported by Williams[114] using Raman spectroscopy, in agreement with this thesis work.

In solid-state insulin, the relative proportions of the sum of α- helix and 3_{10}-helix was 16.5 % as shown in figure 30. Similarly, the sum of the relative proportions of unordered and turn was found to be 18.5 % as shown in figure 30. It signifies that the relative proportion of the sum of unordered and turn is similar to the relative proportion of the sum of α-helix and 3_{10}-helix, as reported in the literature (unordered + turn = 29.3 % and α-helix + 3_{10}-helix = 32.8).[110]

In conclusion, solid-state insulin possesses large proportions of combined β-sheet and irregular helix while the other secondary structures are present in minor proportions.

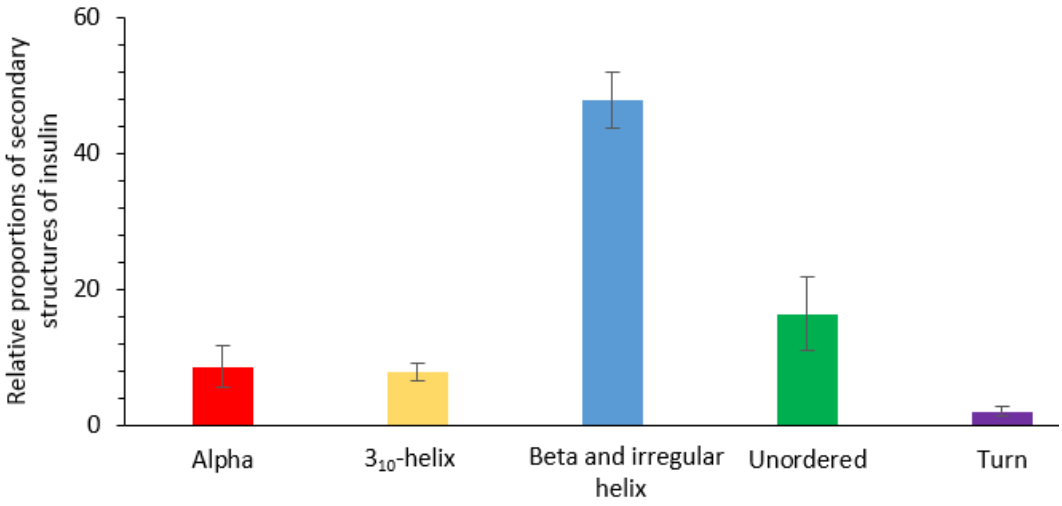

Figure 30: Plot representing the relative proportions of secondary structures of solid-state insulin. Error bars the standard deviations of three trials.

3.3.3 FTIR spectra of hydrated films of aqueous insulin

In order to study the FTIR spectra of hydrated film of aqueous insulin, 2.5 mM aqueous insulin was prepared in 10 mM aqueous HCl. FTIR spectra of the hydrated film of insulin were measured by placing aqueous insulin onto the ATR crystal, accompanied by the complete evaporation of the water. A spectrum of the blank ATR

crystal was always measured before the spectra of insulin. Figure 31 (A) and 31 (B), respectively, represent the region of spectra of the amide I band and the second derivative of the amide I band of the hydrated film of insulin. Like solid-state insulin, a distinct amide I peak was present. The second derivative of the spectra of the amide I peak indicates the presence of the different secondary structures of insulin (e.g., a peak of combined β-sheet and irregular structure at 1637 cm^{-1} and another peak of the unordered structure at 1649 cm^{-1}).[100,110,111]

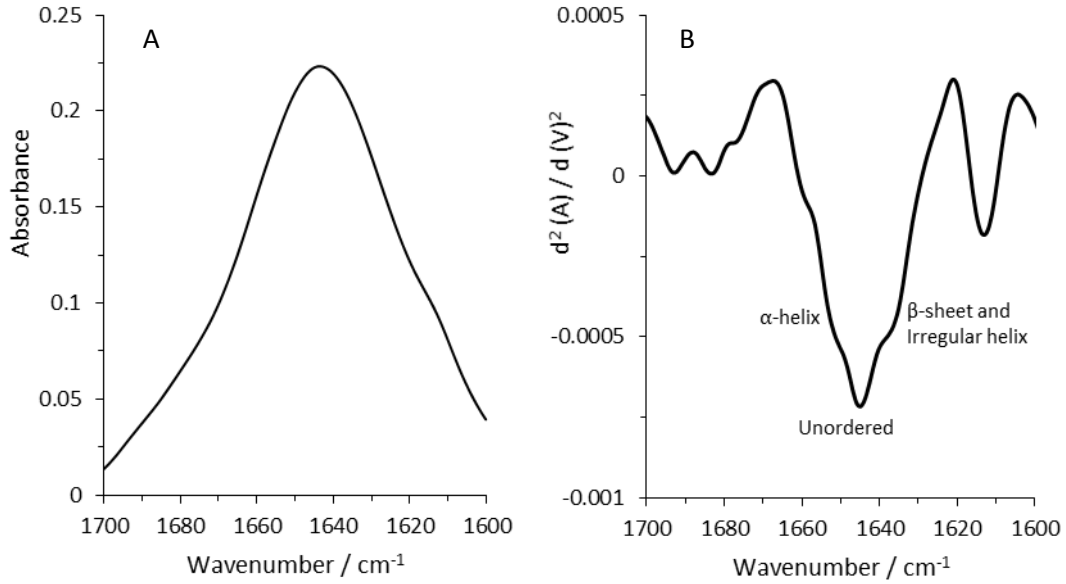

Figure 31: FTIR spectra of hydrated film of insulin (2.5 µM aqueous insulin in 10 mM aqueous HCl representing): (A) amide I band and (B) second derivative of the amide I band. Spectral resolution: 4 cm^{-1}.

The relative proportions of different secondary structures were determined using the curve fitting technique as discussed in chapter 2. Figure 32 illustrates the curve fitted spectra of the hydrated film of insulin. Here, the black solid line indicates the original FTIR band and the black dashed line indicates the calculated band, respectively. Similarly, the red, yellow, blue, green, and violet solid lines correspond to α-helix, 3_{10}-helix, combined β-sheet and irregular helix, unordered, and turn, respectively. The vibrational frequencies of α-helix, 3_{10}-helix, combined β-sheet and irregular helix, unordered, and turns correspond to 1656, 1660, 1637, 1649, and 1680 cm^{-1}, respectively, in aqueous insulin.[100,110,111] Figure 33 represents the relative proportions of secondary structures of the hydrated film of insulin. Like the solid-state insulin, the hydrated film of insulin contains significant proportions of the

combined β-sheet and irregular helix. The total percentage of the combined β-sheet and irregular helix was 44.4 %. Wei et al.[110] also reported a significant proportion of combined β-sheet and irregular helix (37.5 %) of bovine insulin dissolved in D_2O. Similarly, Vecchio et al.[99] also reported the highest proportions of combined β-sheet and irregular helix (38.5 %) of bovine insulin in D_2O. The relative proportion of unordered structures in the hydrated film of insulin was found to be 22.1 % which was similar to that reported by Wei et al. (26.7 %) and Vecchio et al. (21.3 %). This percentage of the unordered structure is highest among the other secondary structures like α-helix (11.7 %), 3_{10}-helix (2.7 %), and turn (0.7 %). These results are also supported by previous results reported by Wei et al.[110] (α-helix (17.5 %), 3_{10}-helix (12.2 %), and turn (6.1 %)) and Vecchio et al.[99] (α-helix (18.9 %), 3_{10}-helix (11 %), and turn (9.4 %)). In this research, turn was found in the least proportions as compared to the other secondary structures, as reported in the literature.[99,110]

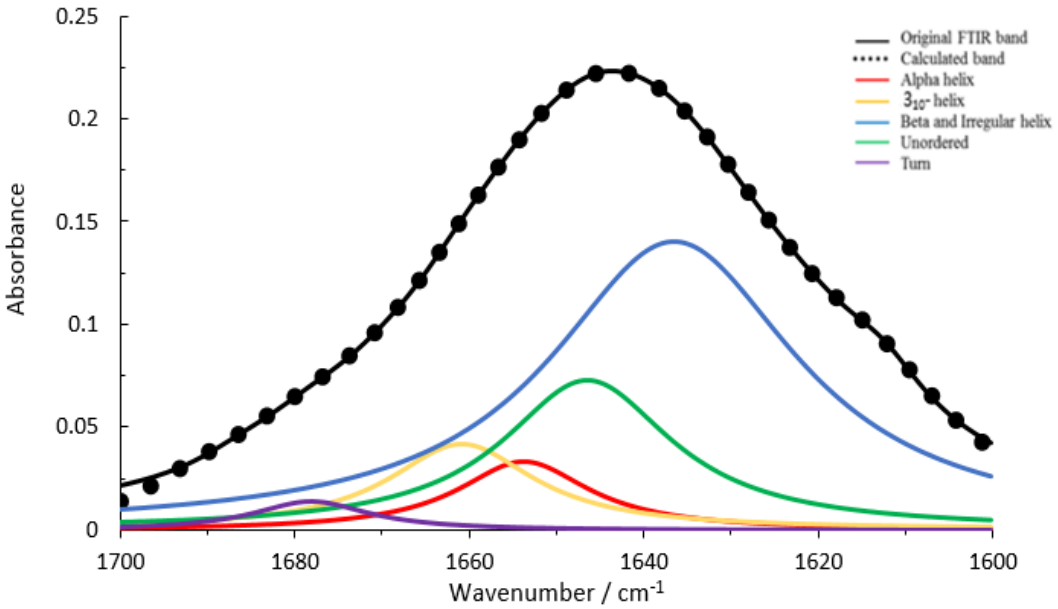

Figure 32: Curve fitted FTIR spectra of hydrated film of insulin representing the original FTIR band (black solid line), calculated band (black dashed line) and the individual component bands (i.e. α-helix (red line), 3_{10}-helix (yellow line), combined β-sheet and irregular helix (blue line), unordered (green line), and turn (violet line)). 2.5 µM insulin in 10 mM aqueous HCl.

Nuclear magnetic resonance (NMR)[138] spectroscopy and X-ray diffraction[139] study have shown that insulin possesses similar secondary structures in its solid-state and aqueous state, but some differences exist. In this thesis, also the majority of the secondary structures of insulin in the solid-state and in hydrated films are combined β-sheet and irregular helix. Although some differences exist in secondary structures, the insulin possesses similar secondary structures in its solid-state and in hydrated films.

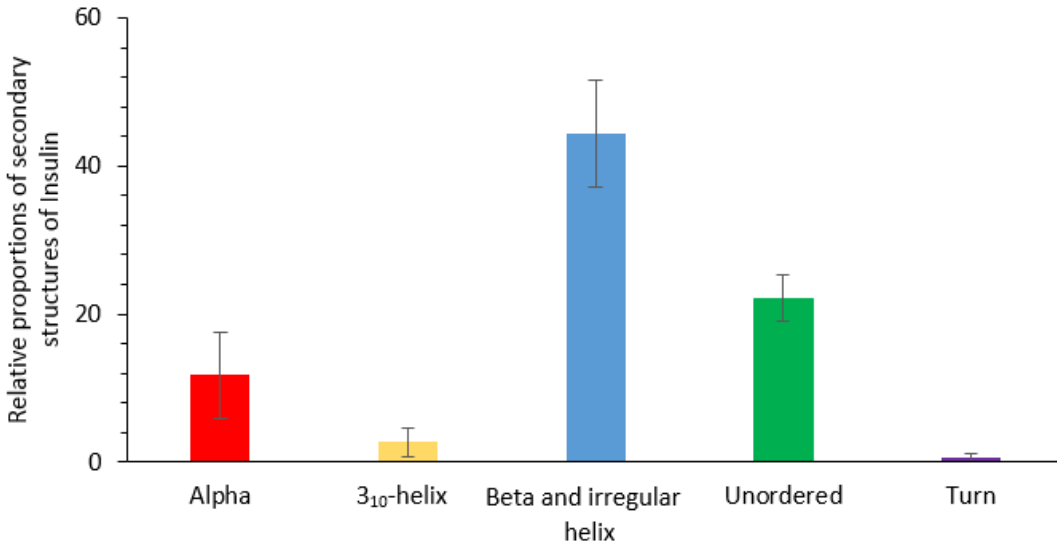

Figure 33: Plot indicating the relative proportions of secondary structures of hydrated film of insulin (2.5 µM aqueous insulin in 10 mM aqueous HCl). Error bars are the standard deviations of three trials.

3.3.4 FTIR spectra of insulin following electroadsorption

As already mentioned the aqueous/1,2-DCE organogel interface can be used as a basis for the analysis of the secondary structures of insulin following electroadsorption. The preparation of organogel, different phases, different electrolytes used, and electrochemical set up used were already discussed in chapter 2. To study the secondary structures of electroadsorbed insulin, firstly a suitable adsorption potential was determined. Secondly, by choosing the suitable adsorption potential, insulin was adsorbed on the interface for a specific interval of time. Finally, the thin layer of organogel having adsorbed insulin was removed from the electrochemical cell and FTIR spectra of electroadsorbed insulin were investigated using FTIR spectroscopy, as discussed below.

3.3.4.1 Selection of suitable adsorption potential of insulin

Although the CV of insulin indicates the adsorption of insulin at 0.70 V as discussed in section 3.2.1, in order to study the secondary structures of electroadsorbed insulin at the interface, a suitable adsorption potential was investigated by choosing six different potentials (i.e. 0.35 V, 0.50 V, 0.60 V, 0.65 V, 0.70 V, and 0.75 V). For all these experiments 30 min adsorption time was deployed. All of these experiments were conducted using the electrochemical cell (Scheme 2 as shown in page 52) with 20 μM insulin. After electroadsorption, the sample was subjected to overnight drying (which was explained in chapter 2) and then the FTIR spectra were recorded. The FTIR spectra of amide I regions of all of the experiments are shown in Figure 34 (A). It clearly shows the distinct amide I response at the potentials 0.65 V, 0.70 V, and 0.75 V, however, amide I peaks did not occur at the potentials 0.35 V, 0.50 V, and 0.60 V. The absence of amide I peaks at potentials $\leq$ 0.6 V is most likely due to less concentration of insulin at the interface. Figure 34 (B) illustrates the relationship between the absorbance of different spectra of 20 μM aqueous insulin at different adsorption potentials. It shows that at potential $\leq$ 0.6 V, the absorbance of insulin is almost negligible as compared to that at potentials $\geq$ 0.65 V in which insulin possesses significant absorbance. This potential study revealed that all potentials are not sufficient for the adsorption of insulin, rather, a suitable potential needs to be chosen for the adsorption of a sufficient amount of insulin at the interface. By considering the CV (Figure 21(A)) and amide I region of spectra of insulin at different adsorption potential, 0.70 V was chosen for the study of the secondary structures of insulin following electroadsorption, which are discussed below.

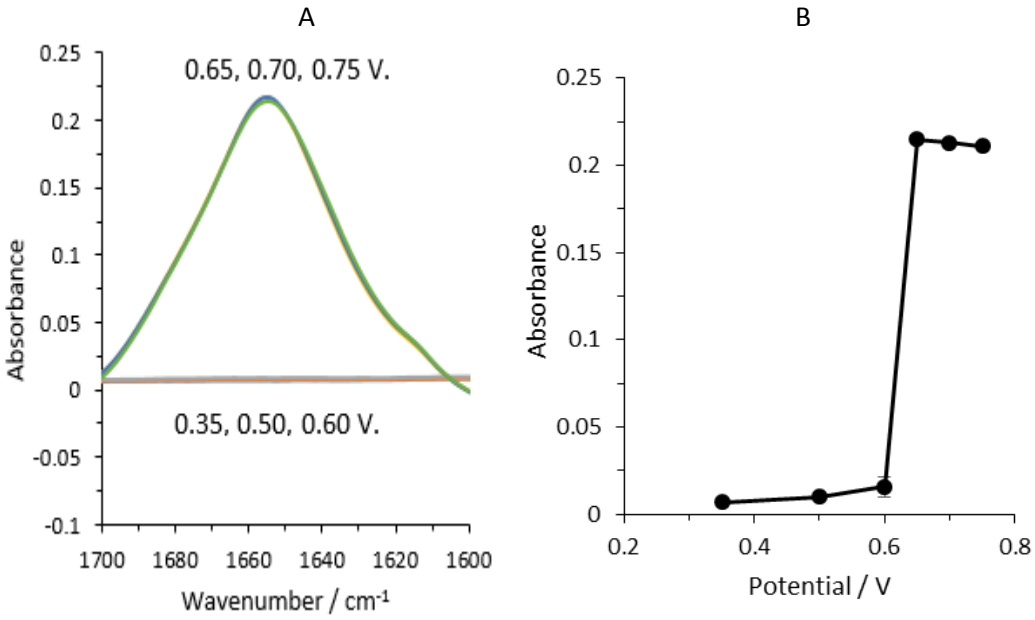

Figure 34: (A) FTIR spectra of insulin showing amide I bands at adsorption potentials of 0.65, 0.70, and 0.75 V, and no amide I bands at adsorption potentials of 0.35, 0.50, and 0.60 V. (B) Plot indicating the variation of absorbance with applied potentials. 20 µM aqueous insulin in 10 mM HCl (aqueous phase). 10 mM BTPPATPBCl-1,2-DCE (10 % w/v PVC) as the organic phase. 30 min adsorption time. Error bars are obtained from the standard deviations of three trials where no error bars are visible, they are smaller than the symbol size.

3.3.4.2 Secondary structures of electroadsorbed insulin at different concentrations.

Four different concentrations (i.e. 5, 20, 50, and 100 µM) of aqueous insulin were used to study the secondary structural variation of electroadsorbed insulin at the ITIES. 30 min adsorption time with 0.70 V adsorption potential was employed. All the electroadsorption was done by using cell (Scheme 2 as shown in page 52). All the electroadsorbed insulin were subjected to overnight drying as discussed in chapter 2. Then, the FTIR spectra of the electroadsorbed insulin were measured. In all samples, distinct amide I peaks were observed. Figures 35 (A) and 35 (B) illustrate the amide I bands and their second derivatives of electroadsorbed insulin at different concentrations. The absorbance frequencies of electroadsorbed insulin shifted with concentrations, indicating underlying changes in protein secondary structure. Specifically, the amide I peaks were shifted towards higher wavenumber region at

low concentrations of insulin, with respect to the amide I peaks from experiments using higher insulin concentration. In addition, the relative intensity of peaks within the second derivatives of the amide I region also changed when insulin was at a lower concentration as compared to the higher insulin concentration. These spectroscopic changes appear to indicate a change in the secondary structures of insulin following electroadsorption. Visual inspection of the second-derivative spectra indicates the changes might be due to the conversion of some combined β-sheet and irregular helix (1637 cm^{-1})[100,110,111] to the α-helical structures (1656 cm^{-1}),[100,110,111] which was further investigated through the curve fitting technique as shown below.

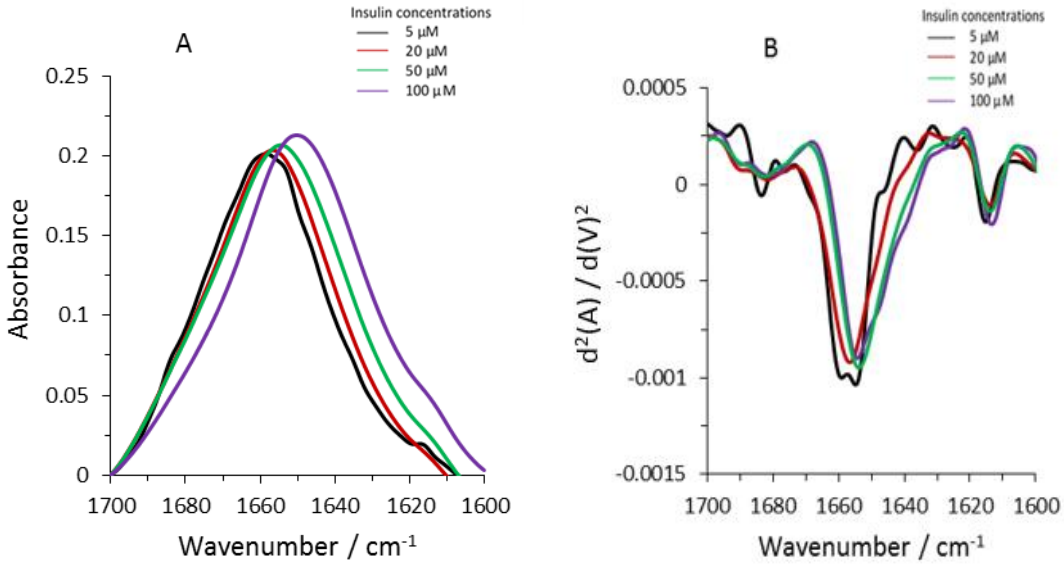

Figure 35: FTIR spectra of insulin following electroadsorption at the ITIES at different concentrations (i.e. 5, 20, 50, and 100 µM) driven by a fixed applied potential of 0.70 V for 30 min. (A) amide I features and (B) second derivative of amide I peak. 10 mM HCl as the organic phase. 10 mM BTPPATPBCl-1,2-DCE (10 % w/v PVC) as the organic phase. Spectral resolution: 4 cm^{-1}.

A Local least squares curve fitting technique, which is discussed in chapter 2, was applied in order to calculate the relative proportions of secondary structures of insulin at different concentrations. Figure 36 (A), 36 (B), 36 (C), and 36 (D), respectively, represent the curve fitted spectra of electroadsorbed insulin at 5, 20, 50, and 100 µM aqueous insulin concentrations. Figure 36 (A) and 36 (B) clearly indicate that, at low aqueous insulin concentrations (i.e. 5 and 20 µM), the α-helical

form was found to be more prominent than the others. Nevertheless, Figure 36 (C) and 36 (D) signify the greater proportions of combined β-sheet and irregular helix at high aqueous insulin concentration (i.e. 50 and 100 µM). The relative proportions of secondary structures of electroadsorbed insulin at different aqueous insulin concentrations were shown in Figure 37. The relative proportions of combined β-sheet and irregular helix were 16 %, 18.1 %, 32.9 %, and 32 % at 5, 20, 50, and 100 µM aqueous insulin concentrations, respectively. It shows that at higher insulin concentration, combined β-sheet and irregular helix are present in major proportions in the electroadsorbed insulin. However, at a low concentration of insulin in the aqueous phase, the electroadsorbed insulin possesses lower proportions of combined β-sheet and irregular helix. The surface coverage study (already discussed in section 3.2.4) has shown that the concentration of adsorbed insulin at the ITIES increases with increasing concentration of insulin in the aqueous phase. So, at high insulin concentration, more insulin might be accumulated at the ITIES. Because of the high concentration of electroadsorbed insulin, the FTIR spectroscopy might have detected only those electroadsorbed insulin which are far from the interface and less impacted by the ITIES. As a result, as in the hydrated film of insulin, the electroadsorbed insulin at high concentration might have possessed larger proportions of combined β-sheet and irregular helix. Nonetheless, at lower insulin concentrations, less insulin might be adsorbed at the ITIES. In this case, FTIR spectroscopy would detect such electroadsorbed insulin that was close to the interface and might have been greatly impacted by it. As a result, the electroadsorbed insulin might have lesser proportions of combined β-sheet and irregular helix.

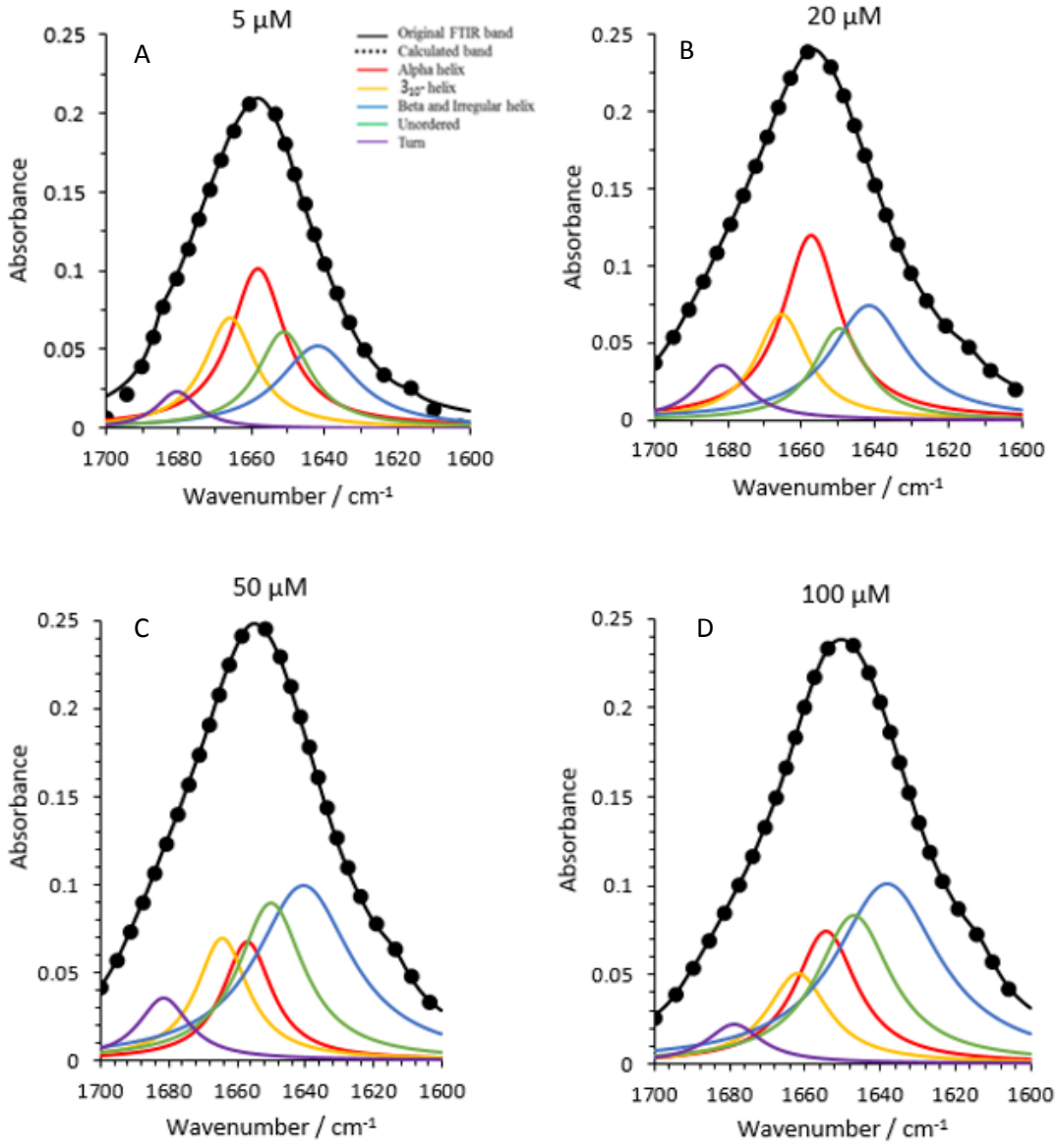

Figure 36: FTIR spectra of insulin following electroadsorption at the ITIES at different concentrations indicating the region of different secondary structures. Curve fitted spectra at: (A) 5 µM (B) 20 µM, (C) 50 µM, and (D) 100 µM aqueous insulin. Fixed applied potential of 0.70 V for 30 min adsorption time. 10 mM HCl as the aqueous phase. 10 mM BTPPATPBCl-1,2-DCE (10 % w/v PVC) as the organic phase.

The relative proportions of α-helix of electroadsorbed insulin were 23.1 %, 28.5 %, 16.4, and % 15.9 % at 5, 20, 50, and 100 µM aqueous insulin, respectively. It revealed that at lower aqueous insulin concentration, the electroadsorbed insulin possesses more α-helical secondary structures. As already discussed, the

accumulation of electroadsorbed insulin increases with an increase in aqueous insulin concentration. So, the α-helical structure is favourable at low aqueous insulin. Likewise, at high insulin concentration, the relative proportion of α-helix was decreased at the ITIES. This is because at high concentrations, more insulin might have accumulated at the ITIES and the insulin that is detected by the FTIR could be far from the ITIES and less impacted by the ITIES. And, hence more combined β-sheet and irregular helix were reported.

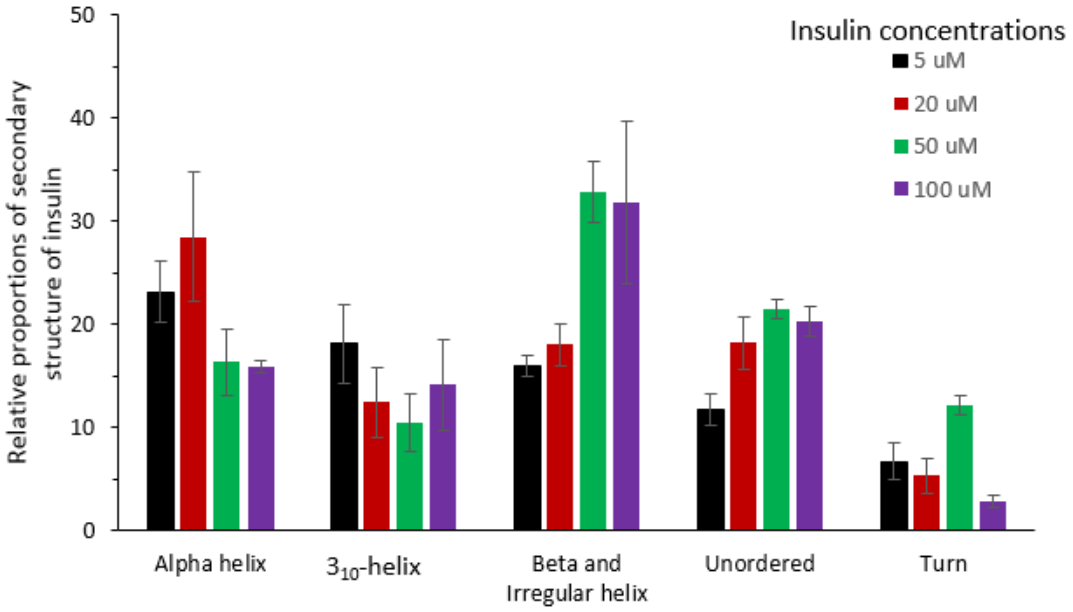

Figure 37: Plot shows the relative proportions of secondary structures of insulin following electroadsorption at different concentrations (i.e. 5, 20, 50, and 100 µM) of aqueous insulin. 0.70 V adsorbed potential for 30 min adsorption time. 10 mM HCl as the aqueous phase. 10 mM BTPPATPBCl-1,2-DCE (10 % w/v PVC) as the organic phase. Error bars are the standard deviations of three trials.

At different aqueous insulin concentrations, the relative proportions of 3_{10}-helix remain unaltered. It means that the 3_{10}-helical structure does not depend upon the concentration of electroadsorbed insulin at the interface. Similarly, a significant difference in relative proportions of unordered structures or turns was not observed between the different insulin concentrations.

3.3.4.3 Secondary structures of electroadsorbed insulin at different applied potentials

20 μM insulin was used to see the impact of applied potentials on any change in the secondary structure of electroadsorbed insulin. 30 min adsorption time was maintained to deposit the insulin at the interface at all applied potentials. Three different potentials (i.e. 0.65, 0.70, and 0.75 V) were chosen. Here, the adsorption of insulin was done by using cell (scheme 2 as shown in page 52). Figure 38 (A) illustrates the curve fitted spectra of electroadsorbed insulin at different adsorption potentials. The curve fitted spectra are almost the same at the three different potentials. Similarly, Figure 38 (B) shows the relative proportions of different secondary structures of electroadsorbed insulin at different potentials. At different potentials, the relative proportions of the α-helical structure remain the same. Similarly, the relative proportions of 3_{10}-helix were found to be the same at all potential. Likewise, the proportions of combined β-sheet and irregular helix were also the same in all the applied potentials studied. In addition, the relative proportions of turn also remain the same in all three potentials studied. This experiment clearly depicts that there is no impact of applied potentials on the relative proportions of secondary structures of electroadsorbed insulin. However, potential has played a significant role in the trigger for insulin adsorption at the interface.

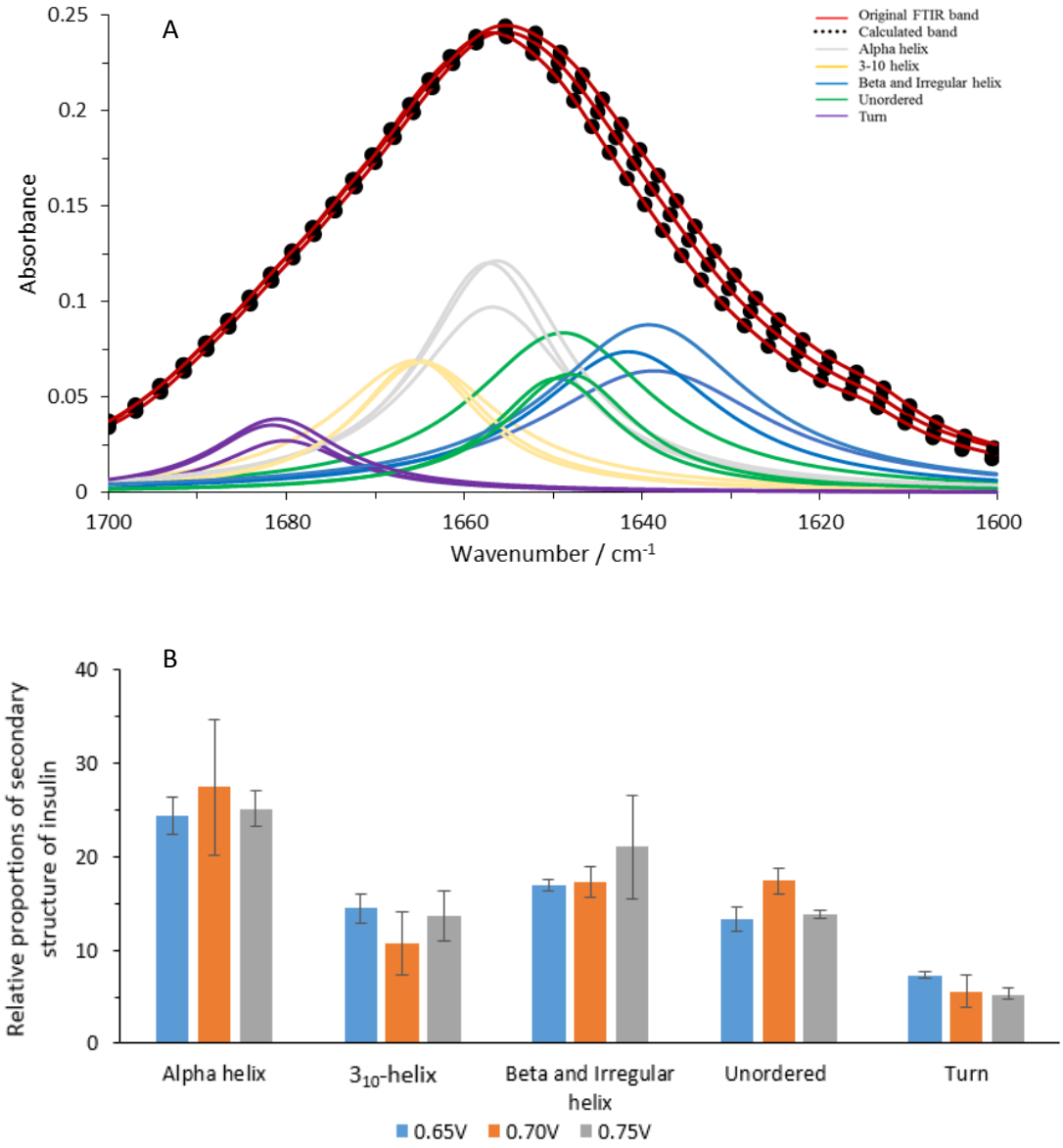

Figure 38: FTIR spectra of insulin following electroadsorption at the ITIES at different adsorption potentials. (A) Curve fitted spectra of electroadsorbed insulin at 20 µM aqueous insulin showing different regions of secondary structures. (B) Relative proportions of secondary structures of insulin. Three adsorption potentials (i.e. 0.65, 0.70, and 0.75 V) were applied for 30 min. 10 mM HCl as the aqueous phase. 10 mM BTPPATPBCl-1,2-DCE (10 % w/v PVC) as the organic phase.

3.3.4.4 Secondary structures of electroadsorbed insulin at different adsorption times

These experiments were conducted to see any change in secondary structures of insulin at different adsorption times by keeping the same aqueous insulin concentration. As already discussed, the applied potential did not have any impact on the secondary structure of electroadsorbed insulin. So, a fixed potential of 0.70 V was chosen for the electroadsorption of insulin at the interface. Two different adsorption times (i.e. 5 and 30 min) were maintained to study the impact of adsorption time on the secondary structures of adsorbed insulin. Two experiments were conducted separately by taking 20 μM and 100 μM aqueous insulin. Figure 39 (A) and 39 (B) give the relative proportions of secondary structures of electroadsorbed insulin at 20 μM and 100 μM aqueous insulin, respectively. At a low concentration of aqueous insulin (20 μM), the relative proportions of α-helix, combined β-sheet and irregular helix, unordered, and turn remains almost the same at the two different adsorption times. These secondary structures did not show any change in their secondary structures. However, the 3_{10}-helix has shown a difference in the relative proportions at different adsorption times. Low insulin concentration with less adsorption time is more favourable for the existence of 3_{10}-helix at the interface. Similarly, at a high concentration of aqueous insulin (100 μM), the relative proportions of α-helix, combined β-sheet and irregular helix, 3_{10}-helix, and turn remain unaltered even at two different adsorption times. Nevertheless, the unordered structure has shown some difference in the secondary structure at two different adsorption times. Figure 39 (A) shows that a high concentration with longer adsorption time is favourable for the unordered structure of electroadsorbed insulin.

This experiment concludes that at low and high concentrations of aqueous insulin, adsorption time has no significant impact on most of the secondary structures of electroadsorbed insulin. However, little impact has occurred on 3_{10}-helix at low concentration and unordered structure at a high concentration of electroadsorbed insulin.

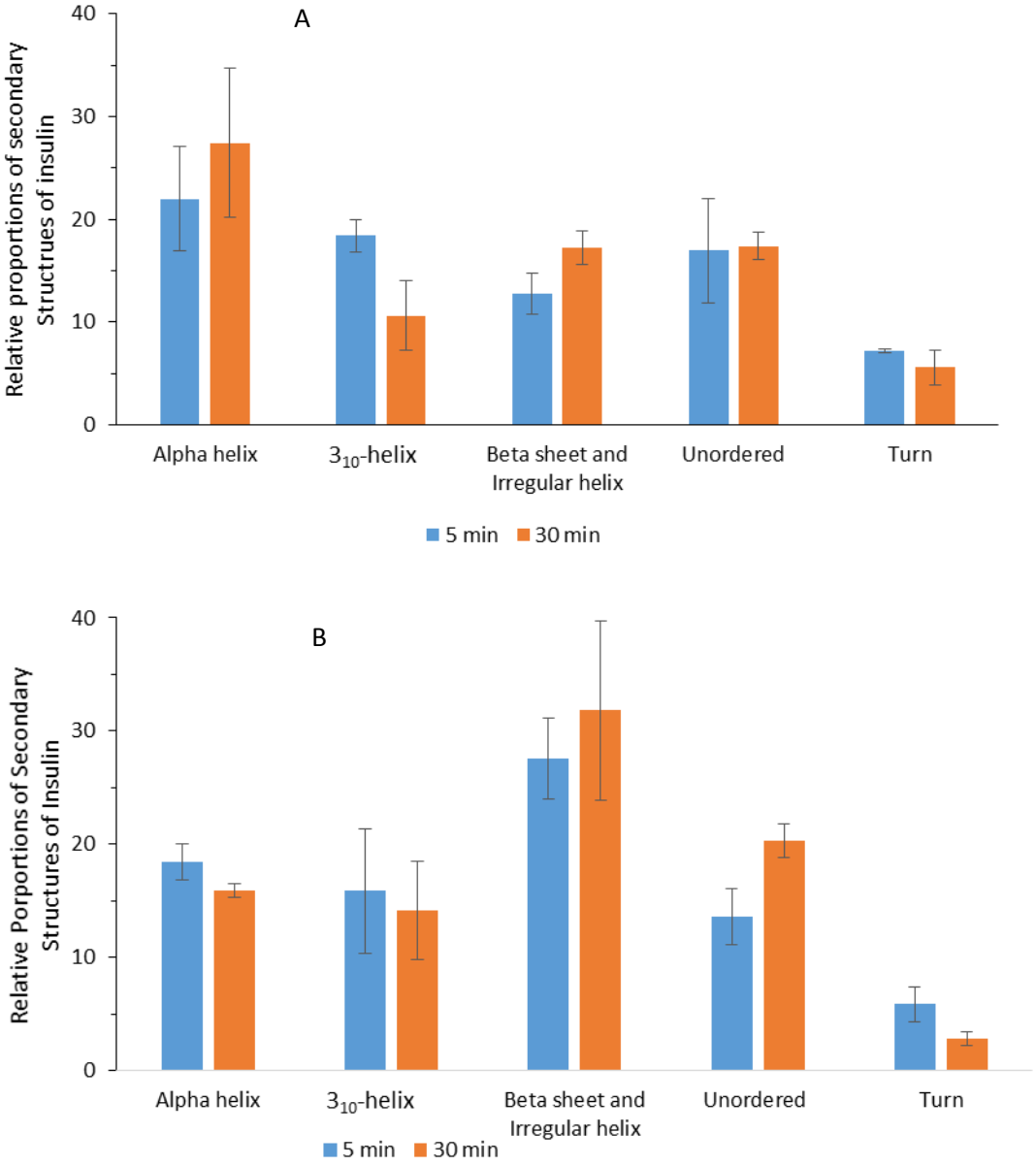

Figure 39: Relative proportions of secondary structures of insulin at different adsorption times (i.e. 5 and 30 min): (A) using 20 µM insulin and (B) using 100 µM insulin. 10 mM aq. HCl as the aqueous phase. 10 mM BTPPATPBCl-1,2-DCE (10 % w/v PVC) as the organic phase.

3.3.4.5 Variation of relative intensities of secondary structures of electroadsorbed insulin with surface coverages

The surface coverage study of electroadsorbed insulin at different concentrations was investigated and the data were analysed in previous section 3.2.4. Four different insulin concentrations (i.e. 5 μM, 20 μM, 50 μM, and 100 μM) were used to study the surface coverage by electroadsorbed insulin at the ITIES. The intensities of different secondary structures of electroadsorbed insulin at different concentrations were determined and the relationship between the intensities and surface coverage was studied. Figure 40 (A) describes the relationship between intensity and surface coverage of electroadsorbed insulin at different concentrations. It indicates that at higher surface coverage, the intensity of the α-helical structure was less than the intensity of combined β-sheet and irregular helix. Nevertheless, the intensities of combined β-sheet and irregular helix were found to be less at low concentration of insulin. So, at low aqueous insulin concentration, surface coverage is lower (only a completely occupied interface surface existing as thin insulin layer) as shown in Figure 40 (B) and therefore the strongest α-helical signal is observed. On the other hand, at high aqueous insulin concentration, the surface coverage is higher (Figure 40 (C)) and protein layers build up. If α-helix structures are only favoured by direct interaction with the interface, then the accumulation of secondary and tertiary protein layers will effectively dilute the α-helix signal of the primary layer. Therefore, increased α-helix signal is not observed at higher concentrations or longer deposition times. Consequently, large proportions of electroadsorbed insulin possess combined β-sheet and irregular helix. As per 3_{10}-helix, unordered, and turn, the intensities of these structures remained almost the same at different surface coverage conditions.

Thus, at low insulin concentration, the interaction of insulin at the ITIES induced a change in secondary structure and hence favouring α-helical secondary structures. At higher insulin concentration, the insulin layers build up, and hence insulin does not show any structural change.

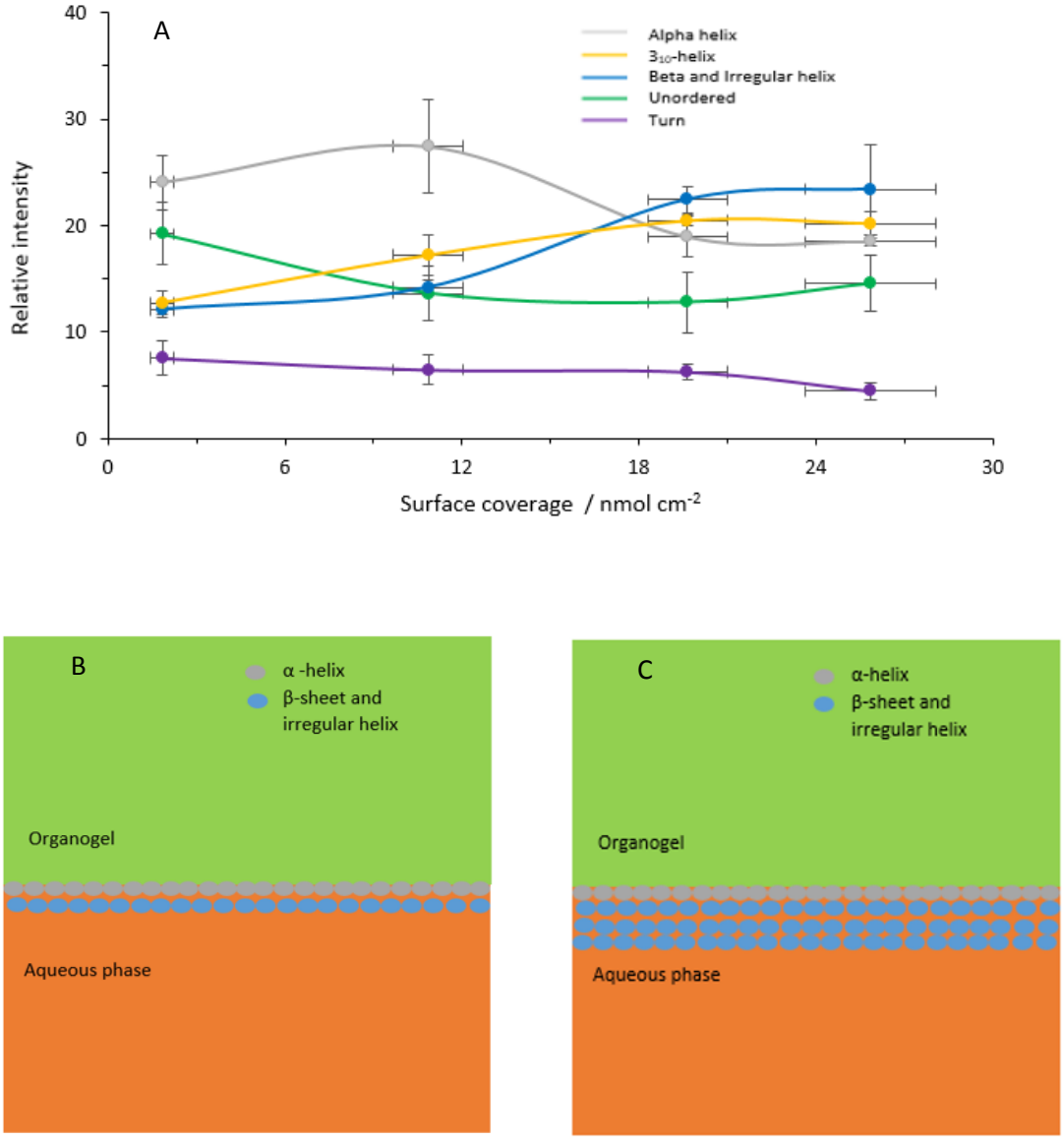

Figure 40: (A) Plot showing the relationship between the relative intensities of secondary structures of electroadsorbed insulin and surface covered by that electroadsorbed insulin. 0.70 V potential for 30 min adsorption time was applied for electroadsorption. Error bars are obtained from the standard deviations of three trials. (B) Cartoon showing thin layers of electroadsorbed insulin at the ITIES at low concentration (C) Cartoon showing the multilayers formation of insulin at the ITIES at high concentration.

3.4 Raman study of the secondary structures of insulin

3.4.1 Raman spectra of organogel

Raman spectroscopy is a vibrational spectroscopy technique that can be used in the detection of substances and characterisation of various chemical reactions. In this study, Raman spectroscopy was used in an attempt to characterise the secondary structures of insulin, to enable comparison with the secondary structures of insulin determined using FTIR.

Like the FTIR study, in the Raman spectroscopy study, aqueous-organic organogel interface was used for the study of secondary structures of electroadsorbed insulin. After that, the Raman spectra of the organogel were measured in the same environmental conditions. Figure 41 (A) and 41 (B), respectively, indicate the Raman spectra and amide I region of the Raman spectra of the organogel. Since no amide I band appeared in the Raman spectra of the organogel, this organogel is useful for the analysis of secondary structures of insulin following electroadsorption.

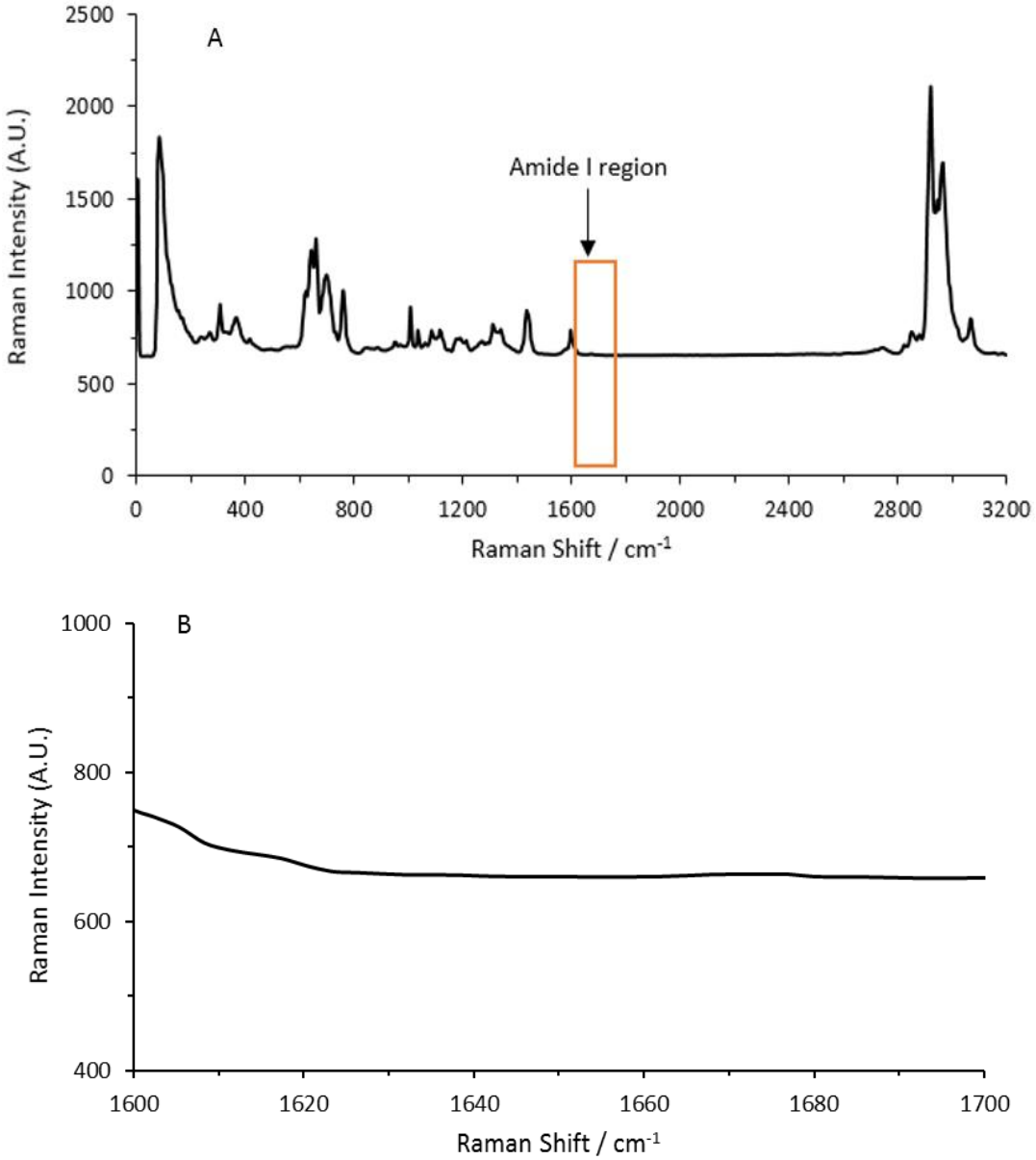

Figure 41: Raman spectra of 10 mM BTPPATPBCl-1,2-DCE (10 % w/v PVC) organogel (A) showing different spectral region, and (B) showing amide I region. Spectral resolution: 1 rel. cm^{-1}. 100 accumulations at an integration time of 100 ms.

3.4.2 Secondary structures of electroadsorbed insulin using Raman spectroscopy

Raman spectroscopy is widely used for the study of structures of insulin.[109,140–143] In this research, the secondary structures of insulin following electroadsorption were attempted to study using Raman spectroscopy. Here, two fixed concentrations (20 and 50 μM) of insulin were used. For the adsorption of insulin 0.70 V potential was maintained at the interface for 30 min. Like the FTIR spectroscopy, the aqueous medium was always 10 mM HCl. The electroadsorption of insulin was achieved using cell (scheme 2 as shown in page 52). After the adsorption of insulin at the organogel, this organogel containing adsorbed insulin was dried overnight and was then analysed using Raman spectroscopy. Figures 42 (A) and 42 (B) illustrate the Raman spectra of electroadsorbed insulin at 20 μM and 50 μM insulin, respectively. Similarly, Figures 42 (C) and 42 (D) represent the regions of amide I spectral band of electroadsorbed insulin at 20 and 50 μM insulin, respectively. The Raman spectra of the oranogel containing electroadsorbed insulin are the same as that of organogel at both concentrations. Likewise, in both concentrations, the amide I region does not show any response of electroadsorbed insulin. It means that the organogel surface does not contain a sufficient amount of electroadsorbed insulin for detection by Raman spectroscopy at these concentrations. Likewise, a poor signal-to-noise ratio was obtained with solid-state insulin (data not shown). So, Raman spectroscopy was not used further for the analysis of the secondary structures of electroadsorbed insulin.

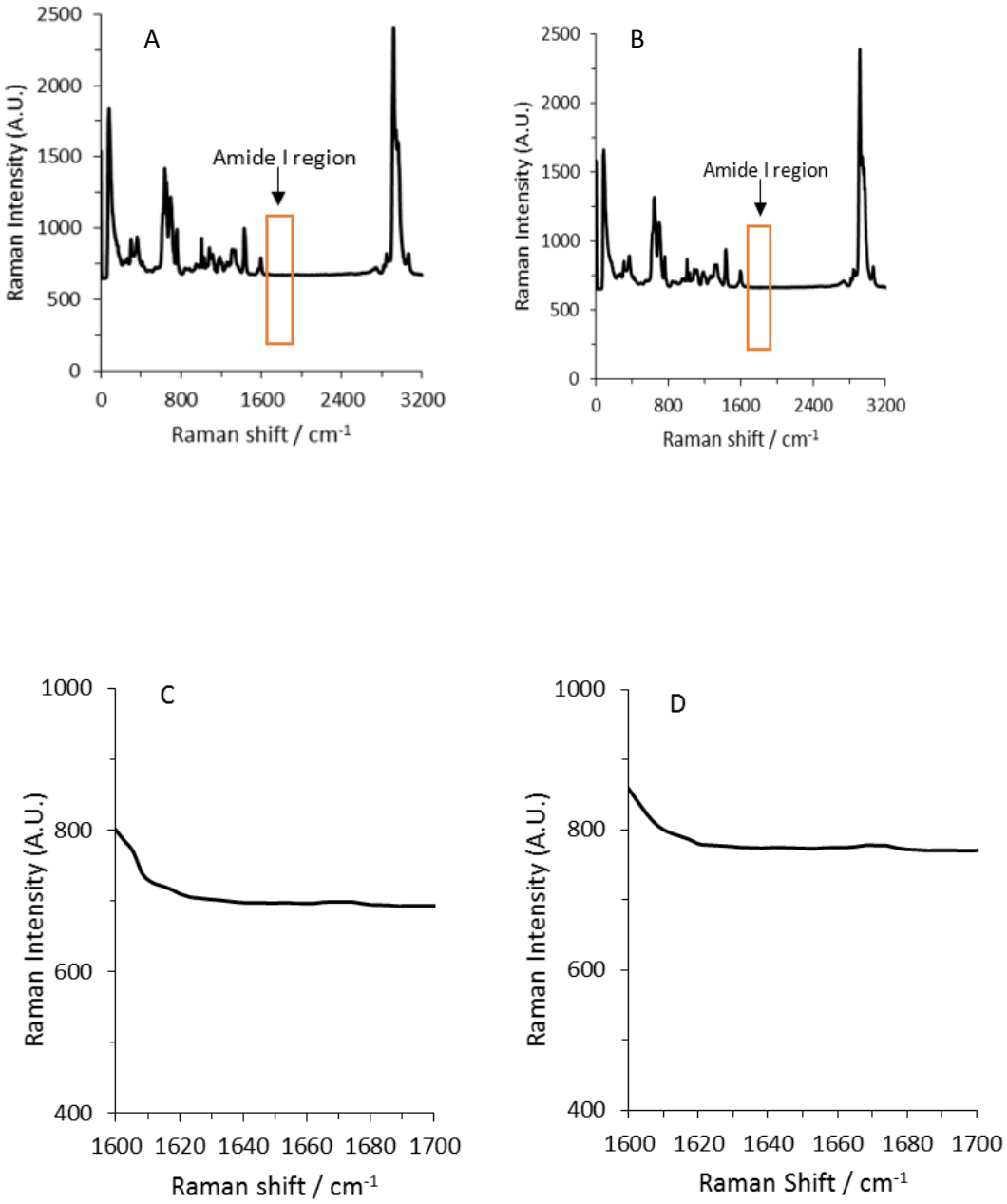

Figure 42: Raman spectra of insulin following electroadsorption using a two-electrode cell. 10 mM aqueous HCl as the aqueous phase. 10 mM BTPPATPBCl-1,2-DCE (10 % w/v PVC) organogel as the organic phase. (A) and (B) represent the Raman spectra of electroadsorbed insulin at 20 and 50 µM aqueous insulin, respectively. (C) and (D) indicate the amide I bands of electroadsorbed insulin at 20 and 50 µM aqueous insulin, respectively. 0.70 V potential applied for 30 min for electroadsorption. Spectral resolution: 1 rel. cm^{-1}. 100 accumulations at an integration time of 100 ms.

3.4.3 Comparative study of sensitivity of Electrochemistry, Fourier transform infrared spectroscopy, and Raman spectroscopy for detection of insulin

Three different techniques (i.e. electrochemistry, Fourier transform infrared (FTIR) spectroscopy, and Raman spectroscopy) were used for the analysis of insulin following electroadsorption. The sensitivity of these three techniques can be compared. From electrochemistry, the lowest limit of detection of electroadsorbed insulin was found to be 0.5 μM as discussed in section 3.2.3. Similarly, FTIR spectroscopy could detect 5 μM insulin following 30 min electroadsorption which was discussed in section 3.3.4.2. However, Raman spectroscopy could not detect insulin following electroadsorption even at 50 μM aqueous insulin which was discussed in section 3.4.2. From this study, it shows that electrochemistry is the most sensitive technique for the detection of insulin following electroadsorption. Raman spectroscopy is the least sensitive technique for the study of electroadsorbed insulin. However, FTIR spectroscopy is the best for secondary structure information. This means that different experimental methods have different strengths and weaknesses for insulin characterisation. While electrochemistry is good for the detection of low concentration, it does not reveal any structural detail. In contrast, FTIR spectroscopy reveals structural information but is less good for the detection of low concentration.

Chapter 4: General conclusions and suggestions for further works

4.1 General conclusions

The work presented in this thesis reported the study of the electrochemical behaviour of tetrapropylammonium ion ($TPrA^+$) and insulin at the interface between the two immiscible electrolyte solutions (ITIES) in a new electrochemical cell based on a plastic membrane. Such ITIES can be further used to study the electrochemical behaviour of other proteins. Likewise, the secondary structures of insulin were investigated at the ITIES, following electroadsorption, using FTIR spectroscopy and Raman spectroscopy.

A two-electrode system at the aqueous / 1,2-DCE organogel interface was used to study the electrochemical behaviour of $TPrA^+$ ions to validate the new electrochemical set up. The study revealed that peak responses (both forward and backward scans) due to $TPrA^+$ ions were directly proportional to the concentration of $TPrA^+$ ions in the aqueous phase. The peak-peak separation for the transfer of $TPrA^+$ at the ITIES was *ca.* 59 mV and the ratio of forward peak current to the backward peak current was *ca.* 1, which were consistent with the data already reported for transfers of single charged species.[134] Likewise, a scan rate study of $TPrA^+$ transfer revealed the diffusion-controlled behaviour of $TPrA^+$ at the ITIES, which is in good agreement with the literature.[14,127,130] The Randles-Sevcik equation was used to calculate the diffusion coefficient of $TPrA^+$ ion in the aqueous phase, which was found to be 5.5×10^{-6} cm^2 s^{-1}, in agreement with the data reported elsewhere.[14,134] These electrochemical experiments validated the new electrochemical cell.

After validation of the new cell, it was also used to study insulin electrochemistry at the aqueous / 1,2-DCE organogel interface. Insulin study has shown that forward and backward peak responses at the ITIES were obtained at 0.70 V and 0.46 V, respectively, and both the peak responses linearly increased with an increase in insulin concentrations. Peak charges also increased with an increase in the concentration of insulin. Nonetheless, the backward peak charges were greater than the forward peak charges. This might be due to the high concentration of electroadsorbed insulin at the gelled ITIES and this gel phase might prevent the

electroadsorbed species diffusing away from the interface. A scan rate study suggested the diffusion-controlled ion transfer process, but the peak shape on the backward scan was as expected for an adsorption/desorption process. So the overall reaction is suggested to be a diffusion-controlled transfer followed by the adsorption of complex species (cation insulin + anion of organic phase) at the interface; these results were in good agreement with the results reported in the literature.[32,137] These studies also validated the new electrochemical set up. Similarly, taking advantage of the adsorption process enabled pre-concentration at the interface for the method of adsorptive stripping voltammetry (AdSV). Using AdSV, the lowest detection limit of insulin at the ITIES formed at a single pore in a plastic membrane was found to be 0.5 μM. Likewise, a surface coverage study at the ITIES was conducted using different concentrations of insulin. Surface coverages consistent with multilayer formation occurred with an increase in the concentration of insulin. Multilayer formation of insulin at the ITIES also increased with increasing adsorption time. It means that the adsorbed insulin amount increased with insulin concentration in the aqueous phase and also with the increasing adsorption time. In this way, the amount of insulin attached to the interface can be controlled by the electrochemical parameters (potential and time).

Furthermore, the secondary structures of solid-state insulin, hydrated film of insulin, and electroadsorded insulin were investigated. Analysis of the spectroscopic data revealed that solid-state insulin and hydrated film of insulin possessed significant proportions of combined β-sheet and irregular helix. Since the adsorption of insulin was potential dependent, 0.70 V potential was chosen to study the secondary structures of insulin following electroadsorption. The absorbance frequencies of electroadsorbed insulin shifted with concentrations. Instead of the peaks overlapping each other, the amide I peaks were shifted towards higher wavenumber region at low concentration than the amide I peak at higher concentration. However, the shifting of peaks from lower wavenumber to higher wavenumber on lowering the concentration of aqueous insulin might provide some information about the change in secondary structures of insulin following electroadsorption. The curve fitting technique revealed that α-helical forms were dominant at low concentration while combined β-sheet and

irregular helix were found in larger proportion in high concentration. However, other secondary structures like 3_{10}-helix, unordered and turn did not show any significant difference at different concentrations. Secondary structures of electroadsorbed insulin at different potentials (i.e. 0.65 V, 0.70 V, and 0.75 V) using 20 μM aqueous insulin with 30 min adsorption time were also investigated. The adsorption potential did not change the relative proportions of secondary structures. However, the applied potential was only responsible for the deposition of insulin at the ITIES. Likewise, by keeping the fixed concentration of insulin and fixed electroadsorbtion potential, the relative proportions of secondary structures of electroadsorbed insulin at different adsorption time were investigated. At different adsorption times, no significant impact on α-helical and combined β-sheet and irregular structures occurred. Nevertheless, lower concentration with shorter adsorption time was favourable for the 3_{10}-helix and higher concentration with longer adsorption time was favourable for unordered structure.

In addition, Raman spectroscopy was also assessed for the identification of the secondary structures of electroadsorbed insulin. However, Raman spectroscopy could not detect insulin following electroadsorption even at 50 μM aqueous insulin. The study revealed that electrochemistry is the most sensitive technique for the detection of insulin following electroadsorption. However, FTIR spectroscopy is the best for obtaining secondary structure information of insulin.

4.2 Suggestions for further works

- This millimetre-sized ITIES can be further used for the study of secondary structures of various biomolecules like proteins, DNA, phospholipids, and carbohydrates following electroadsorption.
- In-situ FTIR study of electroadsorbed insulin would be interesting to perform in the future and can be compared with the ex-situ FTIR study of electroadsorbed insulin.

References

(1) Carrell, R. W.; Lomas, D. A. Conformational Disease. *Lancet* **1997**, *350*, 134–138.

(2) Bard, A. J.; Faulkner, L. R. *Electrochemical Methods: Fundamentals and Applications*, 2nd ed.; John Wiley & Sons, Inc.: New York, **2001**.

(3) Zoski, C. G. *Handbook of Electrochemistry*, 1st ed.; Elsevier: Oxford, 2007.

(4) Wieckowski, A. *Interfacial Electrochemistry: Theory, Experiment, and Applications*; CRC Press, **1999**.

(5) Wang, J. *Analytical Electrochemistry*; John Wiley & Sons: Hoboken, New Jersey, **2006**.

(6) Atkins, P.; De Paula, J. *Elements of Physical Chemistry*; Oxford University Press, **2017**.

(7) Wang, Y.; Kakiuchi, T.; Yasui, Y.; Mirkin, M. V. Kinetics of Ion Transfer at the Ionic Liquid/Water Nanointerface. *J. Am. Chem. Soc.* **2010**, *132* (47), 16945–16952.

(8) Bond, A. M. *Broadening Electrochemical Horizons: Principles and Illustration of Voltammetric and Related Techniques*; Oxford University Press on Demand, **2002**.

(9) Stern, O. The Theory of the Electrolytic Double-Layer. *Z. Elektrochem.* **1924**, *30*, 508–516.

(10) Grahame, D. C. The Electrical Double Layer and the Theory of Electrocapillarity. *Chem. Rev.* **1947**, *41* (3), 441–501.

(11) Silvester, D. S. Electrochemical Studies in Room Temperature Ionic Liquids, University of oxford, PhD Thesis, **2008**.

(12) Matsuura, T. Progress in Membrane Science and Technology for Seawater Desalination. *Desalination* **2001**, *134* (1–3), 47–54.

(13) Henstridge, M. C.; Compton, R. G. Mass Transport to Micro- and Nanoelectrodes and Their Arrays. *Chem. Rec.* **2012**, *12* (1), 63–71.

(14) Samec, Z. Electrochemistry at the Interface between Two Immiscible Electrolyte Solutions. *Pure Appl. Chem.* **2004**, *76*, 2147–2180.

(15) Arrigan, D. W. M. Bioanalytical Detection Based on Electrochemistry at

Interfaces between Immiscible Liquids. *Anal. Lett.* **2008**, *41* (18), 3233–3252.

(16) Samec, Z.; Marecek, V.; Koryta, J.; Khalil, M. W. Investigation of Ion Transfer across the Interface between Two Immiscible Electrolyte Solutions by Cyclic Voltammetry. *J. Electroanal. Chem.* **1977**, *83*, 393–397.

(17) Lillie, G. C.; Holmes, S. M.; Dryfe, R. A. W. Electrochemistry of Cytochrome c at the Liquid-Liquid Interface. *J. Phys. Chem. B* **2002**, *106* (47), 12101–12103.

(18) Sugihara, T.; Hotta, H.; Osakai, T. Electrochemical Control of Glucose Oxidase-Catalyzed Redox Reaction Using an Oil/Water Interface. *Phys. Chem. Chem. Phys.* **2004**, *6* (13), 3563–3568.

(19) Herzog, G.; Arrigan, D. W. M. Electrochemical Strategies for the Label-Free Detection of Amino Acids, Peptides and Proteins. *Analyst* **2007**, *132* (7), 615–632.

(20) Koryta, J. Electrochemical Polarization Phenomena at the Interface of Two Immiscible Electrolyte Solutions. *Electrochim. Acta* **1979**, *24* (3), 293–300.

(21) Campbell, J. A.; Girault, H. H. Steady State Current for Ion Transfer Reactions at a Micro Liquid/Liquid Interface. *J. Electroanal. Chem.* **1989**, *266* (2), 465–469.

(22) Shao, Y.; Mirkin, M. V. Fast Kinetic Measurements with Nanometer-Sized Pipets. Transfer of Potassium Ion from Water into Dichloroethane Facilitated by Dibenzo-18-Crown-6. *J. Am. Chem. Soc.* **1997**, *119* (34), 8103–8104.

(23) Scanlon, M. D.; Arrigan, D. W. M. Enhanced Electroanalytical Sensitivity via Interface Miniaturisation: Ion Transfer Voltammetry at an Array of Nanometre Liquid-Liquid Interfaces. *Electroanalysis* **2011**, *23* (4), 1023–1028.

(24) Nernst, W.; Riesenfeld, E. H. Ueber Elektrolytische Erscheinungen an Der Grenzfläche Zweier Lösungsmittel. **1902**, *313*, 600–608.

(25) Blank, M.; Feig, S. Electric Fields across Water-Nitrobenzene Interfaces. *Science (80-.).* **1963**, *141*, 1173–1174.

(26) Gavach, C.; Seta, P.; D'epenoux, B. The Double Layer and Ion Adsorption at the Interface between Two Non Miscible Solutions. Part I. Interfacial Tension Measurements for the Water-Nitrobenzene Tetraalkylammonium Bromide Systems. *J. Electroanal. Chem.* **1977**, *83* (2), 225–235.

(27) Koryta, J. Electrochemical Polarization Phenomena at the Interface of Two

Immiscible Electrolyte Solutions-II. Progress since 1978. **1984**, *29*, 445–452.

(28) Vanýsek, P.; Hernandez, I. C.; Xu, J. Determination of Choline, Picrate, Dodecyl Sulfate, and Several Quaternary Ammonium Salts on an Electrified Liquid/Liquid Microinterface. *Microchem. J.* **1990**, *41* (3), 327–339.

(29) Ribeiro, J. A.; Miranda, I. M.; Silva, F.; Pereira, C. M. Electrochemical Study of Dopamine and Noradrenaline at the Water/1,6-Dichlorohexane Interface. *Phys. Chem. Chem. Phys.* **2010**, *12* (46), 15190–15194.

(30) Marecek, V.; Samec, Z. Electrolysis At The Interface Between Two Immiscible Electrolyte Solutions : Determination Of Acetylcholine By Differential Pulse Stripping Voltammetry. *Anal. Lett.* **1981**, *14* (15), 1241–1253.

(31) Berduque, A.; Zazpe, R.; Arrigan, D. W. M. Electrochemical Detection of Dopamine Using Arrays of Liquid-Liquid Micro-Interfaces Created within Micromachined Silicon Membranes. *Anal. Chim. Acta* **2008**, *611* (2), 156–162.

(32) Kivlehan, F.; Lanyon, Y. H.; Arrigan, D. W. M. Electrochemical Study of Insulin at the Polarized Liquid-Liquid Interface. *Langmuir* **2008**, *24* (17), 9876–9882.

(33) Scanlon, M. D.; Jennings, E.; Arrigan, D. W. M. Electrochemical Behaviour of Hen-Egg-White Lysozyme at the Polarised Water/1, 2-Dichloroethane Interface. *Phys. Chem. Chem. Phys.* **2009**, *11* (13), 2272–2280.

(34) Herzog, G.; Kam, V.; Arrigan, D. W. M. Electrochemical Behaviour of Haemoglobin at the Liquid/Liquid Interface. *Electrochim. Acta* **2008**, *53* (24), 7204–7209.

(35) Huang, X.; Xie, L.; Lin, X.; Su, B. Detection of Metoprolol in Human Biofluids and Pharmaceuticals via Ion-Transfer Voltammetry at the Nanoscopic Liquid/Liquid Interface Array. *Anal. Chem.* **2017**, *89* (1), 945–951.

(36) Ribeiro, J. A.; Silva, F.; Pereira, C. M. Electrochemical Study of the Anticancer Drug Daunorubicin at a Water/Oil Interface: Drug Lipophilicity and Quantification. *Anal. Chem.* **2013**, *85* (3), 1582–1590.

(37) Guo, J.; Yuan, Y.; Amemiya, S. Voltammetric Detection of Heparin at Polarized Blood Plasma/1,2- Dichloroethane Interfaces. *Anal. Chem.* **2005**, *77* (17), 5711–5719.

(38) Jing, P.; Kim, Y.; Amemiya, S. Voltammetric Extraction of Heparin and Low-Molecular-Weight Heparin across 1,2-Dichloroethane/Water Interfaces.

Langmuir **2009**, *25* (23), 13653–13660.

(39) Horrocks, B. R.; Mirkin, M. V. Cation Binding to DNA Studied by Ion-Transfer Voltammetry at Micropipets. *Anal. Chem.* **1998**, *70* (22), 4653–4660.

(40) Kivlehan, F.; Lefoix, M.; Moynihan, H. A.; Thompson, D.; Ogurtsov, V. I.; Herzog, G.; Arrigan, D. W. M. Interaction of Acridine-Calix[4]Arene with DNA at the Electrified Liquid|liquid Interface. *Electrochim. Acta* **2010**, *55* (9), 3348–3354.

(41) Herzog, G.; Kam, V.; Berduque, A.; Arrigan, D. W. M. Detection of Food Additives by Voltammetry at the Liquid-Liquid Interface. *J. Agric. Food Chem.* **2008**, *56* (12), 4304–4310.

(42) Wang, Y.; Kececi, K.; Velmurugang, J.; Mirkin, M. V. Electron Transfer/Ion Transfer Mode of Scanning Electrochemical Microscopy (SECM): A New Tool for Imaging and Kinetic Studies. *Chem. Sci.* **2013**, *4* (9), 3606–3616.

(43) Wilke, S.; Schürz, R.; Wang, H. Amperometric Ion Detection in Capillary Zone Electrophoresis by Ion Transfer across a Liquid-Liquid Microinterface. *Anal. Chem.* **2001**, *73* (6), 1146–1154.

(44) Lee, H. J.; Girault, H. H. Amperometric Ion Detector for Ion Chromatography. *Anal. Chem.* **1998**, *70* (20), 4280–4285.

(45) Sawada, S.; Torii, H.; Osakai, T.; Kimoto, T. Pulse Amperometric Detection of Lithium in Artificial Serum Using a Flow Injection System with a Liquid/Liquid-Type Ion-Selective Electrode. *Anal. Chem.* **1998**, *70* (20), 4286–4290.

(46) Verwey, E. J. W.; Niessen, K. F. The Electrical Double Layer at the Interface of Two Liquids. *London, Edinburgh, Dublin Philos. Mag. J. Sci.* **1939**, *28* (189), 435–446.

(47) Girault, H. H.; Schiffrin, D. J. Thermodynamic Surface Excess of Water and Ionic Solvation at the Interface Between Immiscible Liquids. *J. Electroanal. Chem.* **1983**, *150*, 43–49.

(48) Senda, M.; Kakiuchi, T.; Osakai, T. Electrochemistry at the Interface Between Two Immiscible Electrolyte Solutions. *Electrochim. Acta* **1991**, *36* (2), 253–262.

(49) Pereira, C. M.; Schmickler, W.; Silva, F.; Sousa, M. J. Ion Association at Liquid|liquid Interfaces. *J. Electroanal. Chem.* **1997**, *436* (1–2), 9–15.

(50) Mitrinovic, D. M.; Zhang, Z.; Williams, S. M.; Huang, Z.; Schlossman, M. L. X-Ray Reflectivity Study of the Water-Hexane Interface. *J. Phys. Chem. B* **1999**, *103*

(11), 1779–1782.

(51) Luo, G.; Malkova, S.; Yoon, J.; Schultz, D. G.; Lin, B.; Meron, M.; Benjamin, I.; Vanýsek, P.; Schlossman, M. L. Ion Distributions near a Liquid Liquid Interface. *Science (80-.).* **2006**, *311*, 216–218.

(52) Mitrinović, D. M.; Tikhonov, A. M.; Li, M.; Huang, Z.; Schlossman, M. L. Noncapillary-Wave Structure at the Water-Alkane Interface. *Phys. Rev. Lett.* **2000**, *85* (3), 582–585.

(53) Strutwolf, J.; Barker, A. L.; Gonsalves, M.; Caruana, D. J.; Unwin, P. R.; Williams, D. E.; Webster, J. R. P. Probing Liquid/Liquid Interfaces Using Neutron Reflection Measurements and Scanning Electrochemical Microscopy. *J. Electroanal. Chem.* **2000**, *483*, 163–173.

(54) Daikhin, L. I.; Kornyshev, A. A.; Urbakh, M. Capillary Waves at Soft Electrified Interfaces. *J. Electroanal. Chem.* **2000**, *483* (1), 68–80.

(55) Vanýsek, P.; Ramírez, L. B. Interface between Two Immiscible Liquid Electrolytes. *J. Chil. Chem. Soc.* **2008**, *53* (2), 1455–1463.

(56) Girault, H. H. Charge Transfer across Liquid-Liquid Interfaces. In *Modern aspects of electrochemistry*; Bockris, J., Ed.; New York, **1993**; pp 1–62.

(57) Girault, H. H. Electrochemistry at Liquid Liquid Interfaces. In *Electroanalytical Chemistry*; Bard, A. J., Zoski, C. G., Eds.; CRC Press: Taylor & Francis: Boca Raton, **2010**; Vol. 23, p 1.

(58) Geblewicz, G.; Kontturi, A. K.; Kontturi, K.; Schiffrin, D. J. Salting out of Hydrophobic Ions at Immiscible Electrolyte Interfaces. *J. Electroanal. Chem.* **1987**, *217* (2), 261–269.

(59) Amemiya, S.; Wang, Y.; Mirkin, M. V. Nanoelectrochemistry at the Liquid/Liquid Interface. In *Specialist Periodical Reports in Electrochemistry*; **2014**; Vol. 12, pp 1–43.

(60) Osakai, T.; Kakutani, T.; Senda, M. Ion-Transfer Voltammetry with the Interfaces Between Polymer-Electrolyte Gel and Electrolyte Solutions. *Japan Soc. Anal. Chem.* **1984**, *33*, E371–E377.

(61) Lee, H. J.; Beriet, C.; Girault, H. H. Amperometric Detection of Alkali Metal Ions on Micro-Fabricated Composite Polymer Membranes. *J. Electroanal. Chem.* **1998**, *453* (1–2), 211–219.

(62) Kakutani, T.; Ohkouchi, T.; Osakai, T.; Kakiuchi, T.; Senda, M. Ion-Transfer Voltammetry and Potentiometry of Acetylcholine with the Interface between and Potentiometry of Polymer-Nitrobenzene Acetyicholine Gel and Water. *Anal. Sci.* **1985**, *1* (3), 219–225.

(63) Alvarez de Eulate, E.; Serls, L.; Arrigan, D. W. M. Detection of Haemoglobin Using an Adsorption Approach at a Liquid-Liquid Microinterface Array. *Anal. Bioanal. Chem.* **2013**, *405* (11), 3801–3806.

(64) Scanlon, M. D.; Strutwolf, J.; Arrigan, D. W. M. Voltammetric Behaviour of Biological Macromolecules at Arrays of Aqueous|organogel Micro-Interfaces. *Phys. Chem. Chem. Phys.* **2010**, *12* (34), 10040–10047.

(65) Berduque, A.; Sherburn, A.; Ghita, M.; Dryfe, R. A. W.; Arrigan, D. W. M. Electrochemically Modulated Liquid-Liquid Extraction of Ions. *Anal. Chem.* **2005**, *77* (22), 7310–7318.

(66) Fantini, S.; Clohessy, J.; Gorgy, K.; Fusalba, F.; Johans, C.; Kontturi, K.; Cunnane, V. J. Influence of the Presence of a Gel in the Water Phase on the Electrochemical Transfer of Ionic Forms of Beta-Blockers across a Large Water/1,2-Dichloroethane Interface. *Eur. J. Pharm. Sci.* **2003**, *18* (2), 251–257.

(67) Zoski, C. G.; Mirkin, M. V. Steady-State Limiting Currents at Finite Conical Microelectrodes. *Anal. Chem.* **2002**, *74* (9), 1986–1992.

(68) Bond, A. M.; Luscombe, D.; Oldham, K. B.; Zoski, C. G. A Comparison of the Chronoamperometric Response at Inlaid and Recessed Disc Microelectrodes. *J. Electroanal. Chem.* **1988**, *249*, 1–14.

(69) Strutwolf, J.; Scanlon, M. D.; Arrigan, D. W. M. Electrochemical Ion Transfer across Liquid/Liquid Interfaces Confined within Solid-State Micropore Arrays - Simulations and Experiments. *Analyst* **2009**, *134* (1), 148–158.

(70) Vanysek, P.; Reid, J. D.; Craven, M. A.; Buck, R. P. Properties of the Interface Between Two Immiscible Electrolytes in the Presence of Proteins. *Electrochem. Soc.* **1984**, *131*, 1788–1791.

(71) Zhan, D.; Mao, S.; Zhao, Q.; Chen, Z.; Hu, H.; Jing, P.; Zhang, M.; Zhu, Z.; Shao, Y. Electrochemical Investigation of Dopamine at the Water/1,2-Dichloroethane Interface. *Anal. Chem.* **2004**, *76* (14), 4128–4136.

(72) Yong, C.; Yi, Y.; Meiqin, Z.; Fei, L.; Peng, S.; Zhao, G.; Yuanhua, S. Systematic

Study of the Transfer of Amino Acids across the Water/1,2-Dichloroethane Interface Facilitated by Dibenzo-18-Crown-6. *Sci. China, Ser. B Chem.* **2004**, *47* (1), 24–33.

(73) Sawada, S.; Osakai, T. Hydrophobicity of Oligopeptides: A Voltammetric Study of the Transfer of Dipeptides Facilitated by Dibenzo-18-Crown-6 at the Nitrobenzene/Water Interface. *Phys. Chem. Chem. Phys.* **1999**, *1*, 4819–4825.

(74) Osakai, T.; Hirai, T.; Wakamiya, T.; Sawada, S. Quantitative Analysis of the Structure-Hydrophobicity Relationship for Di- and Tripeptides Based on Voltammetric Measurements with an Oil/Water Interface. *Phys. Chem. Chem. Phys.* **2006**, *8*, 985–993.

(75) Collins, C. J.; Arrigan, D. W. M. Ion-Transfer Voltammetric Determination of the β-Blocker Propranolol in a Physiological Matrix at Silicon Membrane-Based Liquid|liquid Microinterface Arrays. *Anal. Chem.* **2009**, *81* (6), 2344–2349.

(76) Velický, M.; Tam, K. Y.; Dryfe, R. A. W. Hydrodynamic Voltammetry at the Liquid-Liquid Interface: Application to the Transfer of Ionised Drug Molecules. *J. Electroanal. Chem.* **2012**, *683*, 94–102.

(77) Samec, Z.; Trojánek, A.; Langmaier, J.; Samcová, E. Cyclic Voltammetry of Biopolymer Heparin at PVC Plasticized Liquid Membrane. *Electrochem. commun.* **2003**, *5*, 867–870.

(78) Arrigan, D. W. M. Voltammetry of Proteins at Liquid-Liquid Interfaces. *Annu. Reports Prog. Chem. - Sect. C* **2013**, *109*, 167–188.

(79) O'Sullivan, S.; Arrigan, D. W. M. Electrochemical Behaviour of Myoglobin at an Array of Microscopic Liquid-Liquid Interfaces. *Electrochim. Acta* **2012**, *77*, 71–76.

(80) Alvarez de Eulate, E.; O'Sullivan, S.; Arrigan, D. W. M. Electrochemically Induced Formation of Cytochrome c Oligomers at Soft Interfaces. *ChemElectroChem* **2017**, *4* (4), 898–904.

(81) Alvarez de Eulate, E.; Qiao, L.; Scanlon, M. D.; Girault, H. H.; Arrigan, D. W. M. Fingerprinting the Tertiary Structure of Electroadsorbed Lysozyme at Soft Interfaces by Electrostatic Spray Ionization Mass Spectrometry. *Chem. Commun.* **2014**, *50* (80), 11829–11832.

(82) Vagin, M. Y.; Malyh, E. V.; Larionova, N. I.; Karyakin, A. A. Spontaneous and

Facilitated Micelles Formation at Liquid/Liquid Interface: Towards Amperometric Detection of Redox Inactive Proteins. *Electrochem. commun.* **2003**, *5* (4), 329–333.

(83) Amemiya, S.; Yang, X.; Wazenegger, T. L. Voltammetry of the Phase Transfer of Polypeptide Protamines across Polarized Liquid/Liquid Interfaces. *J. Am. Chem. Soc.* **2003**, *125*, 11832–11833.

(84) Yuan, Y.; Amemiya, S. Facilitated Protamine Transfer at Polarized Water/1,2-Dichloroethane Interfaces Studied by Cyclic Voltammetry and Chronoamperometry at Micropipet Electrodes. *Anal. Chem.* **2004**, *76*, 6877–6886.

(85) Trojánek, A.; Langmaier, J.; Samcová, E.; Samec, Z. Counterion Binding to Protamine Polyion at a Polarised Liquid-Liquid Interface. *J. Electroanal. Chem.* **2007**, *603*, 235–242.

(86) O'Sullivan, S.; Arrigan, D. W. M. Impact of a Surfactant on the Electroactivity of Proteins at an Aqueous-Organogel Microinterface Array. *Anal. Chem.* **2013**, *85* (3), 1389–1394.

(87) Alvarez de Eulate, E.; Arrigan, D. W. M. Adsorptive Stripping Voltammetry of Hen-Egg-White-Lysozyme via Adsorption-Desorption at an Array of Liquid-Liquid Microinterfaces. *Anal. Chem.* **2012**, *84* (5), 2505–2511.

(88) Thomsen, A. E.; Jensen, H.; Jorgensen, L.; Weert, M.; Østergaard, J. Studies on Human Insulin Adsorption Kinetics at an Organic-Aqueous Interface Determined Using a Label-Free Electroanalytical Approach. *Colloids Surfaces B Biointerfaces* **2008**, *63* (2), 243–248.

(89) O'Sullivan, S.; Alvarez de Eulate, E.; Yuen, Y. H.; Helmerhorst, E.; Arrigan, D. W. M. Stripping Voltammetric Detection of Insulin at Liquid-Liquid Microinterfaces in the Presence of Bovine Albumin. *Analyst* **2013**, *138* (20), 6192–6196.

(90) Brocchieri, L.; Karlin, S. Protein Length in Eukaryotic and Prokaryotic Proteomes. *Nucleic Acids Res.* **2005**, *33* (10), 3390–3400.

(91) Caetano-Anollés, G.; Wang, M.; Caetano-Anollés, D.; Mittenthal, J. E. The Origin, Evolution and Structure of the Protein World. *Biochem. J.* **2009**, *417* (3), 621–637.

(92) Madan, B.; Thangappan, J.; Lee, S. G. Engineering a Beta-Turn in Green Fluorescent Protein to a Foreign Loop. *J. Ind. Eng. Chem.* **2016**, *33*, 330–335.

(93) Bezer, S.; Matsumoto, M.; Lodewyk, M. W.; Lee, S. J.; Tantillo, D. J.; Gagné, M. R.; Waters, M. L. Identification and Optimization of Short Helical Peptides with Novel Reactive Functionality as Catalysts for Acyl Transfer by Reactive Tagging. *Org. Biomol. Chem.* **2014**, *12* (9), 1488–1494.

(94) Linding, R.; Jensen, L. J.; Diella, F.; Bork, P.; Gibson, T. J.; Russell, R. B. Protein Disorder Prediction: Implications for Structural Proteomics. *Structure* **2003**, *11* (11), 1453–1459.

(95) Lokappa, S. B.; Suk, J. E.; Balasubramanian, A.; Samanta, S.; Situ, A. J.; Ulmer, T. S. Sequence and Membrane Determinants of the Random Coil-Helix Transition of α-Synuclein. *J. Mol. Biol.* **2014**, *426* (10), 2130–2144.

(96) Chiti, F.; Dobson, C. M. Protein Misfolding, Functional Amyloid, and Human Disease. *Annu. Rev. Biochem.* **2006**, *75* (1), 333–366.

(97) Greenfield, N. J. Using Circular Dichroism Spectra to Estimate Protein Secondary Structure. *Nat. Protoc.* **2007**, *1* (6), 2876–2890.

(98) Wiithrich, K. Protein Structure Determination in Solution by NMR Spectroscopy. *Journal. Biol. Chem.* **1990**, *265* (36), 22059–22062.

(99) Vecchio, G.; Bossi, A.; Pasta, P.; Carrea, G. Fourier-Transform Infrared Conformational Study of Bovine Insulin in Surfactant Solutions. *Int. J. Pept. Protein Res.* **1996**, *48* (2), 113–117.

(100) Nielsen, L.; Frokjaer, S.; Carpenter, J. F.; Brange, J. Studies of the Structure of Insulin Fibrils by Fourier Transform Infrared (FTIR) Spectroscopy and Electron Microscopy. *J. Pharm. Sci.* **2001**, *90* (1), 29–37.

(101) Dong, A.; Huang, P.; Caughey, W. S. Protein Secondary Structures in Water from Second-Derivative Amide I Infrared Spectra. *Biochemistry* **1990**, *29* (13), 3303–3308.

(102) Bouchard, M.; Zurdo, J.; Nettleton, E. J.; Dobson, C. M.; Robinson, C. V. Formation of Insulin Amyloid Fibrils Followed by FTIR Simultaneously with CD and Electron Microscopy. *Protein Sci.* **2000**, *9* (10), 1960–1967.

(103) Hua, Q.; Weiss, M. A. Comparative 2D NMR Studies of Human Insulin and Des-Pentapeptide Insulin: Sequential Resonance Assignment and Implications for

Protein Dynamics and Receptor Recognition. *Biochemistry* **1991**, *30* (22), 5505–5515.

(104) Welch, W. R. W.; Kubelka, J.; Keiderling, T. A. Infrared, Vibrational Circular Dichroism, and Raman Spectral Simulations for β-Sheet Structures with Various Isotopic Labels, Interstrand, and Stacking Arrangements Using Density Functional Theory. *J. Phys. Chem. B* **2013**, *117* (36), 10343–10358.

(105) Booth, S. G.; Felisilda, B. M. B.; Alvarez de Eulate, E.; Gustafsson, O. J. R.; Arooj, M.; Mancera, R. L.; Dryfe, R. A. W.; Hackett, M. J.; Arrigan, D. W. M. Secondary Structural Changes in Proteins as a Result of Electroadsorption at Aqueous–Organogel Interfaces. *Langmuir* **2019**, *35*, 5821–5829.

(106) Byler, M.; Susi, H. Examination of the Secondary Structure of Proteins by Deconvolved FTIR Spectra. *Biopolymers* **1986**, *25* (3), 469–487.

(107) Pelton, J. T.; McLean, L. R. Spectroscopic Methods for Analysis of Protein Secondary Structure. *Anal. Biochem.* **2000**, *277* (2), 167–176.

(108) Sereda, V.; Sawaya, M. R.; Lednev, I. K. Structural Organization of Insulin Fibrils Based on Polarized Raman Spectroscopy: Evaluation of Existing Models. *J. Am. Chem. Soc.* **2015**, *137* (35), 11312–11320.

(109) Zeng, G.; Shou, J. J.; Li, K. K.; Zhang, Y. H. In-Situ Confocal Raman Observation of Structural Changes of Insulin Crystals in Sequential Dehydration Process. *Biochim. Biophys. Acta* **2011**, *1814* (12), 1631–1640.

(110) Wei, J.; Lin, Y. Z.; Zhou, J. M.; Tsou, C. L. FTIR Studies of Secondary Structures of Bovine Insulin and Its Derivatives. *Biochim. Biophys. Acta* **1991**, *1080* (1), 29–33.

(111) Xie, L.; Tsou, C. L. Comparison of Secondary Structures of Insulin and Proinsulin by FTIR. *J. Protein Chem.* **1993**, *12* (4), 483–487.

(112) Krimm, S. Infrared Spectra and Chain Conformation of Proteins. *J. Mol. Biol.* **1962**, *4* (6), 528–540.

(113) Susi, H.; Byler, D. M. Protein Structure by Fourier Transform Infrared Spectroscopy: Second Derivative Spectra. *Biochem. Biophys. Res. Commun.* **1983**, *115*, 391–397.

(114) Williams, R. W. Estimation of Protein Secondary Structure from the Laser Raman Amide I Spectrum. *J. Mol. Biol.* **1983**, *166* (4), 581–603.

(115) Fineberg, S. E.; Kawabata, T. T.; Finco-Kent, D.; Fountaine, R. J.; Finch, G. L.; Krasner, A. S. Immunological Responses to Exogenous Insulin. *Endocr. Rev.* **2007**, *28* (6), 625–652.

(116) Nettleton, E. J.; Tito, P.; Sunde, M.; Bouchard, M.; Dobson, C. M.; Robinson, C. V. Characterization of the Oligomeric States of Insulin in Self-Assembly and Amyloid Fibril Formation by Mass Spectrometry. *Biophys. J.* **2000**, *79* (2), 1053–1065.

(117) Nault, L.; Guo, P.; Jain, B.; Bréchet, Y.; Bruckert, F.; Weidenhaupt, M. Human Insulin Adsorption Kinetics, Conformational Changes and Amyloidal Aggregate Formation on Hydrophobic Surfaces. *Acta Biomater.* **2013**, *9* (2), 5070–5079.

(118) Yeo, S.-D.; Debenedetti, P. G.; Patro, S. Y.; Przybycien, T. M. Secondary Structure Characterization of Microparticulate Insulin Powders. *J. Pharm. Sci.* **1994**, *83* (12), 1651–1656.

(119) Samec, Z.; Mareček, V.; Weber, J. Detection of an Electron Transfer across the Interface between Two Immiscible Electrolyte Solutions by Cyclic Voltammetry with Four-Electrode System. *J. Electroanal. Chem.* **1977**, *96* (2), 245–247.

(120) Bates, R. G.; Macaskill, J. B. Standard Potential of the Silver-Silver Chloride Electrode. *Pure Appl. Chem.* **1978**, *50*, 1701–1706.

(121) Compton, R. G.; Banks, C. E. *Understanding Voltammetry*, 2nd Ed.; Imperical College Press, 2011.

(122) Herzog, G.; Beni, V. Stripping Voltammetry at Micro-Interface Arrays. *Anal. Chim. Acta* **2013**, *769*, 10–21.

(123) Strutwolf, J.; Scanlon, M. D.; Arrigan, D. W. M. The Performance of Differential Pulse Stripping Voltammetry at Micro-Liquid-Liquid Interface Arrays. *J. Electroanal. Chem.* **2010**, *641* (1–2), 7–13.

(124) Garcia-Quintana, D.; Garriga, P.; Manyosa, J. Study of the Structure of Arrestin (S-Antigen) from Bovine Photoreceptors by FTIR Spectroscopy. *Biochim. Biophys. Acta (BBA)/Protein Struct. Mol.* **1992**, *1122* (3), 269–272.

(125) Barth, A. The Infrared Absorption of Amino Acid Side Chains. *Prog. Biophys. Molcular Biol.* **2000**, *74*, 141–173.

(126) Camp, C. H.; Cicerone, M. T. Chemically Sensitive Bioimaging with Coherent Raman Scattering. *Nat. Photonics* **2015**, *9* (5), 295–305.

(127) Samec, Z.; Mareček, V. Charge Transfer between Two Immiscible Electrolyte Solutions Part X. Kinetics of Tetraalkylammonium Ion Transfer across the Water/Nitrobenzene Interface. *J. Electroanal. Chem.* **1986**, *200*, 17–33.

(128) Wilke, S.; Zerihun, T. Standard Gibbs Energies of Ion Transfer across the Water | 2-Nitrophenyl Octyl Ether Interface. *J. Electroanal. Chem.* **2001**, *515*, 52–60.

(129) Toth, P. S.; Dryfe, R. A. W. Novel Organic Solvents for Electrochemistry at the Liquid/Liquid Interface. *Analyst* **2015**, *140* (6), 1947–1954.

(130) Langmaier, J.; Samec, Z. Cyclic Voltammetry of Ion Transfer across a Room Temperature Ionic Liquid Membrane Supported by a Microporous Filter. *Electrochem. commun.* **2007**, *9* (10), 2633–2638.

(131) Ulmeanu, S.; Lee, H. J.; Fermin, D. J.; Girault, H. H.; Shao, Y. Voltammetry at a Liquid-Liquid Interface Supported on a Metallic Electrode. *Electrochem. commun.* **2001**, *3* (5), 219–223.

(132) Kakiuchi, T.; Tsujioka, N. Cyclic Voltammetry of Ion Transfer across the Polarized Interface between the Organic Molten Salt and the Aqueous Solution. *Electrochem. commun.* **2003**, *5* (3), 253–256.

(133) Pletcher, D.; Greef, R.; Peat, R.; Peter, L. M.; Robinson, J. *Instrumental Methods in Electrochemistry*, 2nd ed.; Horwood Publishing Limited: England, **2001**.

(134) Rahaman, A. Doe, H. Ion Transfer of Tetraalkylammonium Cations at an Interface between Frozen Aqueous Solution and 1,2-Dichloroethane. *J. Electroanal. Chem.* **1997**, *424*, 159–164.

(135) Tanford, C.; Epstein, J. The Physical Chemistry of Insulin. I. Hydrogen Ion Titration Curve of Zinc-Free Insulin. *J. Am. Chem. Soc.* **1954**, *76* (8), 2163–2169.

(136) Gao, J.; Mrksich, M.; Whitesides, G. M.; Gomez, F. A. Using Capillary Electrophoresis To Follow the Acetylation of the Amino Groups of Insulin and To Estimate Their Basicities. *Anal. Chem.* **1995**, *67* (18), 3093–3100.

(137) Shinshi, M.; Sugihara, T.; Osakai, T.; Goto, M. Electrochemical Extraction of Proteins by Reverse Micelle Formation. *Langmuir* **2006**, *22* (13), 5937–5944.

(138) Hua, Q. X.; Shoelson, S. E.; Kochoyan, M.; Weiss, M. A. Receptor Binding Redefined by a Structural Switch in a Mutant Human Insulin. *Nature* **1991**, *354* (6350), 238–241.

(139) Blundell, T.; Dodson, G.; Hodgkin, D.; Mercola, D. Insulin: The Structure in the

Crystal and Its Reflection in Chemistry and Biology. In *Laboratory of molecular biophysics*; South parks Road, Oxford, England, **1972**; pp 279–402.

(140) Ferrari, D.; Diers, J. R.; Bocian, D. F.; Kaarsholm, N. C.; Dunn, M. F. Raman Signatures of Ligand Binding and Allosteric Conformation Change in Hexameric Insulin. *Biopolym.* **2001**, *62* (5), 249–260.

(141) Ortiz, C.; Zhang, D.; Xie, Y.; Davisson, V. J.; Ben-Amotz, D. Identification of Insulin Variants Using Raman Spectroscopy. *Anal. Biochem.* **2004**, *332* (2), 245–252.

(142) Yu, N. T.; Liu, C. S.; O'Shea, D. C. Laser Raman Spectroscopy and the Conformation of Insulin and Proinsulin. *J. Mol. Biol.* **1972**, *70* (1), 117–132.

(143) Yu, N.-T.; Jo, B. H.; Chang, R. C. C.; Huber, J. D. Single-Crystal Raman Spectra of Native Insulin Structures of Insulin Fibrils, Glucagon Fibrils, and Intact Calf Lens. *Arch. Biochem. Biophys.* **1974**, *160* (2), 614–622.

List of Presentations

"Structural changes in insulin at soft electrochemical interfaces", H.B. Lamichhane, T.G. Henares, M.J. Hackett, and D.W.M. Arrigan, poster presentation at the 21st Australia and New Zealand Electrochemistry Symposium (21AES), Queensland University of Technology, Brisbane, Australia, April 2019.

"Structural changes in the insulin following electroadsorption at the water-organogel interface", H.B. Lamichhane, T.G. Henares, M.J. Hackett, and D.W.M. Arrigan, poster presentation at the MLS HDR Science Symposium, Curtin University, Perth, Australia, December 2019.

To Whom It May Concern

In relation to a planned draft manuscript to be submitted for journal publication:

I, Hum Bahadur Lamichhane, contributed to the design of experiments, the gathering of data by performing these experiments, undertaking of data analysis and interpretation, and preparation of the draft manuscript prepared under the draft title of "Structural Changes in Insulin at Soft Electrochemical Interfaces".

[redacted]

Hum Bahadur Lamichhane

I, as a Co-Author, endorse that this level of contribution by the candidate indicated above is appropriate.

[redacted]

Prof. Damien W.M. Arrigan

[redacted]

Dr. Mark J. Hackett

[redacted]

Dr. Terence G. Henares

To Whom It May Concern

In relation to a planned draft manuscript to be submitted for journal publication:

I, Hum Bahadur Lamichhane, contributed to the design of experiments, the gathering of data by performing these experiments, undertaking of data analysis and interpretation, and preparation of the draft manuscript prepared under the draft title of "Structural Changes in Insulin at Soft Electrochemical Interfaces".

[redacted]

Hum Bahadur Lamichhane

I, as a Co-Author, endorse that this level of contribution by the candidate indicated above is appropriate.

Prof. Damien W.M. Arrigan

[redacted]

Dr. Mark J. Hackett

Dr. Terence G. Henares